Metallic Ruthenium Nanoparticles Derived from Arene Ruthenium Complexes: Synthesis, Characterization and Applications

Thèse présentée à la Faculté des Sciences par

Farooq-Ahmad KHAN

Chimiste diplômé de l'Université de Bretagne Occidentale, France

Pour l'obtention du grade de Docteur ès Sciences

Directeur de thèse : Prof. Georg Süss-Fink

Membres du jury :

Prof. G. Süss-Fink
Directeur de thèse,
Université de Neuchâtel

Dr. B. Therrien
Rapporteur interne,
Université de Neuchâtel

Prof. K. Fromm
Rapporteur externe,
Université de Fribourg

UNIVERSITÉ DE NEUCHÂTEL

Institut de Chimie, Université de Neuchâtel
Novembre 2011

swissuniversity

Université de Neuchâtel

FACULTE DES SCIENCES
Secrétariat-Décanat de la faculté
Rue Emile-Argand 11
CH-2000 Neuchâtel

IMPRIMATUR POUR LA THESE

Metallic Ruthenium Nanoparticles Derived from Arene Ruthenium Complexes : Synthesis, Characterization and Applications

Farooq-Ahmad KHAN

UNIVERSITE DE NEUCHATEL

FACULTE DES SCIENCES

La Faculté des sciences de l'Université de Neuchâtel,
sur le rapport des membres du jury

Prof. Georg Süss-Fink (directeur de thèse),
Dr Bruno Therrien,
Prof. Katharina M. Fromm (Université de Fribourg)

autorise l'impression de la présente thèse.

Neuchâtel, le 25 janvier 2012

Le doyen :
P. Kropf

Acknowledgments

This manuscript describes the results of my doctoral research work done during the last four years at Université de Neuchâtel, Switzerland. Financial support of this work from Swiss National Science Foundation is gratefully acknowledged.

I am deeply indebted to my advisor, Professor Georg Süss-Fink, for giving me the opportunity to join his group and explore the fascinating research area of nanoparticles. His guidance and support throughout this project helped me to carry out this research work to successful conclusions. I also thank him for the confidence that he testified by giving me many responsibilities within the group.

I would express my gratitude to my friends and colleagues, Dr. Mona Anca Furrer, Dr. Julien Boudon, Dr. Altaf Malik, Dr. Cyril Gautier, Dr. Nicolas Barry, Dr. Mathieu Auzias, Dr. Johan Mattsson, Dr. Michael Gras, Dr. Trieu-Tien Thai, Julien Freudenreich, Sun Bing, Amine Garci, Marie Anne-Flore Ibao, Jîri Tauchman, John Peter Justin Paul Raj, Dr. Ulaganatha Raja and Dr. Si Satyabrata for all the good moments that we have shared and for their collaboration.

I owe my sincere gratitude to my apprentice, Luca Nori for the contribution to the work described in this thesis.

I must also thank the technical staff, especially Heinz Bursian and Dr. Julien Furrer for nuclear magnetic resonance spectroscopy services, Dr. Armelle Vallat and Marie Eve for mass spectrometry and chromatography services, the X-ray diffraction experts Dr. Bruno Therrien and Prof. Helene Stoekli-Evans. I especially thank the people of CSEM Neuchâtel, Dr. Masood Dadras, Dr. Vladislav Spassov for nanoscopic analysis and Dr. Olha Sereda, Dr. Antonia Neels for XRD studies, the people of EPFL Lausanne Prof. Paul J. Dyson, Olivier Zava, Dr. Anna K. Renfrew for cytotoxic studies, Jean David Teuscher, Michael Gorcel and Elena Rossel for ICP-OES analysis and the people of ETH Zurich Prof. Anne Marie Hirtz and Hans-Peter Hächler for the magnetic measurements. Their help and their kindness are sincerely acknowledged.

I also thank the friendly people of STF, especially Christian Hèche, Thierry Delhove, Dominique Schenker, Daniel Varidel and many more.

I am grateful to Prof. Rober Dischneux and the people of his group especially Anaïs Pitto-Barry, Philippe Bourgun, Stéphane Frein, Sebastiano Guerra and Sylvain Mischler for their kind help regarding the synthesis and mesogenic studies.

Many thanks to Mrs. Tissot for aid in administrative problems, Philippe Stauffer and Jean Luc for help in technical problems and the staff of the chemical store – Maurice Binggeli and Claire-Lise Rosset.

Cordial gratitude to my siblings Rauf Khan, Rehana, Rabia and Jahanzaib for their love and patience.

In final instance, this thesis is dedicated to my parents, Ahmad Khan and Saeeda Khanam, for their unselfish support and encouragement throughout my life.

Summary

The present work deals with the preparation of ruthenium nanoparticles using an organometallic approach. In the first part, the synthesis of ruthenium nanoparticles stabilized by mesogenic isonicotinic ester ligands is presented. We have been interested in the use of long-chain isonicotinic esters as lipohilic components in order to increase the anticancer activity of arene ruthenium complexes, while using them as stabilizers for ruthenium nanoparticles with the aim of exploring self-organization and biological (anticancer) properties of these new hybrid materials. The ruthenium nanoparticles thus obtained as well as their organometallic precursors showed anticancer activity comparable to cisplatin or superior to cisplatin in the cancer cell lines A2780 and cisplatin-resistant cell line A2780cisR, the highest cytotoxicity being 0.179 µM, a value 9 fold lower than cisplatin – a platinum-based chemotherapy drug widely used to treat different types of cancers.

In second part, silicate-supported ruthenium nanoparticles with a special emphasis on hectorite-supported Ru(0) is presented. Size- and shape-selective preparation of hectorite-supported ruthenium nanoparticles was achieved by using either molecular hydrogen or solvothermal reduction route employing different organometallic precursors. The catalytic efficiency of these nanoparticles was evaluated for different arenes, furfuryl alcohol and α,β-unsaturated ketones. Hectorite-supported ruthenium nanoparticles were found to be promising hydrogenation catalysts. It was observed that the modification of intercalated particles size and reaction conditions tune the catalytic activity for chemo-selective reactions. Thus, these nanoparticles preferentially reduce the C=C olefinic bond in α,β-unsaturated ketones at 35 °C. However, change in particle size results in high selectivity towards C=O bond of α,β-unsaturated ketones, if an excess of solvent is used at low temperatures. A selectivity > 98 % for an unconstrained α,β-unsaturated ketone, *trans*-4-phenyl-3-penten-2-one, was observed at 0 °C. This kind of selectivity is unique for a heterogeneous catalyst especially when the C=C olefinic bond in α, β-unsaturated moiety is sterically not hindered. It was believed that such a preferential C=O bond hydrogenation in α,β-unsaturated ketones was not possible with heterogeneous catalysts.

In the last part, superparamagnetic core-shell-type Fe_3O_4/Ru nanoparticles (particle size ~ 15 nm), synthesized by co-precipitation, adsorption and reduction methods, are presented. Their catalytic efficiency for selective C=O hydrogenation in an unconstrained α,β-unsaturated ketone was evaluated using *trans*-4-phenyl-3-penten-2-one. These particles present a green and sustainable approach towards catalyst separation from the reaction mixture, as they can be efficiently separated from the reaction mixture by applying an external magnetic field.

It was the aim of this study to develop metallic ruthenium nanoparticles stabilized by mesogenic isonicotinic ester ligands, intercalated in hectorite and supported on magnetite and to evaluate their catalytic and biological potential.

Keywords

Ruthenium nanoparticles, anticancer activity, arene ruthenium complexes, supported nanoparticles, superparamagnetic nanoparticles, core-shell type nanoparticles, catalytic hydrogenation, selective hydrogenation

Mots Clés

Nanoparticules de Ruthénium, activité anti-cancéreuse, complexes arène-ruthénium, nanoparticules supportées, nanoparticules superparamagnétiques, les nanoparticules de type core-shell, l'hydrogénation catalytique, l'hydrogénation sélective

dedicated to my parents

Ahmad Khan & Saeeda Khanam

Table of Contents

1

Introduction

1.1 Historical Background

Nanoparticles are usually considered an invention of modern science, but they have a long history. Since ancient times, colloidal gold solutions were prescribed as tonics and elixirs.[1] Gold and Silver nanoparticles were often employed as pigments by roman glass makers of 4th century in order to generate glittering effect on pottery.[2] In 1857, Michael Faraday was the first to explain tentatively how metal particles affect the color of church windows. He presented a proper method to prepare deep red sols containing colloidal gold by reduction of chloroaurate solutions in a paper published in the periodical *Philosophical Transactions of the Royal Society*.[3] A recent reproduction of those preparations in Faraday's original laboratory at the Royal Institution in London showed these gold sols to contain gold nanoparticles of 3 to 30 nm in size.[4] Photography became a mature technology during 19th century, being largely dependent on the production of light-sensitive silver nanoparticles on photographic films.[5] The advent of colloidal science, however, is marked by Ostwald's seminal paper in 1907, in which he developed the relation between particle size and surface area.[6] One year later, Gustav Mae explained the color dependence of the glasses on metal size in a paper published in a German journal *Annalen der Physik* (Leipzig). As far as catalytic applications are concerned, Nord reported in a pioneering study as early as 1941 the catalytic

activity of palladium for nitrobenzene reduction to depend critically on the size of the metallic particles.[7]

A breakthrough in this area came, when the term "nanoparticles" was forged for metallic colloids in the wake of the emergence of nanotechnology, following the often-cited Feynman lecture entitled "There is plenty of room at the bottom".[8] The science of nanoparticles grew largely after the publication of Brust *et al.* in 1994, which presented a facile biphasic method to obtain 2 nm size gold nanoparticles.[9] The last two decades have seen an exponential growth in the number of publications in the nanopaticle field. Pioneered by Schmid, Bönnemann, Bradley, Chaudret, Reetz, Crooks, Astruc, Bürgi, Roucoux and others, metallic nanoparticles have received much attention in recent years, in particular with respect to catalytic applications.[10] Today, many technologies depend crucially on processes that take place on the nanometer scale. Nanohybrid materials have wide range of advance applications such as opto-electronic[11] and photovoltaic devices,[12] bioimaging and biosensors,[13] catalysis,[14] targeted drug delivery,[15] energy storage,[16] and information storage applications.[17]

1.2 Understanding Nanoparticles

In nanotechnology, a particle is defined as a small object that behaves as a whole unit in terms of its transport and properties.[18] These units have a size between 1 and 100 nanometers in at least one dimension.[19] Nanopaticles can be considered as being intermediary between atomic and bulk matter, but displaying properties different from their atomic and bulk counterparts.[20] They have unique physical properties which are often dictated by their size, shape and surface characteristics. These physical properties can be combined with chemical and biological properties of other materials usually functionalized at the surface of these nanoparticles, thus resulting in new type of hybrid materials – a domain where chemistry, physics and biology meets.[21,22]

Although metallic nanoparticles are known for almost all metals, the vast majority of publications in the field is concerned with gold nanoparticles (the "New Gold Rush"), palladium being the second metal to be extensively studied in the form of nanoparticles. Commercially, nanoparticles with different Au, Pd, Pt, Ag, Rh and Co formulations are available.[23] Ruthenium nanoparticles have been studied to a much lesser extent, and they are not commercially available so far, although ruthenium has meanwhile become the most

interesting metal for homogeneous catalysis due to the seminal work of Grubbs and of Noyori.[24]

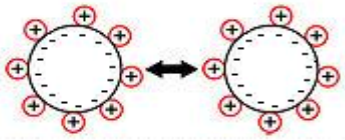

Electrostatic Stabilization[19b]

Electric charges due to ionic species on the particle surface are responsible for the repulsion between dispersed particles.

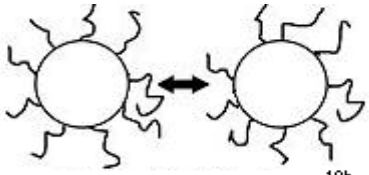

Steric Stabilization[19b]

Hydrophobic chains of the species adsorbed at the particle surface are responsible for the repulsion between particles.

Because of their small size, nanoparticles have large surface to volume ratio. They tend to aggregate into bulk metal in order to minimize their surface energy. It is, therefore, imperative to use some stabilizing agent to prevent undesired aggregation and precipitation. Stability can be obtained by surrounding the particles either with an electrical double layer (electrostatic stablization) or by using polymeric materials adsorbed or grafted at the surface (steric stablization).[19b] Thus, nanoparticles are usually stabilized by the addition of a support, a surfactant, a polymer, or an organic ligand to the reaction mixture.[19,25]

1.3 Organometallic Precursors

The past ten years have witnessed an exponential growth in the number of publications especially for supported nanoparticles with the aim of improving their activities, selectivities and mechanistic understandings.[26] Several methods are being employed for the preparation of nanoparticles which can be subdivided into physical, chemical and physicochemical routes.[27] Among these, chemical routes have been the most extensively investigated and currently include vapor deposition,[28] co-precipitation,[29] sol-gel synthesis,[22] ion adsorption,[30] deposition-precipitation,[31] electrochemical reduction,[32] immobilization and impregnation methods.[26,27]

Classical precursors for the synthesis of metallic nanoparticles are simple metal salts or complexes. In recent years, easily reducible organometallic compounds have also been used as precursors.[33] Of particular interest are water-soluble organometallics which can be

reduced in aqueous solution,[34] the most promising ones being water-soluble arene ruthenium complexes.

In 1967, the first arene ruthenium complex was synthesized by Winkhaus and Singer by the reduction of ruthenium tri-chloride hydrate ($RuCl_3 \cdot x\ H_2O$) using 1,3-cyclohexadiene in refluxing ethanol. The diamagnetic compound obtained was considered to be a polymeric material, for which the empirical formula $[RuCl_2(C_6H_6)]_n$ was proposed.[35] Later studies by Baird *et al.*[36] and by Bennett *et al.*[37] revealed that this complex had in fact a dimeric $[(C_6H_6)RuCl_2]_2$ structure, in which the two bridging chlorides connect two mononuclear $(C_6H_6)RuCl$ units, in analogy to the complexes $[(\eta^5\text{-}C_5H_5)M(\mu_2\text{-}Cl)Cl]_2$ (M = Ir, Rh) published by Maitlis in 1969.[38]

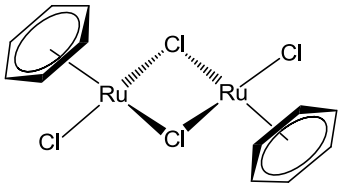

After this discovery, various arene ruthenium complexes have been synthesized during the last forty years. For example, the dimeric $[(\eta^6\text{-}p\text{-}MeC_6H_4Pr^i)Ru(\mu_2\text{-}Cl)Cl]_2$ *p*-cymene complex, a precursor being extensively used for the preparation of anticancer drugs today, was synthesized by the dehydrogenation of (-)-(α)-phellandrene using ruthenium tri-chloride hydrate in refluxing ethanol.[39] However, this method cannot be employed with the electronically rich arenes, such as hexamethylbenzene (C_6Me_6) and durene (1,2,4,5-$Me_4C_6H_2$). In such cases, the arene exchange at elevated temperatures (~ 200 °C) usually give rise to the corresponding dimeric complex.[40,41]

1.4 Stabilizing Nanoparticles

A wide variety of materials is available as support and stabilizer for controlling the growth of nanoparticles. Each support has its own advantages regarding thermal stability and selectivity.

1.4.1 Ruthenium Nanoparticles Stabilized by Organic Materials

Many methods have been developed to prepare ruthenium nanoparticles using various organic compounds as stabilizers. Even simple organic solvents[42] such as methanol[43] are reported to stabilize the ruthenium nanoparticles satisfactorily.

Polymers as Stabilizer: Functional polymers are known to be effective protective agents to stabilize ruthenium colloid solutions due to steric bulk of their framework.[44] Polymers such as poly(4-vinylpyridine),[45] polyvinylpyrrolidine,[46] cellulose derivatives[47] and optically active CO/styrene copolymer[48] are used to stabilize ruthenium nanoparticles.

Ligands as Stabilizer: Ligands usually provide steric stabilization by coordinating with the metal nanoparticles surface. Different small organic ligand molecules such as alkynes,[49] alkyl thiols,[50] alkylamines,[51] dithiocarbamates (surfactants)[52] and carbenes[53] are reported to passivate the ruthenium nanoparticles.

Organic Solvents as Stabilizer: Since ruthenium is the metal of choice for numerous catalytic applications, a clean metal surface is required.[54] Water[55] and simple organic solvents such as methanol,[42] methanol/THF mixture,[56] propanol,[42a] pentanol,[42a] heptanol[57] and polyols[54] can stabilize the ruthenium nanoparticles satisfactorily. The stabilization of the particles is believed to be due to the electrostatic repulsion that results from solvent-induced polarization of the surface.[56]

1.4.2 Ruthenium Nanoparticles Stabilized by Inorganic Materials

Among the range of solid supports available these days, carbonaceous materials, polymers and inorganic metal oxides are the three main families of solid supports being extensively used for the preparation of supported metallic nanoparticles.[58]

Inorganic Salts and Minerals as Stabilizers: Water-soluble nanoparticles are desired for several applications. In this case, electrostatic stabilization by cations[55] or by anions is an interesting alternative.[59-61] Different inorganic salts such as sodium acetate trihydrate[50a] and inorganic minerals, for example hydroxylapatit,[59] are reported in the literature to stabilize the ruthenium nanoparticles effectively.

Ionic Liquids as Stabilizers: These are liquid salts which usually have melting point below 100 °C. Their intrinsic ionic charge and polymeric nature provide a unique electronic and steric protection for metal nanoparticles.[62] Ionic liquids, in particular those based on imidazolium cation,[63] are emerging as alternative liquid templates for the generation and stabilization of ruthenium nanoparticles.[62,64]

Carbonaceous Materials: Carbonaceous materials are known to be an ideal material for nanoparticles support/stabilization due to their nano-scale size, high surface to volume ratio

and chemical stability.[65] Therefore, different carbonaceous materials such as charcoal,[66] carbon nanofibers,[58,67] carbon nanotubes (CNT),[68] MgO-CNT,[69] multiwalled carbon nanotubes (MWCNT)[70] have been quoted in the literature for the passivation of ruthenium nanoparticles.

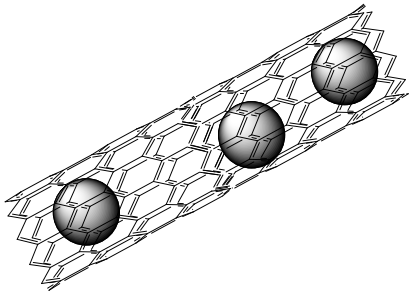

Figure 1. Nanoparticles stabilized inside carbon nanotubes.

Inorganic Metal Oxides: Inorganic oxides are used as both host and stabilizer of nanoparticles. Uptill now, many inorganic oxides such as Al_2O_3,[71] titanated-Al_2O_3,[72] TiO_2,[73] SiO_2,[74] Y_2O_3,[75] CeO_2,[76] and MgO[77] have been employed for the support and stabilization of nano-ruthenium. Of particular interest are microporous and mesoporous materials such as silicas (e.g. SBA-15) and faujasite zeolites in which caging effect help to limit the growth of ruthenium nanoparticles inside these pourous materials.[78]

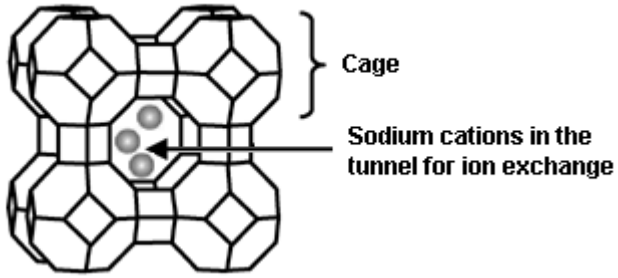

Figure 2. Zeolite cage structure which shows tunnels containing sodium cations for ion exchange. These tunnels help to control the growth of nanoparticles.[78]

Layered clays are alumino-silicate materials. They are relatively less explored as supports but are believed to have significant potential due to soft dimensional constraints.[79] They possess an exceptional swelling property (up to 35x for hectorite) in aqueous medium. The expanded interlayer space facilitates the introduction of water soluble organometallic complexes by cation exchange, thus resulting in heterogenisation of a homogeneous

catalyst.[80] Ruthenium nanoparticles intercalated in montmorillonite[81] and hectorite[34] are reported in the literature for different catalytic applications.

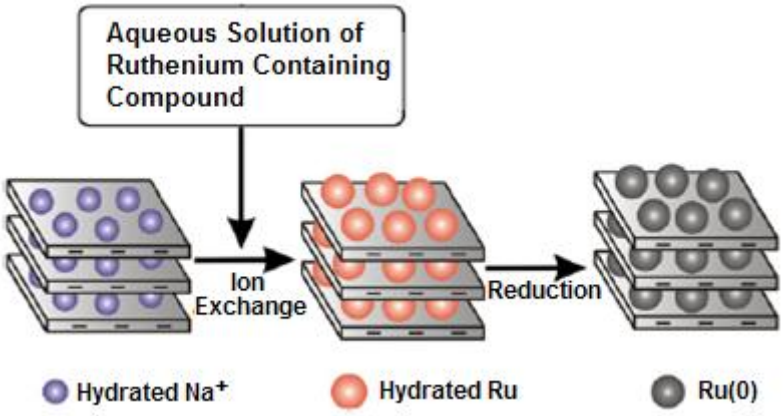

Figure 3. Preparation of ruthenium nanoparticles in layered clays.[79]

1.4.3 Ruthenium Nanoparticles on Magnetite Cores

Recently, the use of magnetic materials as catalyst support has attracted much attention,[82] because solid catalysts with magnetic properties can efficiently be separated from the reaction mixture by applying an external magnetic field.[83] This green and sustainable approach has many advantages, since it is a fast, economical and environmentally acceptable way of product separation and catalyst recycling.[84]

Magnetic nanoparticles mainly of Fe_3O_4, γ-Fe_2O_3 or Co have been widely studied, especially for medical diagnostics, magnetic hyperthermia treatment, imaging and data storage;[85] magnetically separable materials have also found catalytic applications.[86] While silica-coated Fe_3O_4 nanoparticles decorated with metallic palladium (nanoPd@Fe_3O_4) have been synthesized and reported to catalyze the hydrogenation of cyclohexene to cyclohexane,[87] for ruthenium only ruthenium complexes supported on Fe_3O_4 are known: [Ru(binap´)(dpen)-Cl_2] bound to Fe_3O_4 (binap´ = (*R*)-2,2´-bis(diphenylphosphino)-1,1´-binaphthyl-4phosphonic acid, dpen = (*R*,*R*)-1,2diphenylethylenediamine) as a catalyst for the asymmetric hydrogenation of ketones[88] and [$Ru(OH)_x$] supported on Fe_3O_4 as a catalyst for the hydration of nitriles to amides.[89] So far, magnetically recoverable metallic ruthenium is only known to be supported by $NiFe_2O_4$ nanoparticles, which catalyze the hydrogenation of alkynes to

alkanes.[90] Despite the interesting catalytic potential to be expected from such a material, Fe_3O_4 nanoparticles decorated with metallic ruthenium (nanoRu@Fe_3O_4) have never been reported to the best of our knowledge. The easy separability of magnetic nanoparticles from a reaction mixture by means of an external magnet makes nanoRu@Fe_3O_4 an interesting material for catalytic transformations.

1.5 Aim of this Work

Nano-sized molecular materials have raised much interest because of their unique properties and their potential applications. For such materials, functional qualities such as anticancer, magnetic or catalytic properties can be introduced by transition metals, while the self-organization and stabilization can be induced by mesogenic ligands.

In our case, we decided to use long-chain isonicotinic ester ligands, which usually have mesogenic properties.[91] Isonicotinic acid is widely used for the synthesis of antibiotics and antituberculosis preparations,[92] and it has strong bactericide effects.[93] We have been interested in the use of long-chain isonicotinic esters as lipohilic components in order to increase the anticancer activity of arene ruthenium complexes, while at the same time, using them as stabilizer for ruthenium nanoparticles with the aim of exploring self-organization and biological (anticancer) properties of these new hybrid materials.

Developing green chemical transformations to reduce waste in liquid phase organic reactions is a major challenge today. Heterogeneous catalysts are considered clean technologies because they help minimize consumption of energy and raw materials used in the synthesis. Layered clays are relatively less explored as supports but are believed to have significant potential in organic chemical processing due to soft dimensional constraints.[94] Clays possess an exceptional swelling properties (up to 35 times for hectorite) in aqueous medium. The expanded interlayer space facilitates the introduction of catalytically active arene ruthenium complexes by cation exchange, thus resulting in heterogenisation of a homogeneous catalyst. This approach has many benefits i.e. easily tunable catalyst with low cost, high activity and selectivity and the ease with which reactions are carried out.[79] We have been interested in using arene ruthenium complexes intercalated in hectorite as a precursor for size- and shape-selective preparation of ruthenium nanoparticles and their possible catalytic potential in hydrogenation reactions.

Based on the experience gained from hectorite-supported nano-ruthenium and on well established procedures to make magnetite nanoparticles by co-precipitation from aqueous solutions of Fe^{2+} and Fe^{3+} salts[95] using the Massart method,[96] we have been interested in developing ruthenium-coated magnetite (core-shell type) nanoparticles by the aqueous organometallic route. The easy separability of magnetic nanoparticles from a reaction mixture by means of an external magnet makes nanoRu@Fe_3O_4 an interesting material for catalytic transformations.

It was, therefore, the aim of this study to develop metallic ruthenium nanoparticles stabilized by mesogenic isonicotinic ester ligands, intercalated in hectorite and supported on magnetite for catalytic and biological applications.

2

Ruthenium Nanoparticles Stabilized by Mesogenic Ligands

2.1 State of the Art

Arene ruthenium complexes containing chloro ligands are both lipophilic and water-soluble, which preconditions these organometallics for bio-medical applications such as anticancer agents.[97] The field of antitumoural and antimetastatic arene ruthenium complexes has, in recent years, received considerable attention,[98,99] following the notion of using arene ruthenium compounds as anticancer agents by Tocher *et al.* in 1992, who observed a cytotoxicity enhancement by coordinating the anticancer agent metronidazole [1-β-(hydroxyethyl)-2-methyl-5-nitro-imidazole] to a benzene ruthenium dichloro fragment.[100] Later on, two prototype arene ruthenium(II) complexes were evaluated in 2001 for anticancer properties *viz.* (*p*-$MeC_6H_4Pr^i$)Ru(P-pta)Cl_2 (pta = 1,3,5-triaza-7-phospha-tricyclo-[3.3.1.1]decane), termed RAPTA-C,[101] and [(C_6H_5Ph)Ru(*N*,*N*-en)Cl][PF_6] (en = 1,2-ethylenediamine).[102]

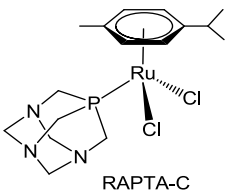

RAPTA-C

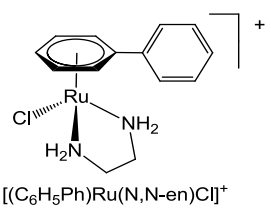

[(C_6H_5Ph)Ru(N,N-en)Cl]$^+$

Isonicotinic acid is widely used for the synthesis of antibiotics and antituberculosis preparations,[92] and it has strong bactericidal effects.[93] We have been interested in the use of long-chain isonicotinic esters as lipohilic components in order to increase the anticancer activity of arene ruthenium complexes, while at the same time, using a molecule that is known to be tolerated *in vivo*.

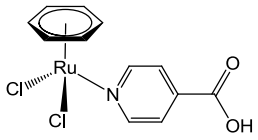

Only one arene ruthenium complex containing isonicotinic acid has been reported so far, namely $[(C_6H_6)Ru(NC_5H_4COOH)Cl_2]$ by J. G. Małecki *et al.*,[103] but the biological properties of the complex were not studied. The long-chain isonicotinic ester ligands also have mesogenic properties. Several metallomesogens have already been reported by using these ligands.[91]

Nanoparticles are finding increasing application in medicinal chemistry being used as drug delivery agents, in photodynamic therapy, as luminescent imaging agents and magnetic imaging agents. In particular, the selective accumulation of nanoparticles in tumor tissue through the enhanced permeability and retention effect, and tunable physical and chemical properties, are attractive properties for such applications.[104] The "enhanced permeability and retention" (EPR) effect is a phenomenon in which macromolecules are able to accumulate at the tumor site due to the dramatic increase in blood vessel permeability within diseased tissues compared to normal tissues.[105] Ruthenium based lipovectors that assemble to form lamellar vesicles have already been reported.[106] In this section, we describe the synthesis and characterization of arene ruthenium complexes of the type "piano-stool" containing long-chain isonicotinic ester ligands and of ruthenium nanoparticles stabilized by these ligands. It should be noted that, while most attention has been focused towards mononuclear arene ruthenium anticancer compounds,[98,99,107] there has been increasing interest in polynuclear complexes,[108] including clusters,[109] which also display excellent pharmacological properties.

2.2 Long-Chain Isonicotinic Ester Ligand-Containing Arene Ruthenium Complexes and Nanoparticles

2.2.1 Synthesis of Alkylated Long-Chain Isonicotinic Ester Ligands

Promesogenic long-chain *N*-ligands of type NC_5H_4-4-COO-C_6H_4-4-O-C_nH_{2n+1} derived from isonicotinic acid were synthesized using a four-step method. Alkyl bromide reacts with benzyl hydroquinone to give an ether according to Williamson's etherification[110] (Step 1). The benzyl group can be removed[111] using Pd/C under 4 bar H_2 pressure at room temperature to produce an alcohol (Step 2).

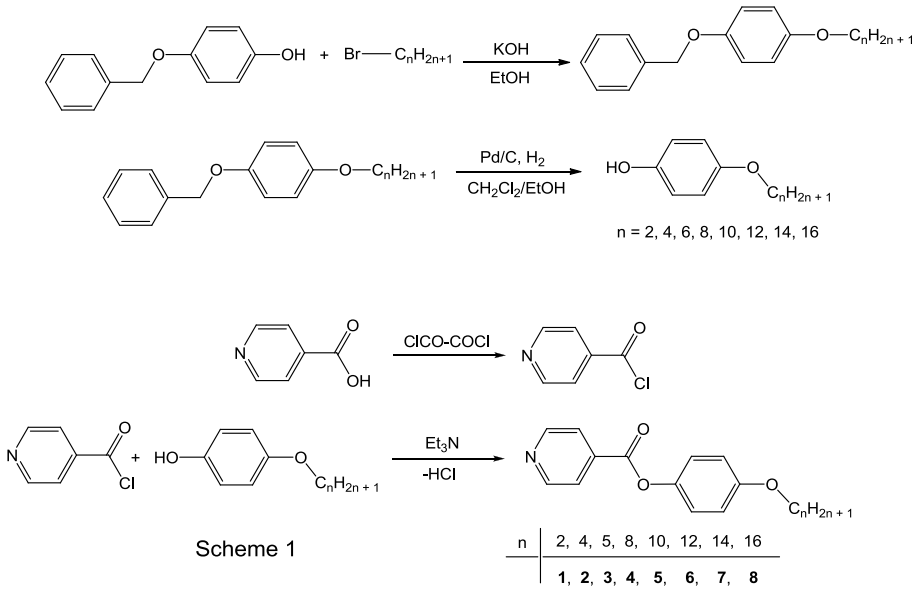

Scheme 1

Isonicotinic acid is transformed into the corresponding acyl chloride (Step 3) by oxalyl chloride,[112] in order to facilitate the nucleophilic substitution with the alcohol to give the esters[113] **1 – 8**. The reaction is done in the presence of triethylamine to bind the eliminated HCl. Alkylated long-chain isonicotinic ester ligand **4** is a new organic compound, the characterization of which is presented in the Experimental Part.

2.2.2 Alkylated Long-Chain Isonicotinic Ester Ligand-Containing Arene Ruthenium Complexes

The dinuclear complexes $[(C_6H_6)RuCl_2]_2$, $[(p\text{-}MeC_6H_4Pr^i)RuCl_2]_2$ and $[(C_6Me_6)RuCl_2]_2$ react in dichloromethane with 2 equivalents of the isonicotinic ester ligands **1** – **8** to give the neutral complexes [(arene)Ru(L)Cl_2] (**9** – **18**) in quantitative yield, see

Scheme 2. All the complexes are obtained as air-stable yellow to yellow/brown powders, which are soluble in polar organic solvents, in particular in dichloromethane and chloroform. The complexes are also sparingly soluble in water.

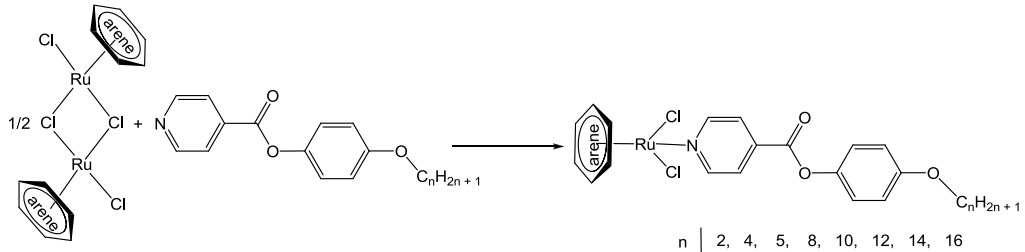

Scheme 2

	n	2,	4,	5,	8,	10,	12,	14,	16
arene	C_6H_6	-	-	-	-	**13**	-	-	-
	p-$MeC_6H_4Pr^i$	**9**,	**10**,	**11**,	**12**,	**14**,	**16**,	**17**,	**18**
	C_6Me_6	-	-	-	-	**15**	-	-	-

X-Ray Structural Analysis of ***9***

Suitable orange crystals of **9** were obtained by slow evaporation of a methylene chloride solution. This compound crystallizes in the monoclinic centrosymmetric space group $P2_1/c$. The structure of this complex is pseudo-tetrahedral having "piano stool" like arrangement in which a ruthenium atom is coordinated to the *p*-$MeC_6H_4Pr^i$ ligand, a nitrogen atom and two chloro ligands. The molecular structure of **9** is shown in Fig. 4. Characteristic distances and angles are summarized in Table 1.

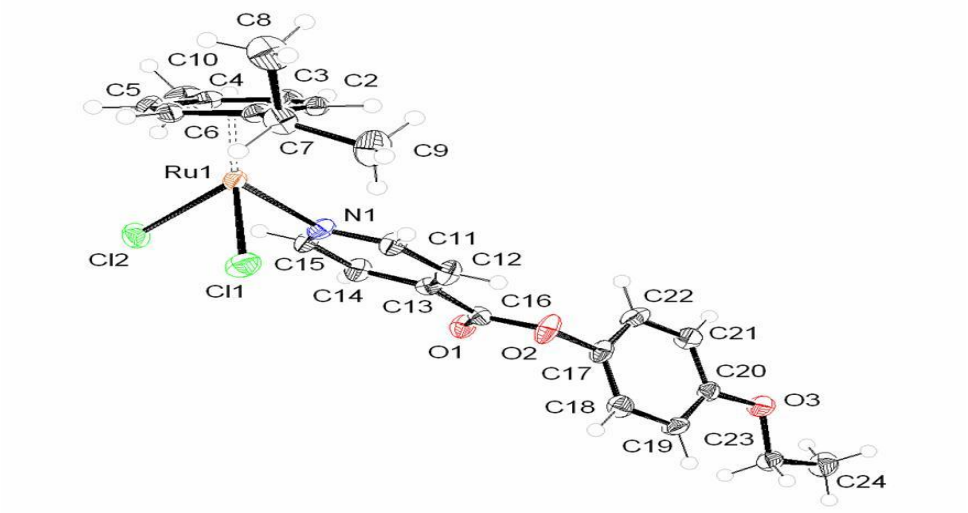

Figure 4. ORTEP diagram of complex **9** with 50% probability thermal ellipsoids

Table 1. Selected bond lengths (Å) and angles (°) for **9**

Bond lengths (Å)		Angles (°)	
Ru(1)-N(1)	2.142(3)	Cl(1)-Ru(1)-N(1)	128.59(14)
Ru(1)-C(1)	2.216(4)	Cl(2)-Ru(1)-N(1)	86.13(9)
Ru(1)-C(2)	2.181(4)	Cl(1)-Ru(1)-Cl(2)	88.02(4)
Ru(1)-C(3)	2.144(5)		
Ru(1)-C(4)	2.177(4)		
Ru(1)-C(5)	2.153(4)		
Ru(1)-C(6)	2.188(4)		
Ru(1)-Cl(1)	2.4251(12)		
Ru(1)-Cl(2)	2.3934(11)		

Silver salts such as Ag_2SO_4 in aqueous or $AgCF_3SO_3$ in organic medium are usually employed to remove chloro ligands as chloride anions from arene ruthenium complexes to give the corresponding aqua complexes. In the case of the neutral complexes [(arene)Ru(L)Cl_2] containing the long-chain *N*-ligand L = **5**, the removal of both chlorides results in the precipitation of the free isonicotinic ester ligand (Scheme 3). The triaqua arene ruthenium complexes **19** – **21** can then be isolated as sulfate salts after filtration from the reaction mixture.

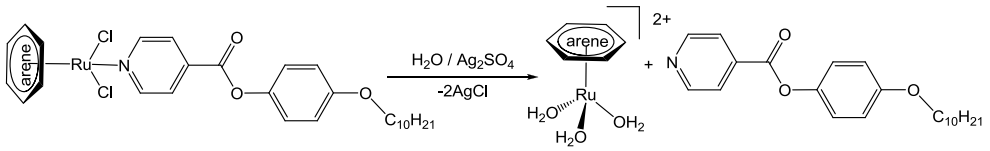

Scheme 3

	arene
19	C_6H_6
20	*p*-$MeC_6H_4Pr^i$
21	C_6Me_6

On the other hand, it is possible to remove only one chloro ligand as silver chloride from the neutral complexes [(arene)Ru(L)Cl_2] and to coordinate a second isonicotinic ester ligand **5**. This reaction yields the cationic complexes **22** – **23**, which can be isolated as triflate salts (Scheme 4). In the ^{1}H NMR spectra of complex **22**, the signals for the α-protons in the pyridine ring appear at higher field as the signals of the corresponding protons in **13**. However, for complexes **23 – 24**, these signals appear at lower field as the signals of the

corresponding protons in **14 – 15**. Moreover, the benzene signal in **22** is shifted low field with respect to the one in **13**.

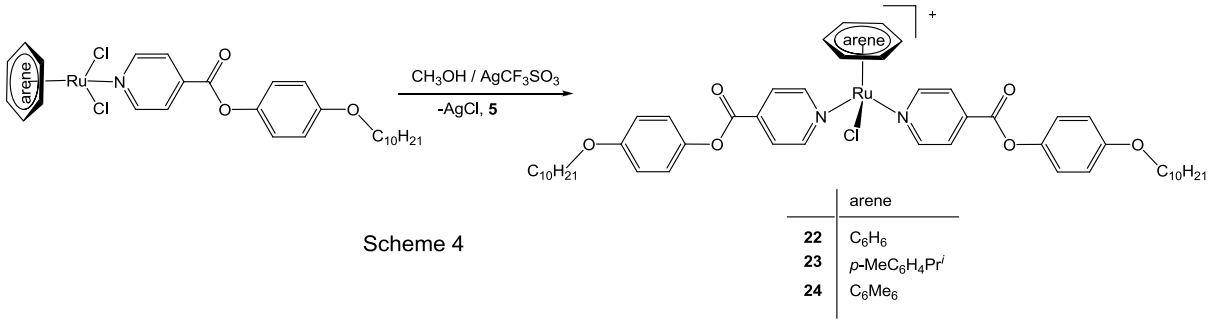

	arene
22	C_6H_6
23	*p*-$MeC_6H_4Pr^i$
24	C_6Me_6

Scheme 4

2.2.3 Preparation of Nanoparticles from Alkylated Long-Chain Isonicotinic Ester Ligand-Containing Arene Ruthenium Complexes

When an ethanol solution of **13** (5mg, 5mL) is stirred for 14 h under hydrogen (50 bar) at 100 °C, a black material **25** is obtained. This material can be purified by centrifugation and washing with dichloromethane. The ^{1}H NMR shows that isonicontinic ester ligand has been hydrogenated. The TEM analysis reveals the presence of aggregated Ru(0) particles having particle size of 3 nm. Selected-area-electron-diffraction of the sample shows that these particles are crystalline in nature. On the other hand, the complexes **14** and **15** are not reduced under these conditions; they give dark red or yellow solutions respectively.

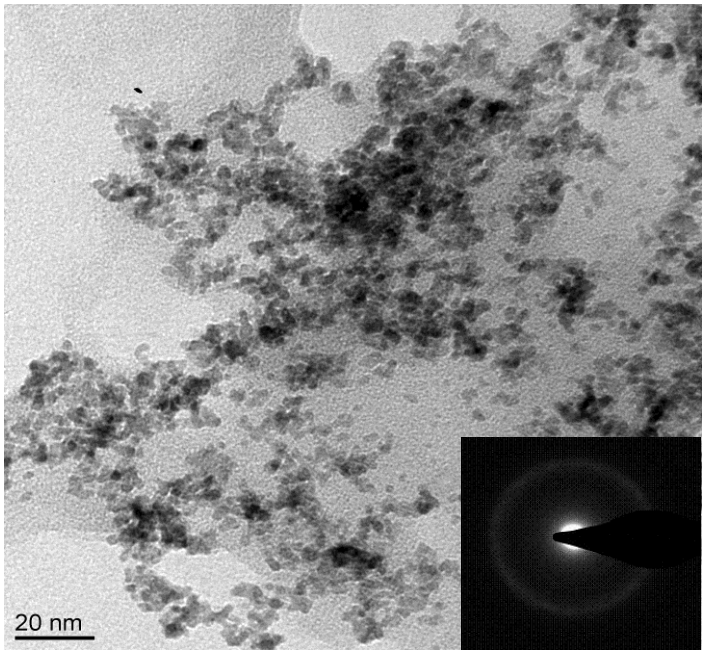

Figure 5. TEM micrograph and SAED analysis (inset) of ruthenium nanoparticles **25**

2.2.4 Preparation of Nanoparticles from Triaqua Arene Ruthenium Complexes Stabilized by Alkylated Long-Chain Isonicotinic Ester Ligands

Evaluation of Reduction Potential of Triaqua Arene Ruthenium Complexes

Ruthenium nanoparticles are known to show no interaction with light during UV-Vis spectroscopy.[114] This behavior of Ru(0) can be used to evaluate the reduction potential of different triaqua arene ruthenium complexes. In the absence of stabilizing agent, the triaqua benzene complexe $[(C_6H_6)Ru(H_2O)_3]^{2+}$ (**19**) is reduced to black Ru(0) precipitates at 90 °C under a pressure of 50 bar H_2. The dispersion thus obtained shows almost no interaction with light in UV-Vis spectroscopy. The analogues $[(p\text{-}MeC_6H_4Pr^i)Ru(H_2O)_3]^{2+}$ (**20**) and $[(C_6Me_6)Ru(H_2O)_3]^{2+}$ (**21**) give a lustrous metallic ruthenium surface on the walls of the glass tube upon reduction with hydrogen (50 bar) at higher temperatures (> 90 °C).

*Preparation of the Ruthenium Nanoparticles (**26** - **29**)*

The Ru nanoparticles **26** stabilized by ligand **5**, are prepared by reducing complex **13** (5 mg, 8.26 x 10^{-3} mmol) under solvent-free conditions in a magnetically stirred stainless-steel autoclave (volume 100 mL) with H_2 (50 bar) at 100 ˚C for 16 h.

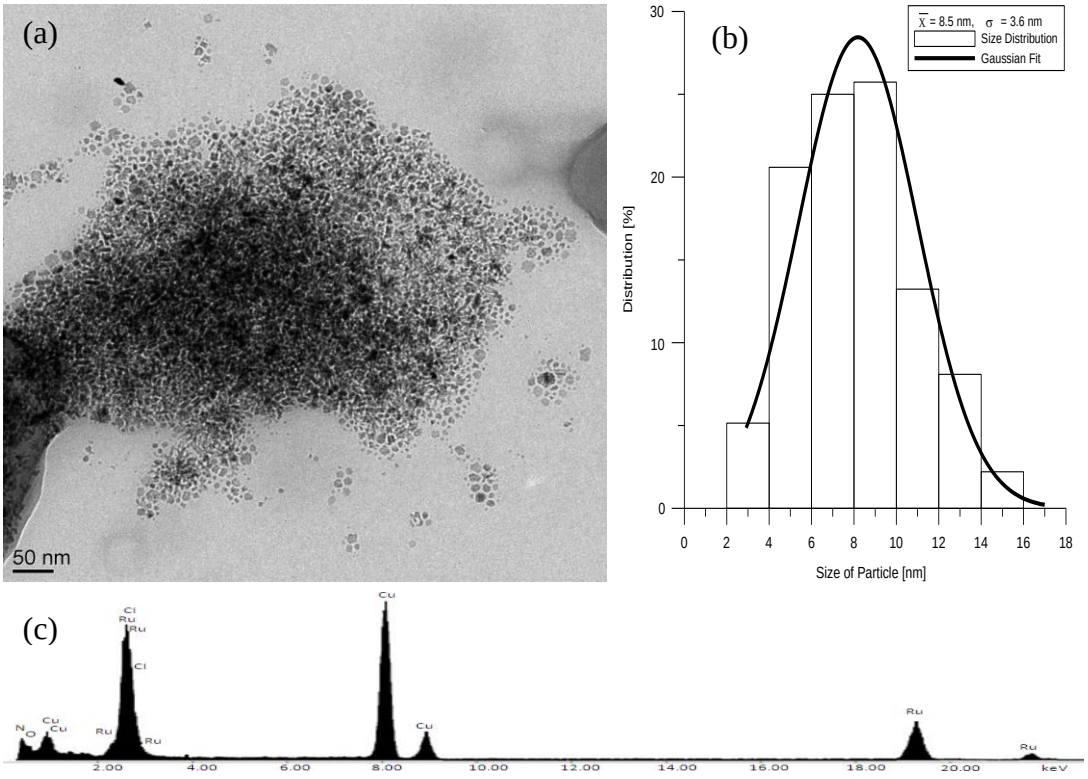

Figure 6. TEM micrograph (**a**) histogram (**b**) and EDAX analysis (**c**) of ruthenium nanoparticles **26**

Alternatively, the **5** stabilized Ru nanoparticles **27 – 29** are obtained by reacting 5 mg of [(arene)Ru(H_2O)$_3$]SO_4 (**27**: arene = C_6H_6; **28**: arene = *p*-MeC_6H_4Pr^i; **29**: arene = C_6Me_6) with one equivalent of **5** in absolute ethanol (1 mL) in a magnetically stirred stainless-steel autoclave (volume 100 mL) under a 50 bar pressure of H_2 at 100 ˚C for 14 h. After pressure release, the solvent was removed and the nanoparticles were dried *in vacuo*. The characterization of the nanoparticles **27 – 29** is presented in Fig. 6 – 9. The size distribution of the ruthenium(0) nanoparticles was studied by transmission electron microscopy (TEM) using the "ImageJ" software[115] for image processing and analysis. The mean particle size was estimated from image analysis of *ca.* 100 particles at least.

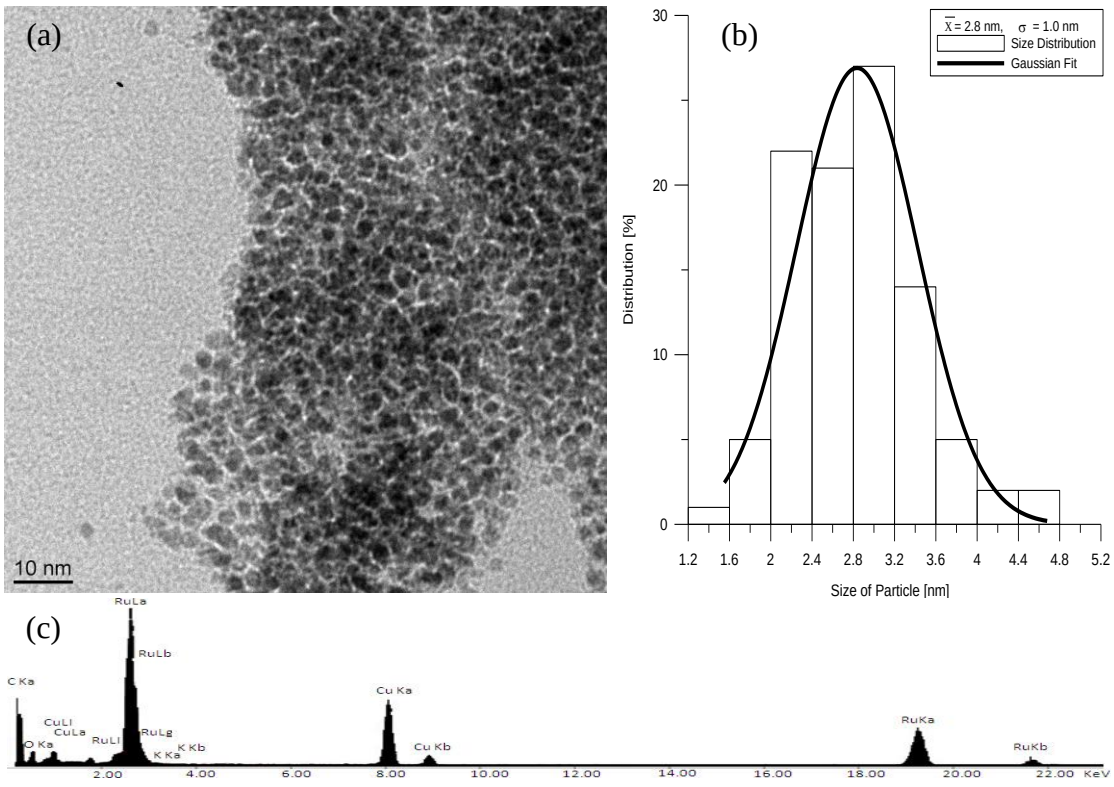

Figure 7. TEM micrograph (**a**) histogram (**b**) and EDAX analysis (**c**) of ruthenium nanoparticles **27**

The solventless reduction of solid **13** with H_2 (50 bar, 50 °C) gives ruthenium nanoparticles **26** stabilized by the isonicotinic ester ligand **5**, which have a mean particle size of 8.5 nm (established by TEM). The size distribution of these nanoscopic ruthenium particles (2 – 16 nm) is relatively large. Smaller ruthenium nanoparticles stabilized by the isonicotinic ester ligand **5** are obtained by reducing

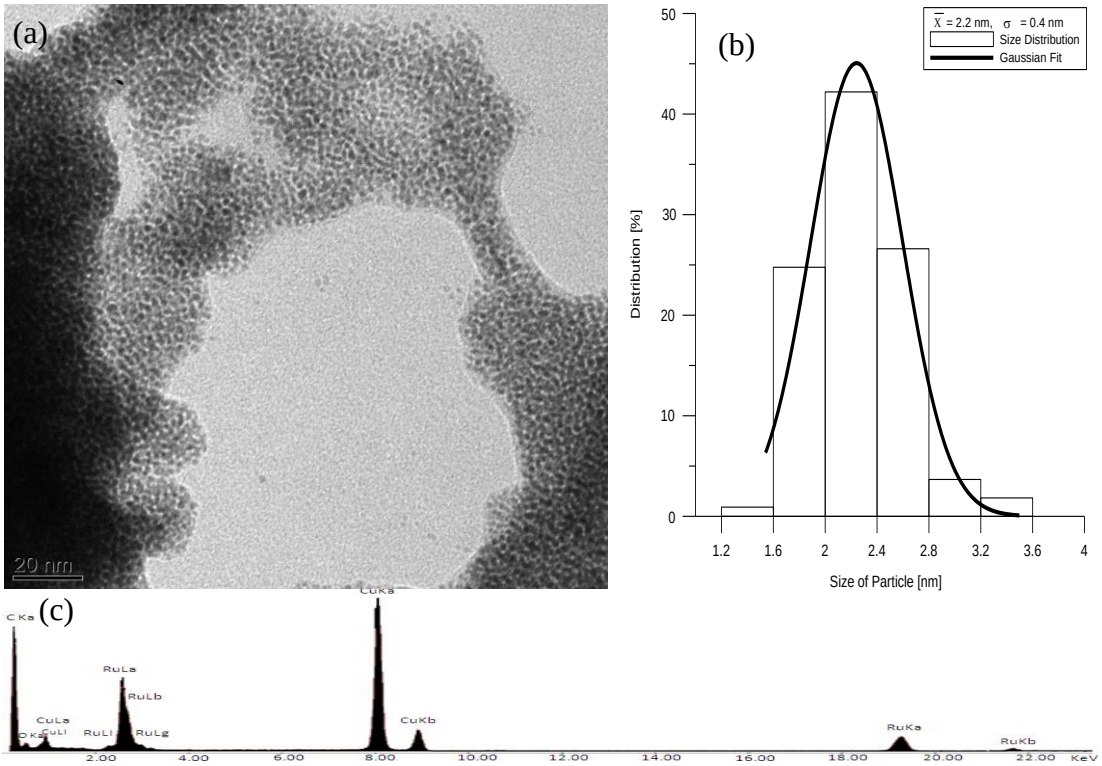

Figure 8. TEM micrograph (**a**) histogram (**b**) and EDAX analysis (**c**) of ruthenium nanoparticles **28**

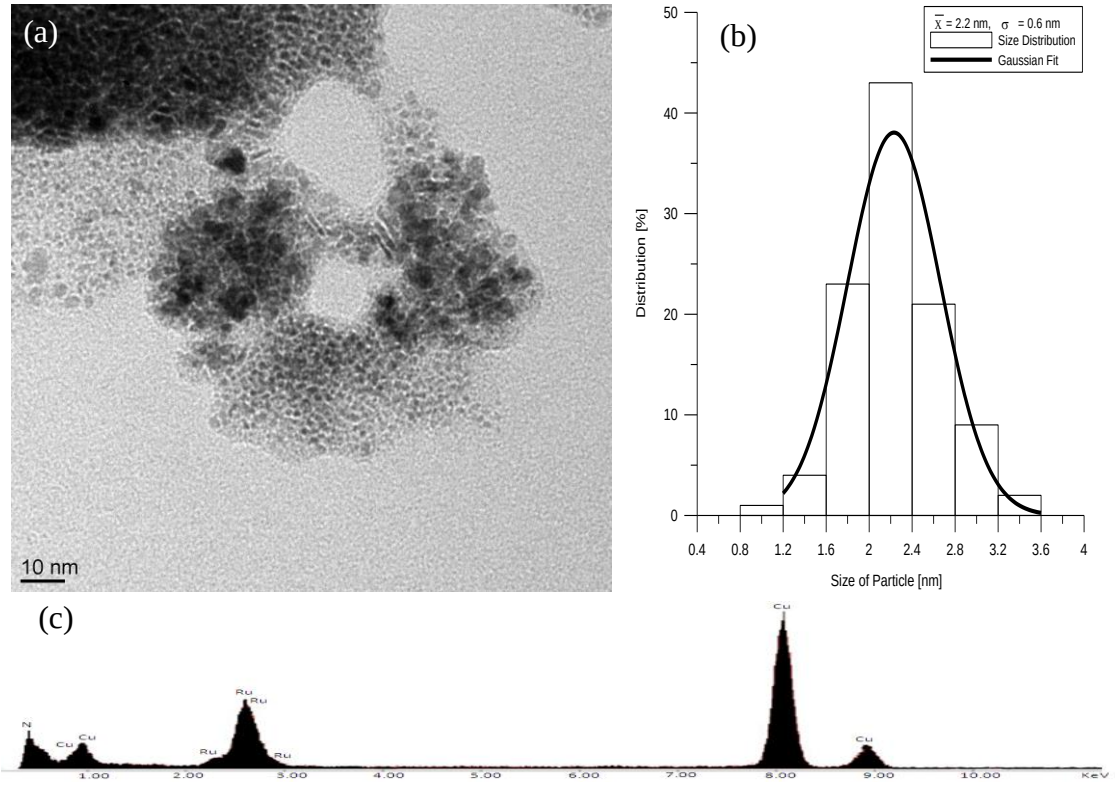

Figure 9. TEM micrograph (**a**) histogram (**b**) and EDAX analysis (**c**) of ruthenium nanoparticles **29**

[(arene)Ru(H_2O)$_3$]SO_4 in ethanol at 100 °C with molecular hydrogen (50 bar) in the presence of **5** (1 equivalent): The ruthenium nanoparticles **27** obtained from [(C_6H_6)Ru(H_2O)$_3$]SO_4 have a mean particle size of 2.8 nm, the Ru nanoparticles **28** obtained from [(*p*-$MeC_6H_4Pr^i$)Ru(H_2O)$_3$]SO_4 have a mean particle size of 2.3 nm, and the Ru nanoparticles **29** obtained from [(C_6Me_6)Ru(H_2O)$_3$]SO_4 have a mean particle size of 2.2 nm. The ^{1}H NMR spectra of **26** – **29** in $CDCl_3$ show the presence of the ligand **5**, the signals of the pyridine ring being weak.

2.2.5 Alkylated Long-Chain Isonicotinic Ester Ligand Exchange on Pyridine-Stabilized Nanoparticles

In recent years, the preparation of nanoparticles having a clean surface state has attracted much attention due to their potential applications.[42,54-56] We have been able to prepare well dispersed bare-surface ruthenium nanoparticles, avoiding traditional protective agents, with the aim of using these particles for ligand exchange at their surface and prepare a new series of hybrid materials.

When an ethanol solution of **20** (5mg, 5mL) containing one equivalent of pyridine is stirred for 14 h under hydrogen (50 bar) at 100 °C, a brownish black material **30** is obtained.

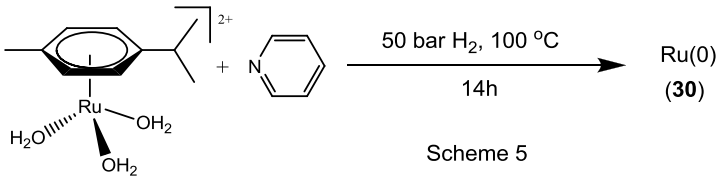

Scheme 5

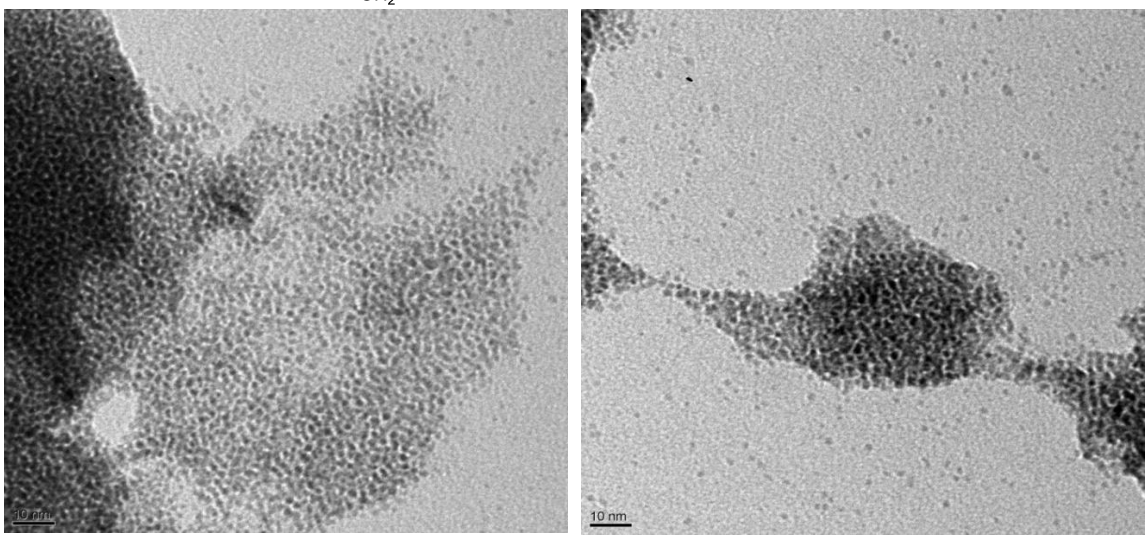

Figure 10. TEM micrograph of ruthenium nanoparticles **30**

The ^{1}H NMR spectrum of **30** shows the presence of piperidine (reduced pyridine) at the surface of these particles. TEM analysis reveals the presence of well dispersed Ru(0) having particles size of 2 nm.

When an ethanol solution of **19** (5mg, 5mL) containing one equivalent of pyridine is stirred for 14 h under hydrogen (50 bar) at 100 °C, a black material **31** is obtained. The TEM analysis reveals the presence of rather aggregated ruthenium nanoparticles. If the solvent is removed by evaporation and **31** is dried overnight under vacuum (~ 10^{-2} mbar), these nanoparticles burn in the air. This shows that **31** has clean metal surface, probably due to absolute removal of protective agents under high vacuum.

When an ethanol solution of **31** is stirred overnight after adding one equivalent of **5** dissolved in CH_2Cl_2, the piperidine ligand at the surface is exchanged against the long-chain isonicotinic ester ligand **5**, to give **32**. Thermogravimetric analysis of **32** shows the presence of 2.3% of **5** at the surface of these nanoparticles.

2.2.6 Catalytic Properties of Long-Chain Isonicotinic Ester Ligand-Stabilized and Pyridine-Stabilized Ruthenium Nanoparticles

*Hydrogenation of Arenes Catalyzed by **27** and **30***

The ruthenium nanoparticles **27** (stabilized by the long-chain isonicotinic ester ligand **5**) and **30** (stabilized by piperidine) efficiently catalyse the hydrogenation of arenes (5 mL) under a hydrogen pressure of 50 bar at 50˚C using ethanol (5 mL) as solvent. After a 15 bar decrease in pressure, the reaction is quenched in an ice bath, and the product was decanted off and analyzed by ^{1}H NMR spectroscopy.

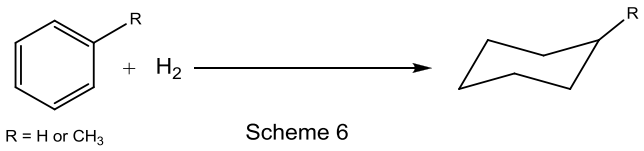

Scheme 6

Table 2. Catalytic hydrogenation of arenes using **27** and **30** in ethanol

Catalyst	Substrate	Reaction time (h)	Conversion (%)	Activity TOF (h^{-1})[a]
27	Benzene	12.6	49	170
30	Benzene	1.3	29	979
27	Toluene	18	57	116
30	Toluene	61.7	17	28

[a]TOF, turnover frequency was calculated as moles of converted benzene per mol Ru per hour

It can be seen (Table 2) that the piperidine-stabilized ruthenium nanoparticles **30** are more active than the long-chain isonicotinic stabilized ruthenium nanoparticles **27** for the hydrogenation of benzene.

*Selective C=C Hydrogenation of α,β-Unsaturated Ketones Catalyzed by **30***

The ruthenium nanoparticles **30** (stabilized by piperidine) catalyze the selective hydrogenation of 3-butene-2-one under a hydrogen pressure of 5 bar at 35°C using ethanol as solvent. These nanoparticles exclusively hydrogenate the olefinic C=C bond in the substrate.

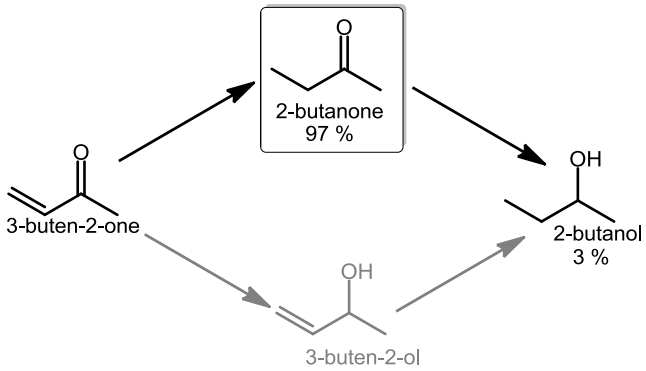

Scheme 7. Selective hydrogenation of 3-butene-2-one catalyzed by **30**

2.2.7 Anticancer Properties of Long-Chain Isonicotinic Ester Ligands, their Arene Ruthenium Complexes and Nanoparticles

The *in vitro* cytotoxicity of long-chain isonicotinic ester ligands (**1** – **8**), complexes **(9** – **21)** and their nanoparticles **(26 – 29)** has been studied in the A2780 ovarian cancer cell line and cisplatin resistant variant A2780cisR using the MTT assay. The monomeric dichloro complexes **13** – **15** of ligand **5** exhibit a very high cytotoxicity in cancer cell lines, A2780 and the cisplatin resistant cell line A2780cisR. In particular, the benzene and *p*-cymene complexes **13** – **14** have IC_{50} values equivalent to cisplatin in the A2780 line (1.6 μM) and are 2-3 times more active in the A2780cisR cell line.[116]

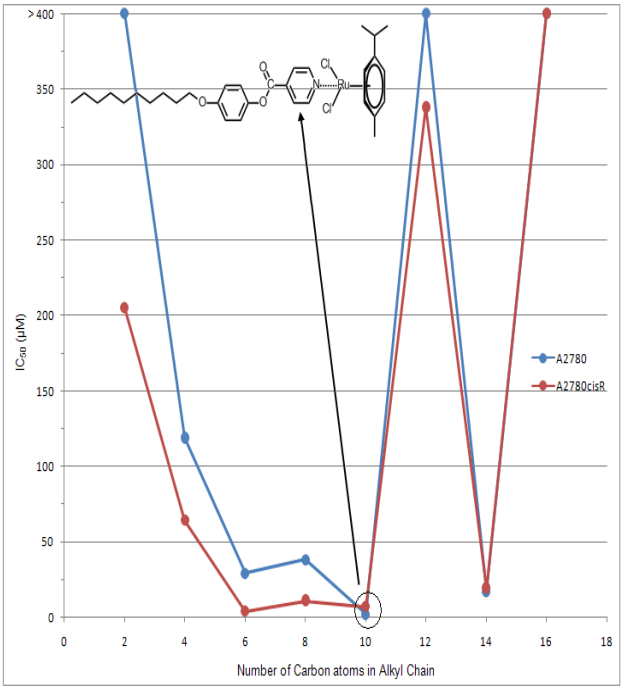

Compound	A2780 IC_{50} [μM]	A2780cisR IC_{50} [μM]
9	>400	205
10	119	64
11	29	4
12	38	11
13	3	10
14	2	7
15	29	28
16	>400	338
17	17	19.3
18	>400	>400
cisplatin[116]	1.6	8.6

Figure 11. Cytotoxicity values of arene ruthenium complexes **9 – 18** containing long chain isonicotinic ester ligands and the graphical representation of carbon atom chain length effect in para-cymene derived complexes on IC_{50} values

Interestingly, the analogous pyridine complex [(*p*-$MeC_6H_4Pr^i$)Ru(py)Cl_2] is essentially inactive (IC_{50} = 750 μM) under comparable conditions in these cancer cell lines,[117] suggesting that the cytotoxicity of these complexes may be due to the long-chain isonicotinic ester group. This is supported by the very low IC_{50} values observed for the free ligands (Fig. 12).

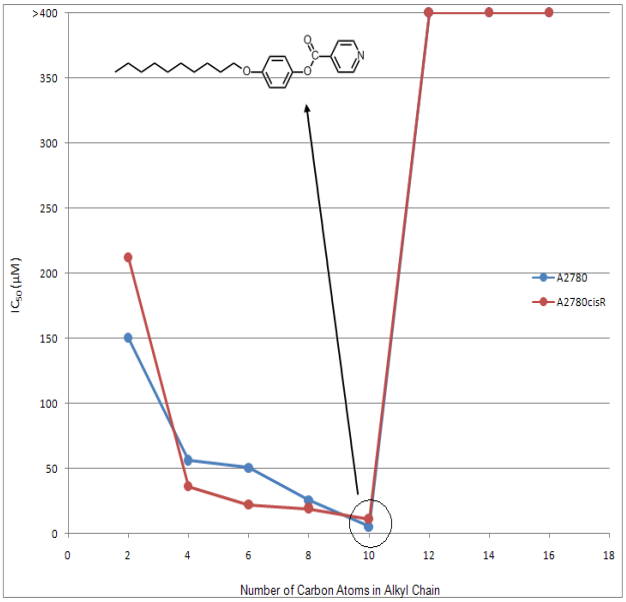

Compound	A2780 IC_{50} [μM]	A2780cisR IC_{50} [μM]
1	150	212
2	56	36
3	50	22
4	25	19
5	5	11
6	>400	>400
7	>400	>400
8	>400	>400

Figure 12. Cytotoxicity values of long chain isonicotinic ester ligands **1 – 8** and the graphical representation of carbon atom chain length effect in these ligands on IC_{50} values

By contrast, the triaqua arene ruthenium complexes **19 – 21** are much less cytotoxic in spite of their good solubility in water as sulfate salts (see Table 3).

Table 3. Cytotoxicity values of triaqua arene ruthenium complexes **19 – 21**

Compound	A2780 IC_{50} [μM]	A2780cisR IC_{50} [μM]
19	>200	-
20	>200	-
21	74	-

The **5**-stabilized Ru nanoparticles **26** – **29**, also exhibit a moderate cytotoxicity in the ovarian cancer cell line A2780, with the exception of *p*-cymene-derived system **28,** which was unusually inactive (Table 4) probably due to their insolubility in water and DMSO. For the other compounds, the size of the nanoparticles and the nature of the ligands in the precursor complex appear to have little effect on the cytotoxicity, all three compounds exhibiting similar IC_{50} values (29 - 39 μM). It seems probable that the

isonicotinic ester ligand **5** is important for the *in vitro* activity of the complexes, given that the free ligand is so cytotoxic.

Table 4. Cytotoxicity values of ruthenium nanoparticles **26 – 29**

Compound	A2780 IC_{50} [µM]	A2780cisR IC_{50} [µM]
26	29	-
27	34	-
28	>200	-
29	39	-

2.3 Cyanobiphenylic Long-Chain Isonicotinic Ester Ligand-Containing Arene Ruthenium Complexes and Nanoparticles

2.3.1 Synthesis of a Cyanobiphenyl-Containing Long-Chain Isonicotinic Ester Ligand and its Arene Ruthenium Complexes

The mesogenic long-chain *N*-ligand NC_5H_4-4-COO-$(CH_2)_{10}$-O-C_6H_4-4-COO-C_6H_4-4-C_6H_4-4-CN (**32**), derived from isonicotinic acid, is synthesized by reacting isonicotinoyl chloride hydrochloride with 4'-cyanobiphenyl-4-yl-4-(10-hydroxydecyloxy)benzoate using triethylamine to facilitate the esterification process. The reaction gives **32** in high yield, it is a new organic compound, the characterization of which is presented in the Experimental Part.

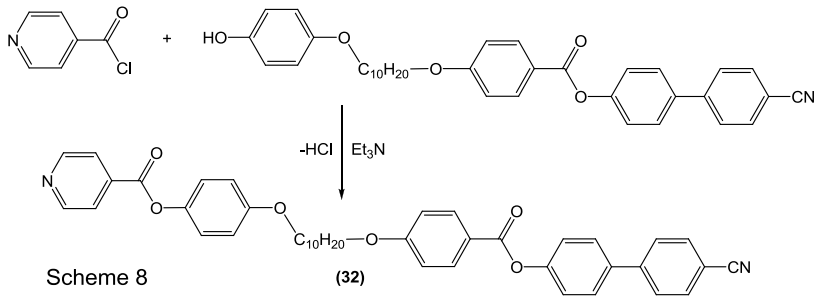

Scheme 8 **(32)**

The dinuclear complexes $[(C_6H_6)RuCl_2]_2$, $[(p\text{-}MeC_6H_4Pr^i)RuCl_2]_2$ and $[(C_6Me_6)RuCl_2]_2$ react in dichloromethane with 2 equivalents of the cyanobiphenyl containing

long-chain isonicotinic ester ligands **32** to give the neutral complexes [(arene)Ru(L)Cl_2] (**33** – **35**) in quantitative yield, see Scheme 9. All the complexes are obtained as air-stable orange powders, which are soluble in polar organic solvents, in particular in dichloromethane and chloroform. The complexes are also sparingly soluble in water.

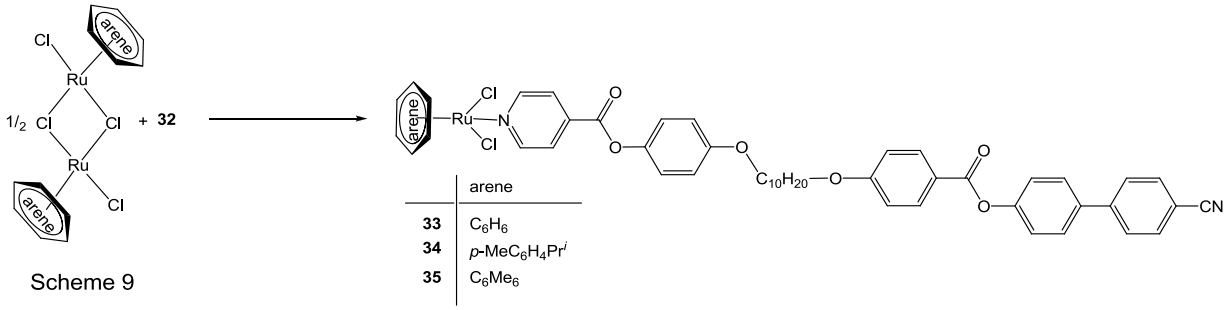

	arene
33	C_6H_6
34	*p*-$MeC_6H_4Pr^i$
35	C_6Me_6

Scheme 9

2.3.2 Preparation of Nanoparticles from Triaqua Arene Ruthenium Complexes Stabilized by a Cyanobiphenyl-Containing Long-Chain Isonicotinic Ester Ligand

The Ru nanoparticles **36** are prepared by reducing **20** with one equivalent of **32** in absolute ethanol in a magnetically stirred stainless-steel autoclave (volume 100 mL) under a 35 bar pressure of H_2 at 100 °C for 14 h. After pressure release, the brownish black solution was isolated and treated with CH_2Cl_2 followed by centrifugation in order to remove excess of **32**. These nanoparticles are insoluble in polar solvents such as alcohols and water. The ^{1}H NMR shows that cyanobiphenyl containing isonicotinic ester ligand has been hydrogenated. The characterization of these nanoparticles is presented in Fig. 13. The size distribution of the ruthenium(0) nanoparticles was studied by transmission electron microscopy (TEM). The mean particle size was estimated from image analysis of *ca.* 100 particles at least.

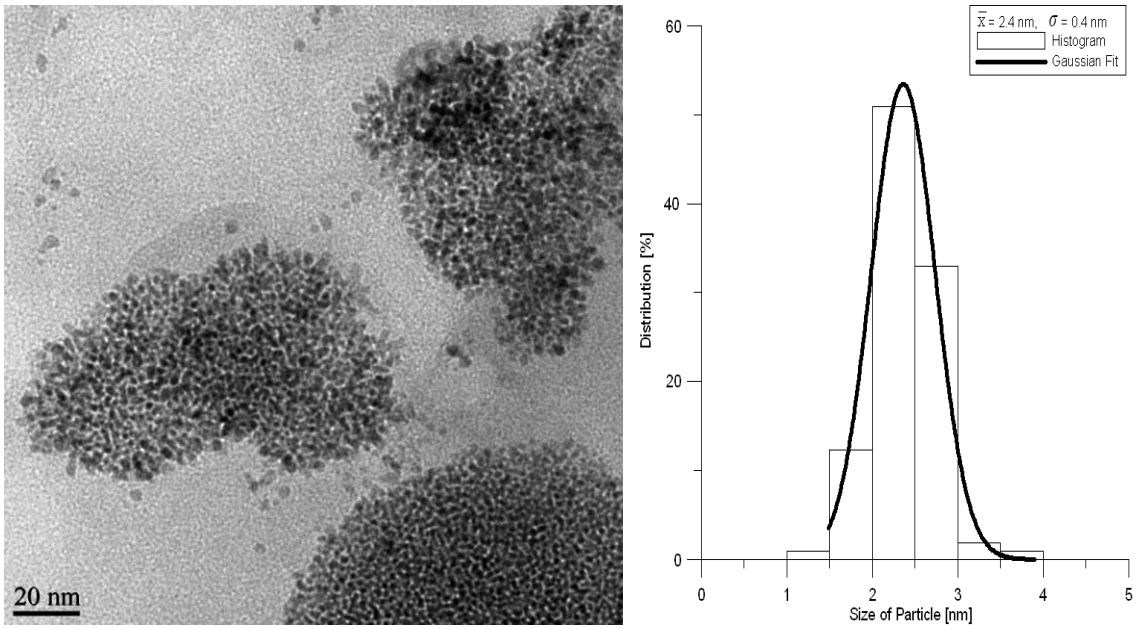

Figure 13. TEM micrograph and histogram of ruthenium nanoparticles **36**

Transmission electron microscopic analysis of these particles also shows the presence of ruthenium nanoplates **37**, sees Fig. 14. However, it was not possible to separate them from nanoparticles **36** by size-exclusion chromatography.

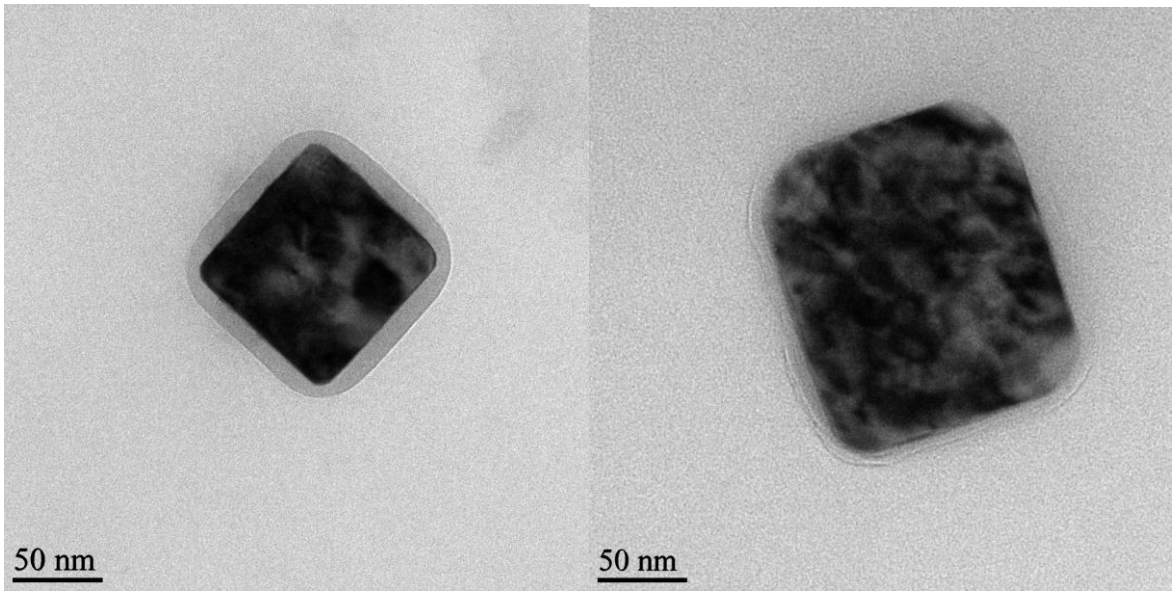

Figure 14. Ruthenium nanoplates **37** observed along with ruthenium nanoparticles **36** in transmission electron microscopy

2.3.3 Cyanobiphenyl-Containing Long-Chain Isonicotinic Ester Ligand Exchange on Pyridine-Stabilized Nanoparticles

When an ethanol solution of **31** is stirred overnight after adding one equivalent of **32** dissolved in CH_2Cl_2, the piperidine ligand at the surface is exchanged against the cyanobiphenyl containing long-chain isonicotinic ester ligand **32** to give **38**. The thermogravimetric analysis of **38** shows the presence of < 1 % of **32** at the surface of these nanoparticles.

2.3.4 Catalytic Properties of Cyanobiphenyl-Containing Long-Chain Isonicotinic Ester Ligand-Stabilized and Pyridine-Stabilized Ruthenium Nanoparticles

The catalytic activity of the ruthenium nanoparticles **36** was studied for the hydrogenation of arenes (5 mL) under a hydrogen pressure of 50 bar at 50˚C using ethanol (5 mL) as solvent. After 15 bar decrease in pressure, the reaction was quenched in an ice bath, product was decanted off and analyzed by ^{1}H NMR spectroscopy. It turned out that **36** is less efficient for toluene hydrogenation as compared to benzene hydrogenation (see Table 5).

Table 5. Catalytic hydrogenation of arenes using **36** in ethanol

Substrate	Reaction time (h)	Conversion (%)	Activity TOF (h^{-1})[a]
Benzene	3.2	42	555
Toluene	18	50	101

[a]TOF, turnover frequency was calculated as moles of converted benzene per mol Ru per hour

2.3.5 Anticancer Properties of a Cyanobiphenylic Long-Chain Isonicotinic Ester Ligand, its Arene Ruthenium Complexes and Nanoparticles

The *in vitro* cytotoxicity of cyanobiphenyl containing long-chain isonicotinic ester ligand **32** and their complexes **(33 – 35)** has been studied in the A2780 ovarian cancer cell line and cisplatin resistant variant A2780cisR using the MTT assay. Cyanobiphenyl containing long-chain isonicotinic ester ligand **32** and their arene ruthenium complexes **33 – 35** show much lower cytotoxicity as compared to

previously described alkylated long-chain containing isonicotinic ester ligand **5** and the corresponding arene ruthenium complexes **13** – **15**. This is probably due to the poor solubility of **32** – **35** in water. Cytotoxicity studies for ruthenium nanoparticles **36** are not possible due to the non-solubility of these particles in water and DMSO.

Table 6. Cytotoxicity values of the compounds **32 – 35**

Compound	A2780 IC_{50} [µM]	A2780cisR IC_{50} [µM]
32	255	303
33	36	264
34	28	253
35	38	278

2.4 Long-Chain Isonicotinic Ester-Alcohol Ligand-Containing Arene Ruthenium Complexes and Nanoparticles

2.4.1 Synthesis of a Long-Chain Alcohol-Containing Isonicotinic Ester Ligand

The long-chain NC_5H_4-4-COO-C_6H_4-4-O-$(CH_2)_{10}$-OH (**39**), derived from isonicotinic acid and containing a free alcohol function, is synthesized using a four-step method. 10-Bromodecanol is prepared by selective bromination of 1,10-decandiol using 48 % HBr solution in a liquid-liquid extractor[118] (Step 1). 10-Bromodecanol reacts with benzyl hydroquinone in the presence of potassium carbonate and 18-crown-6 to give ether according to a literature modified etherification process[119] (Step 2). The benzyl group can be removed using Pd/C under 4 bar H_2 pressure at room temperature to produce an alcohol (Step 3).

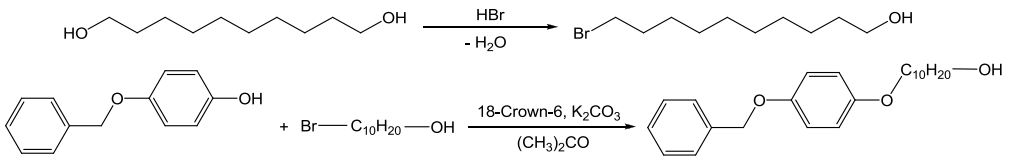

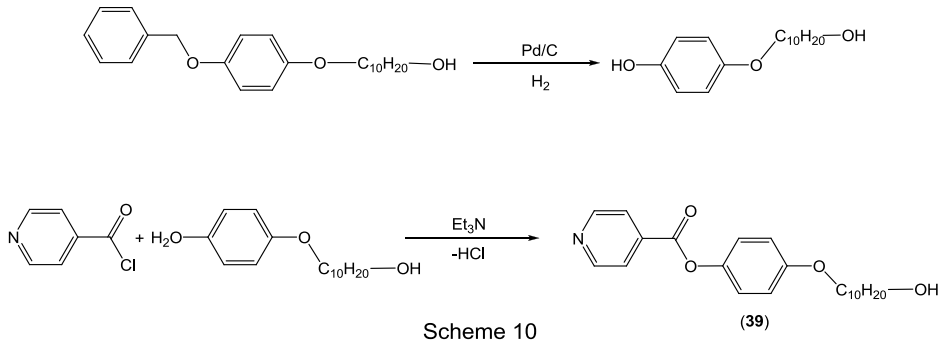

Scheme 10

The final ligand **39** is synthesized by reacting isonicotinoyl chloride hydrochloride with the alcohol *viz.* 4-(10-hydroxydecyloxy)phenol (Step 4). The reaction is done in the presence of triethylamine to bind the HCl eliminated. The reaction gives **39** in good yield, it is a new organic compound, the characterization of which is presented in the Experimental Part.

2.4.2 Long-Chain Isonicotinic Ester-Alcohol Ligand-Containing Arene Ruthenium Complexes

The dinuclear complexes $[(C_6H_6)RuCl_2]_2$, $[(p\text{-}MeC_6H_4Pr^i)RuCl_2]_2$ and $[(C_6Me_6)RuCl_2]_2$ react in dichloromethane with 2 equivalents of the isonicotinic ester ligands **39** to give the neutral complexes [(arene)Ru(L)Cl_2] (**40 – 42**) in quantitative yield, see Scheme 11. The complexation of ligand at the ruthenium centre can be concluded from the ^{1}H NMR spectra of the complex **40 – 42**, in which the signals for the α-protons in the pyridine ring appear at lower field as compared to those of the corresponding protons in **39**. All complexes are obtained as air-stable yellow to yellow/brown powders, which are soluble in polar organic solvents, in particular in dichloromethane and chloroform. The complexes are also soluble in DMSO and sparingly soluble in water.

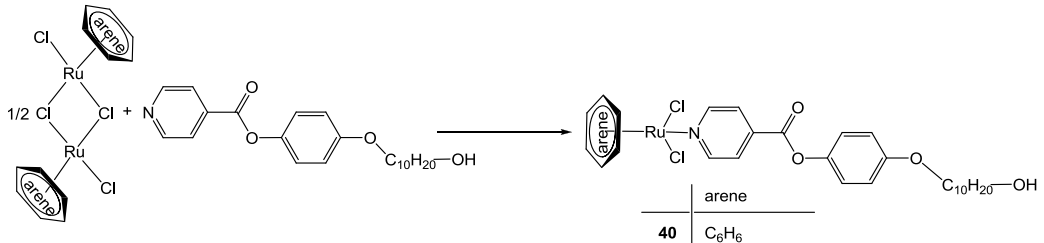

	arene
40	C_6H_6
41	p-$MeC_6H_4Pr^i$
42	C_6Me_6

Scheme 11

2.4.3 Preparation of Nanoparticles from Triaqua Arene Ruthenium Complexes Stabilized by a Long-Chain Isonicotinic Ester-Alcohol Ligand

The Ru nanoparticles **43** are prepared by reducing **20** with one equivalent of **39** in absolute ethanol in a magnetically stirred stainless-steel autoclave (volume 100 mL) under a 40 bar pressure of H_2 at 100 °C. This mixture is stirred for 14 h in order to facilitate the Ostwald ripening process of ruthenium nanoparticles. After pressure release, the brownish black solution is isolated and treated with CH_2Cl_2 followed by centrifugation in order to remove excess of **39**. These nanoparticles are insoluble in polar solvents such as alcohols and water. The ^1H NMR of **43** in $CDCl_3$ shows that the aromatic ring adjacent to the isonicotinic ester function in ligand **39** has been hydrogenated. However, the pyridine ring of the isonicotinic ester function itself is not hydrogenated. The characterization of these nanoparticles is presented in Fig. 15.

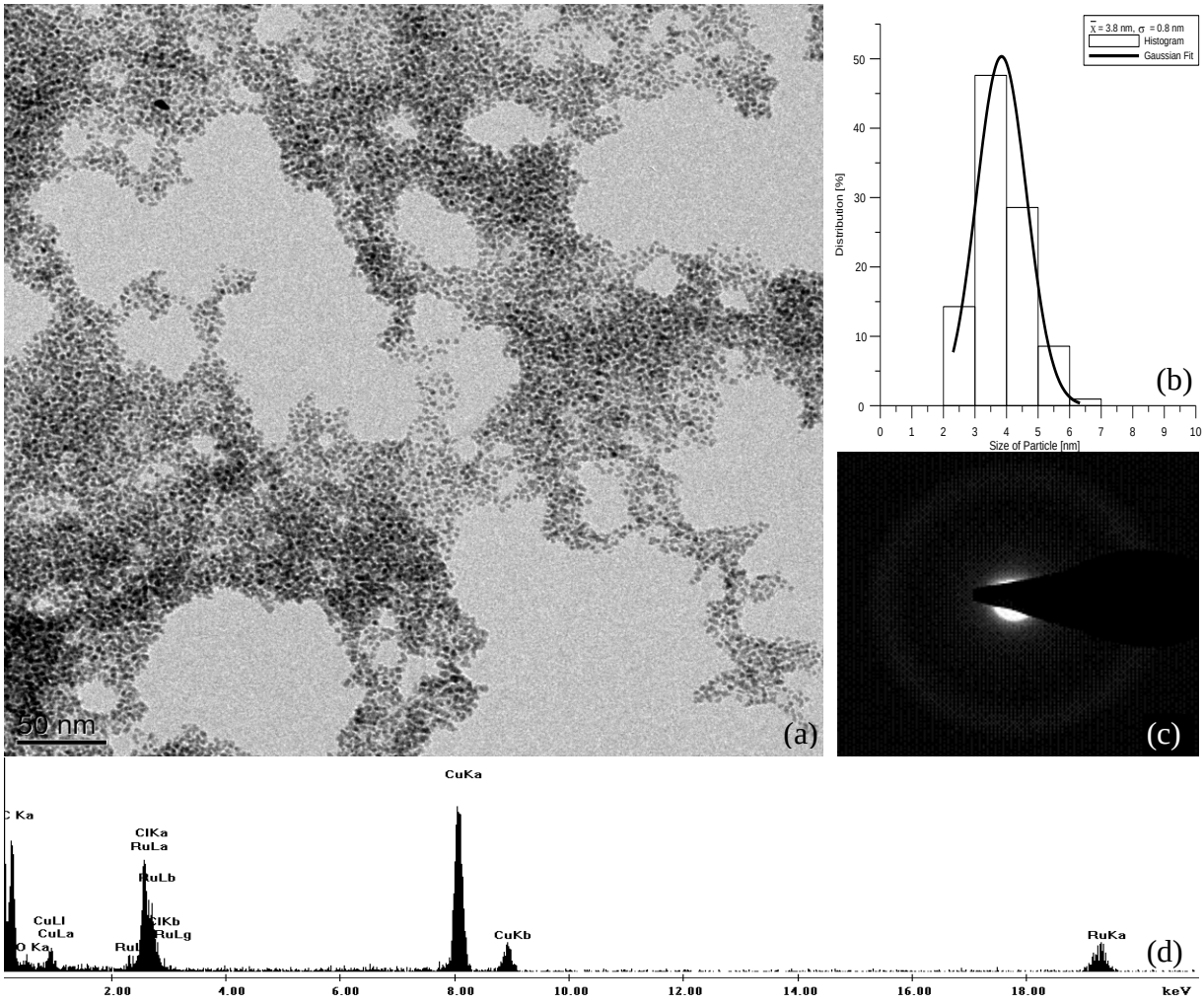

Figure 15. TEM micrograph (**a**) histogram (**b**) SAED (**c**) and EDAX analysis (**d**) of ruthenium nanoparticles **43**

The size distribution of the ruthenium(0) nanoparticles was studied by transmission electron microscopy (TEM). The mean particle size is estimated from image analysis of *ca.* 100 particles at least. The mean particle size was calculated by using the equation:[120]

$$\bar{d} = \sum n_i d_i / n_i$$

Where $\bar{d}$ is the mean particle size, d_i is the individual particle size and n is the total number of particles measured.

These ruthenium(0) nanoparticles are well dispersed having the mean size 3.8 nm with a narrow range of size distribution, the standard deviation (σ) being less than 25 % of mean particle size. Selected-area-electron-diffraction of the sample shows that these particles are crystalline in nature. The presence of ruthenium was inferred from energy dispersive X-ray spectroscopic (EDAX) analysis.

2.4.4 Anticancer Properties of a Long-Chain Isonicotinic Ester-Alcohol Ligand, its Arene Ruthenium Complexes and Nanoparticles

The *in vitro* cytotoxicity of long-chain isonicotinic ester-alcohol ligand **39** and complexes **40** – **42** has been studied in the A2780 ovarian cancer cell line and cisplatin resistant variant A2780cisR using the MTT assay. The monomeric dichloro complexes **40** – **42** of ligand **39**, exhibit very high cytoxicity in both the A2780 and resistant cell line, see Table 7. In particular, the *p*-cymene complex is highly cytotoxic (IC_{50} = 0.179 μM), the value being 9 fold lower than cisplatin in the A2780 line (1.6 μM) and 2-3 fold lower in the cisplatin resistant line A2780cisR.[116]

Table 7. Cytotoxicity values of the compounds **39 – 42**

Compound	A2780 IC_{50} [μM]	A2780cisR IC_{50} [μM]
39	162	208
40	0.598	3.564
41	0.179	3.036
42	2.995	9.566

Arene ruthenium complexes of alcoholic-long-chain containing isonicotinic ester ligand (**40** – **42**) show much higher cytotoxicity as compared to previously described arene ruthenium complexes of alkylated long-chain containing isonicotinic ester ligand **12** – **15**. It is worth noting that for **12** – **15**, the cytotoxicities reflect, to some extent, those of the free ligands **4** – **5**. Interestingly, the isonicotinic ester ligand **39** is almost inactive (IC_{50} = 162 and 208 μM) under comparable conditions, suggesting that the cytotoxicity of these complexes may be due to their good solubility in DMSO, thus resulting in efficient uptake of these mononuclear complexes. However, it is too early to say whether these complexes exert their cytotoxic effect via a similar mechanism to cisplatin or whether different mechanisms are in operation. Cytotoxicity studies for ruthenium nanoparticles **43** are not possible due to the precipitation of these particles in DMSO.

2.5 Alkylated Long-Chain Bipyridine Ligand-Containing Arene Ruthenium Complexes and Nanoparticles

2.5.1 Synthesis of a 5,5´-Disubstituted Bipyridine Ligand

5,5´-Dimethyl-2,2´-bipyridine reacts with N-bromosuccinimide (NBS) in carbon tetrachloride to give 5,5´-Bis(bromomethyl)-2,2´-bipyridine.[121] 5,5´-Bis(bromomethyl)-2,2´-bipyridine reacts with 4-(decyloxy)phenol in the presence of potassium carbonate and 18-crown-6 ether to yield **44** according to a literature-modified etherification process.[119]

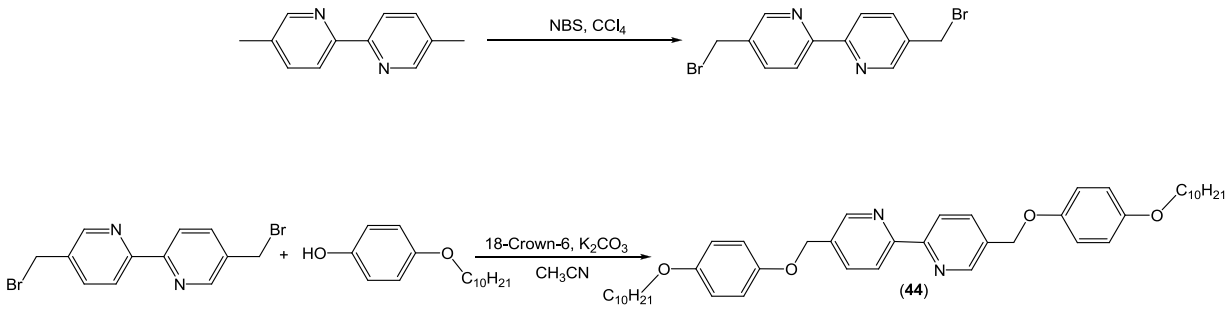

Scheme 12

The reaction gives **44** in good yield, it is a new organic compound, the characterization of which is presented in the Experimental Part.

2.5.2 Arene Ruthenium Complexes of 5,5´-Disubstituted Bipyridine Ligand

The dinuclear complexes $[(C_6H_6)RuCl_2]_2$, $[(p\text{-}MeC_6H_4Pr^i)RuCl_2]_2$ and $[(C_6Me_6)RuCl_2]_2$ react in refluxing dichloromethane/methanol (1:1) mixture with 2 equivalents of **44** to give the cationic complexes **45** – **47**, which can be isolated as chloride salts in quantitative yield, see Scheme 13. The complexation of ligand at the ruthenium centre can be concluded from NMR spectra. In the ^1H NMR spectrum of the ligand, the two CH_2 protons adjacent to the bipyridine rings appear as a singlet at 5.09 ppm. However, in complexes **45** – **47**, these two protons appear as two doublets with a germinal coupling constant (^2J) of ~ 14 Hz. These light-sensitive complexes are obtained as yellow to yellow/brown powders, and are soluble in polar organic solvents, in particular in dichloromethane and chloroform. The complexes are also soluble in DMSO and sparingly soluble in water.

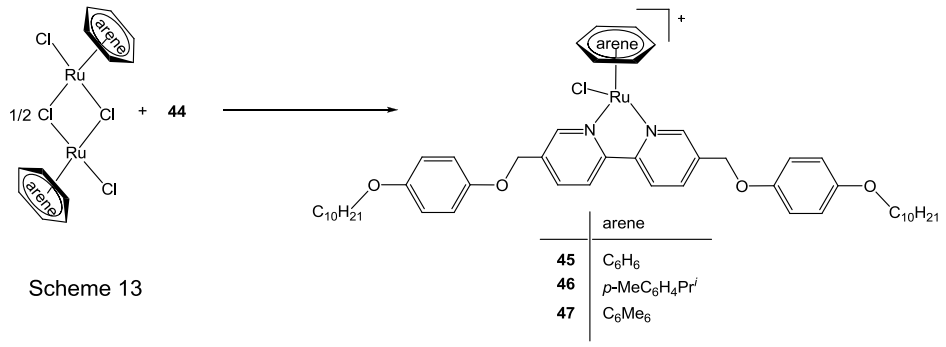

Scheme 13

Silver salts are usually employed to remove chloro ligands as chloride anions from arene ruthenium complexes to give the corresponding aqua complexes. In the case of **45** – **47**, the removal of the chloro ligand by silver sulfate results in the formation of the monoaqua arene ruthenium complexes **48** – **50**, which can then be isolated as sulfate salts after filtration from the reaction mixture, see Scheme 14.

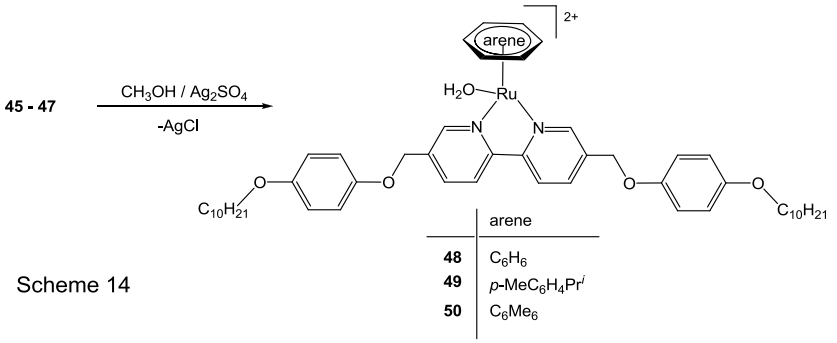

Scheme 14

2.5.3 Ruthenium Nanoparticles from Arene Ruthenium Complexes Containing the 5,5´-Disubstituted Bipyridine Ligand

The Ru nanoparticles **51** are prepared by reducing **48** in refluxing methanol. After 96 h, the black solution was evaporated under reduced pressure. The ^{1}H NMR of this black material shows the presence of the free ligand **44** and the absence of an arene peak. The stabilization of the ruthenium nanoparticles is maintained by **44**, as shown by the weak bipyridine signals having lost their sharpness. Some fragmentation of the ligand has also occured, a breakdown being observed for the ether linkage between the two aromatic rings in **44**. Transmission electron microscopy (TEM) observation shows that this black material contains agglomerated ruthenium nanoparticles. The other complexes **49** – **50** cannot be reduced and give instead a green solution upon reflux in methanol.

2.5.4 Anticancer Properties of the 5,5´-Disubstituted Bipyridine Ligand and its Arene Ruthenium Complex

The *in vitro* cytotoxicity of 5,5´-disubstituted bipyridine ligand **44** and its *p*-cymene complex **46** has been studied in the A2780 ovarian cancer cell line and cisplatin resistant variant A2780cisR using the MTT assay. The compounds **44** and **46** show a much lower cytotoxicity as compared to previously described compounds, see Table 8. This is probably due to the poor solubility of **44** and **46** in water and DMSO.

Table 8. Cytotoxicity values of the compounds **44** and **46**

Compound	A2780 IC_{50} [µM]	A2780cisR IC_{50} [µM]
44	>50	>50
46	>50	>50

2.5.5 Synthesis of a 4,4´-Disubstituted Bipyridine Ligand

4,4´-Bis(bromomethyl)-2,2´-bipyridine[122] reacts with 4-(decyloxy)phenol in the presence of potassium carbonate and 18-crown-6 ether to gives **52** according to a literature modified etherification process.[119]

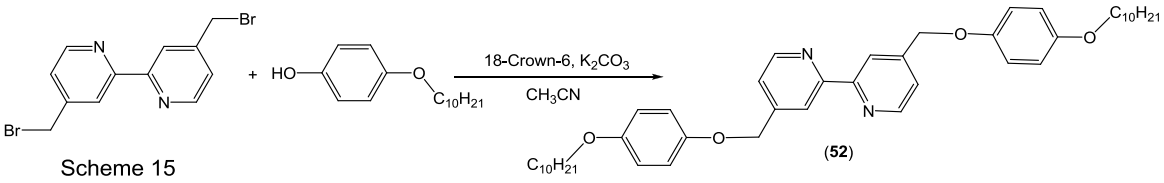

Scheme 15

The reaction gives **52** in good yield, it is a new organic compound, the characterization of which is presented in the Experimental Part.

2.5.6 Arene Ruthenium Complex of the 4,4´-Disubstituted Bipyridine Ligand and the Preparation of Ruthenium Nanoparticles

The dinuclear complexes $[(C_6H_6)RuCl_2]_2$ react in refluxing dichloromethane/methanol (1:1) mixture with 2 equivalents of **52** to give the cationic complexes **53**, which can be isolated as the chloride salts in quantitative yield, see Scheme 16.

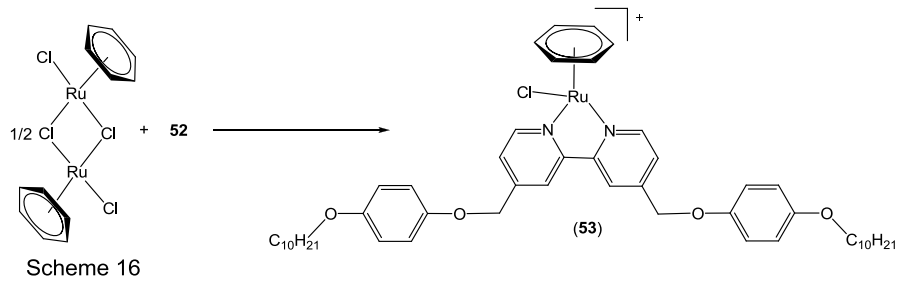

Scheme 16

It is not possible to reduce **53** by a solvothermal route. A green solution is always obtained upon refluxing these complexes in alcohols such as methanol and ethanol. Alternatively, the Ru nanoparticles **54** are prepared by reducing **20** in the presence of one equivalent of **52** in absolute ethanol in a magnetically stirred stainless-steel autoclave (volume 100 mL) under a 50 bar pressure of H_2 at 100 °C for 14 h. After pressure release, the black material is isolated and treated with CH_2Cl_2 followed by centrifugation in order to remove excess of ligand. The ^1H NMR shows ligand

fragmentation at the ether linkage between the two aromatic rings in **53**. The transmission electron microscopic images of these nanoparticles are presented in Fig. 16.

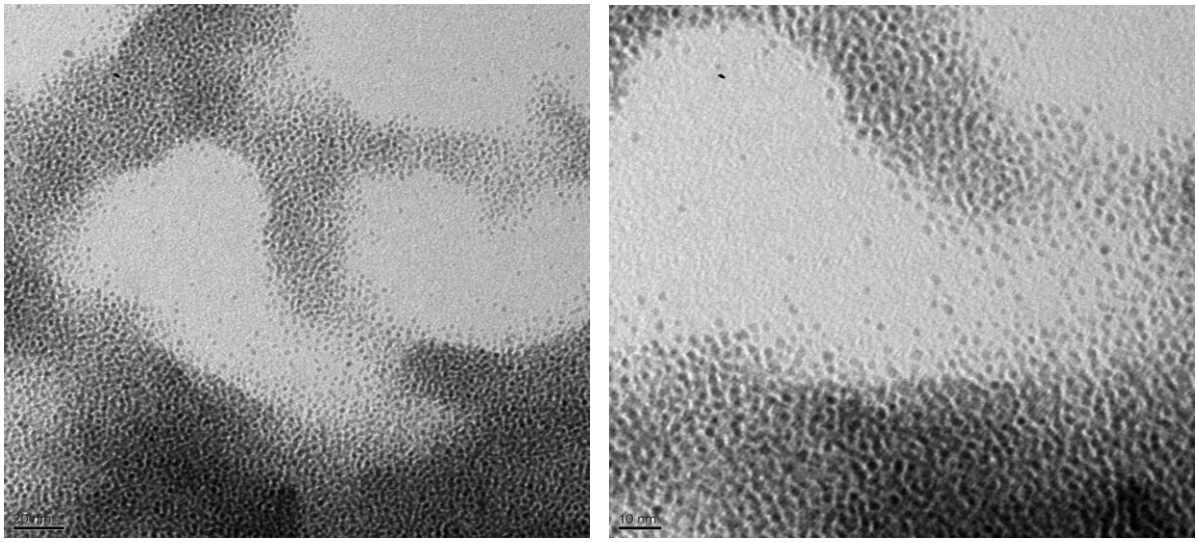

Figure 16. TEM micrographs of ruthenium nanoparticles **54**

3

Ruthenium Nanoparticles Supported by Silicate Materials

3.1 State of the Art: Silicas, Zeolites and Clays

In recent years, metallic nanoparticles received much attention due to their potential applications as catalysts. The design of nanocomposites consisting of functional metals and adequate matrices is a challenge for the fabrication of recyclable catalysts. Highly active metallic nanoparticles must be stabilized by a suitable support in order to prevent aggregation to bulk metal.[123] Therefore, ruthenium nanoparticles have been supported by montmorillonite,[81] by nonporous[74] or mesoporous silica[78] or by zeolites of the types beta[124] or faujasite.[125] All these materials have been shown to catalyze the hydrogenation of benzene to give cyclohexane with excellent activities,[34,81b,74b, 78d,124,125] while polymer-supported (on PVP) ruthenium nanoparticles proved to be completely inactive.[126] The very recent JACS paper (2010) by Özkar on faujasite-supported ruthenium nanoparticles[125] claims this material to fulfill the majority of the "green chemistry requirements" for catalysts.[127] We had observed earlier that the cationic complex $[(C_6H_6)Ru(H_2O)_3]^{2+}$ intercalates in aqueous solution into the cationic sheets of layered materials such as synthetic hectorite by ion exchange against sodium cations.[34] We used this strategy for the generation of metallic ruthenium nanoparticles using different supports such as clays, silicas and zeolites. The

catalytic efficiency of these supported ruthenium nanoparticles was studied for arene hydrogenation reactions. Hectorite, being the most efficient layered clay support, was further systematically studied for the shape- and size-selective preparation of ruthenium nanoparticles, and selective C=C and C=O bond hydrogenation reactions.

3.2 Shape- and Size-Selective Formation of Ruthenium Nanoparticles Intercalated in Hectorite

Since the physical and chemical properties of metallic nanoparticles are often related to their size and shape,[128] controlling their growth has been an area of active research for decades.[129] In the field of catalytic research, an effective size control of metal nanoparticles helps the rational design of catalyst for practical use.[130] Size and shape of nanoparticles are usually controlled by varying different reaction parameters. For example, *Yan et al.* was able to control the size of ruthenium nanoparticles in the range of 1 – 7 nm by changing the reducing agent, temperature and stabilizer.[131] *Bonet et al.* synthesized very small PVP-stabilized ruthenium nanoparticles (2 nm) with narrow size distribution by using ethylene glycol.[132] Recently, *Chen et al.* found that the sizes and standard deviations of ruthenium nanoparticles decrease on increasing the temperature of reaction medium.[133]

In this section, practical methods to efficiently control the growth of hectorite-supported ruthenium nanoparticles are discussed in detail. This work has significance on both fundamental and practical viewpoints, because a better shape- and size-selectivity of these supported nanoparticles is necessary to investigate their novel catalytic properties.

3.2.1 Preparation of Ruthenium Nanoparticles from $[(C_6H_6)Ru(H_2O)_3]^{2+}$

The dinuclear complex benzene ruthenium dichloride dimer dissolves in water with hydrolysis to give, with successive substitution of chloro ligands by aqua ligands, a mixture of mononuclear benzene ruthenium complexes being in equilibrium.[134] The benzene ^{1}H NMR signals in a D_2O solution have been assigned to $[(C_6H_6)RuCl_2(H_2O)]$ (δ = 5.89 ppm), $[(C_6H_6)RuCl(H_2O)_2]^+$ (δ = 5.97 ppm), and $[(C_6H_6)Ru(H_2O)_3]^{2+}$ (δ = 6.06 ppm) (Scheme 17).[135] The dication $[(C_6H_6)Ru(H_2O)_3]^{2+}$, which has been isolated as the sulfate and structurally characterized,[136] is the major species present in the hydrolytic mixture over the pH range from 5 to 8 according to NMR spectrum.

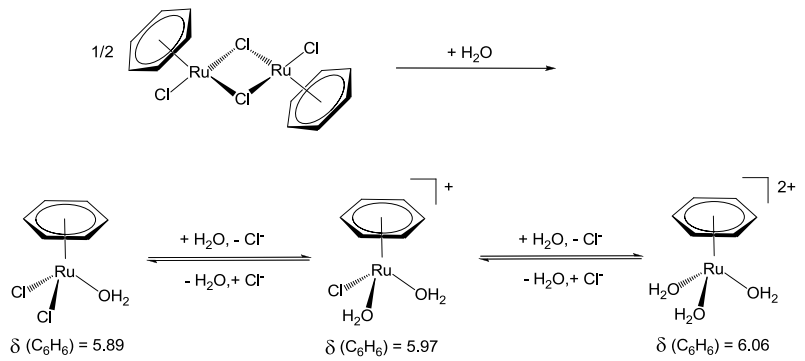

Scheme 17. Hydrolysis of the dinuclear complex $[(C_6H_6)RuCl_2]_2$ in water to give a mixture of mononuclear benzene ruthenium complexes, the dicationic triaqua complex $[(C_6H_6)Ru(H_2O)_3]^{2+}$ being the major product

When the yellow solution obtained from dissolving the dinuclear complex $[(C_6H_6)RuCl_2]_2$ in water after adjusting the pH to 8 by NaOH is added to white sodium hectorite (**55**), the main hydrolysis product $[(C_6H_6)Ru(H_2O)_3]^{2+}$ intercalates into the solid, replacing the appropriate amount of sodium cations, to give the yellow ruthenium(II)-modified hectorite **56**. This material, which can be dried and stored in air, reacts either with hydrogen under pressure (50 bar) at 100 °C or refluxing alcohols by reduction of $[(C_6H_6)Ru(H_2O)_3]^{2+}$ to give the black ruthenium(0)-modified hectorite **57** (Scheme 18).

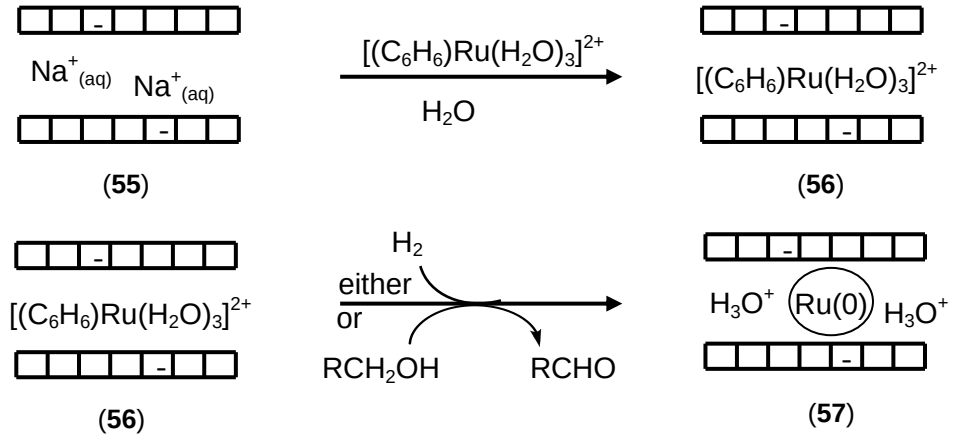

Scheme 18. Ion exchange of Na^+ cations in sodium hectorite **55** (white) against $[(C_6H_6)Ru(H_2O)_3]^{2+}$ cations to give ruthenium(II)-modified hectorite **56** (yellow) and reduction of $[(C_6H_6)Ru(H_2O)_3]^{2+}$ in **56** either by molecular hydrogen or by refluxing alcohols to give ruthenium nanoparticles in the ruthenium(0)-containing hectorite **57**

The ruthenium loading of the black hectorite **57** was assumed to be 3.2 wt%, based upon the molar ratio of $[(C_6H_6)RuCl_2]_2$ used (corresponding to 75% of the experimentally determined[137] cation exchange capacity of **55**), and the presence of metallic ruthenium was proven by its typical reflections in the X-ray diffraction pattern. The specific surface of **57** was determined by low-temperature nitrogen adsorption to be 207 m^2/g, which is significantly higher than for the unmodified hectorite **55** (87 m^2/g), the pore size distribution in **57** showing a maximum of 1.98 nm.[135]

The size distribution of the ruthenium(0) nanoparticles in **57** was studied by transmission electron microscopy (TEM) using the "ImageJ" software for image processing and analysis. The micrographs show particles varying from 2 to 60 nm depending on method of reduction and nature of solvent used. At the edges of superimposed silicate layers nanoparticles are visible, the lighter tone of which is typical for intercalated particles. The mean particle size and standard deviation (σ) were estimated from image analysis of *ca.* 100 particles at least.

Formation of Hectorite-Stabilized-Ru(0) Nanoparticles under Hydrogen Pressure

When yellow ruthenium(II)-containing hectorite **56** is reduced in an aqueous medium, a black suspension is obtained, which represents a stable dispersion of ruthenium(0)-containing hectorite **57** in water. Even after storage for several weeks, the dispersed solid does not precipitate. The TEM analysis of this material shows the presence of hexagonally shaped ruthenium nanoparticles intercalated in hectorite, the nanoparticles having mean size of 38 nm with a wide range of size distribution ($\sigma = 11.6$), see Fig. 17.

Hexagonally shaped ruthenium nanoparticles are also obtained in water/methanol mixtures, indicating that water is essential for the formation of hexagons in hectorite **57**. Whereas the reduction with H_2 in alcohols alone produces more or less spherically shaped ruthenium particles (see below), the nanoparticles obtained in aqueous methanol are also hexagonally shaped, the size of which depends on the ratio of methanol/water: For example, the reduction of **56** in an aqueous solution containing 50% methanol results in a hectorite **57** containing relatively small hexagons with an average size up to 20.7 nm having a standard deviation $\sigma < 25\%$ of the mean particle size (Fig. 18), which is fairly narrow as compared to that observed in pure water (Fig. 17). If the water content is inferior to 20%, hexagonally shaped nanoparticles are not observed any more.

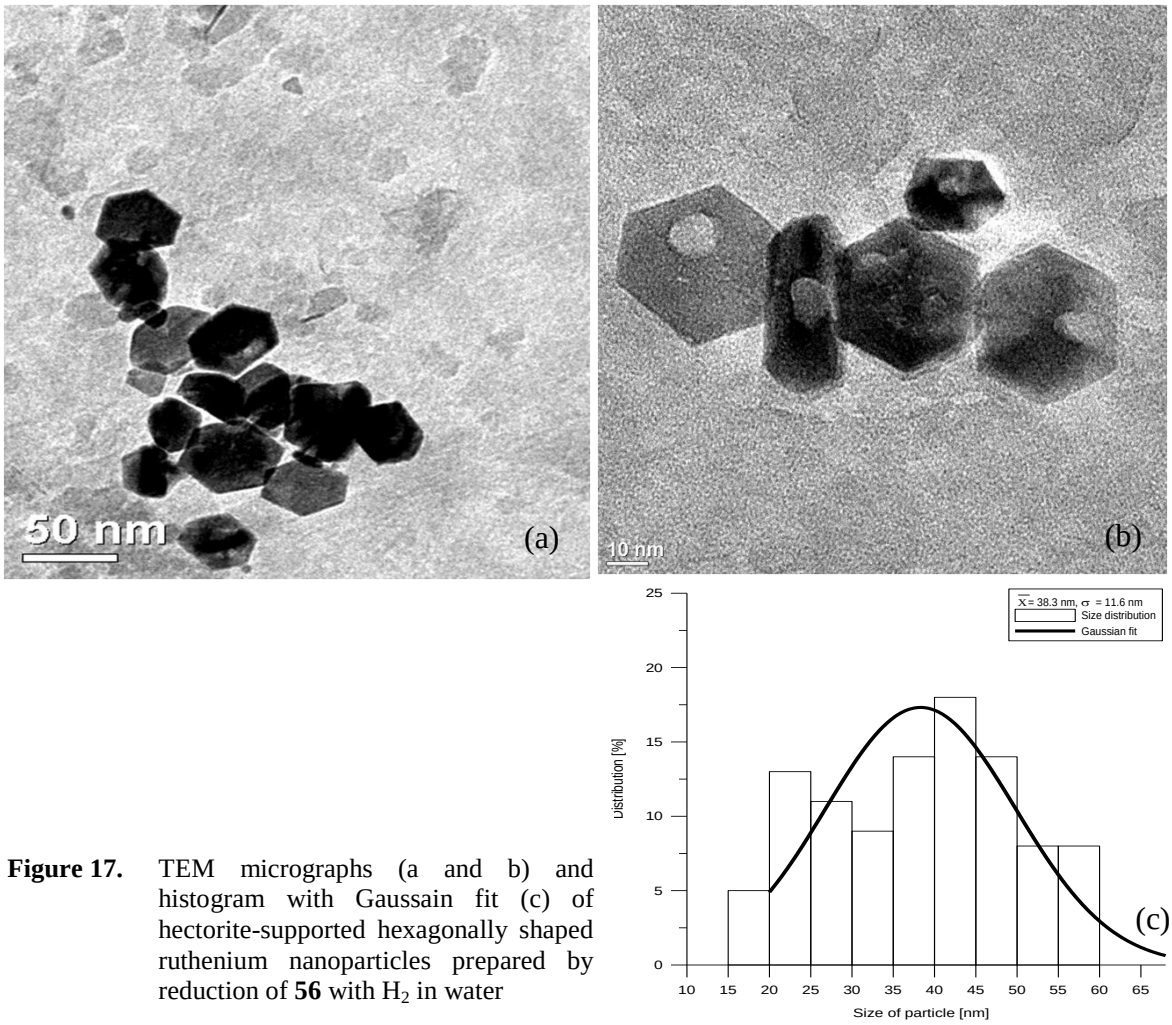

Figure 17. TEM micrographs (a and b) and histogram with Gaussain fit (c) of hectorite-supported hexagonally shaped ruthenium nanoparticles prepared by reduction of **56** with H_2 in water

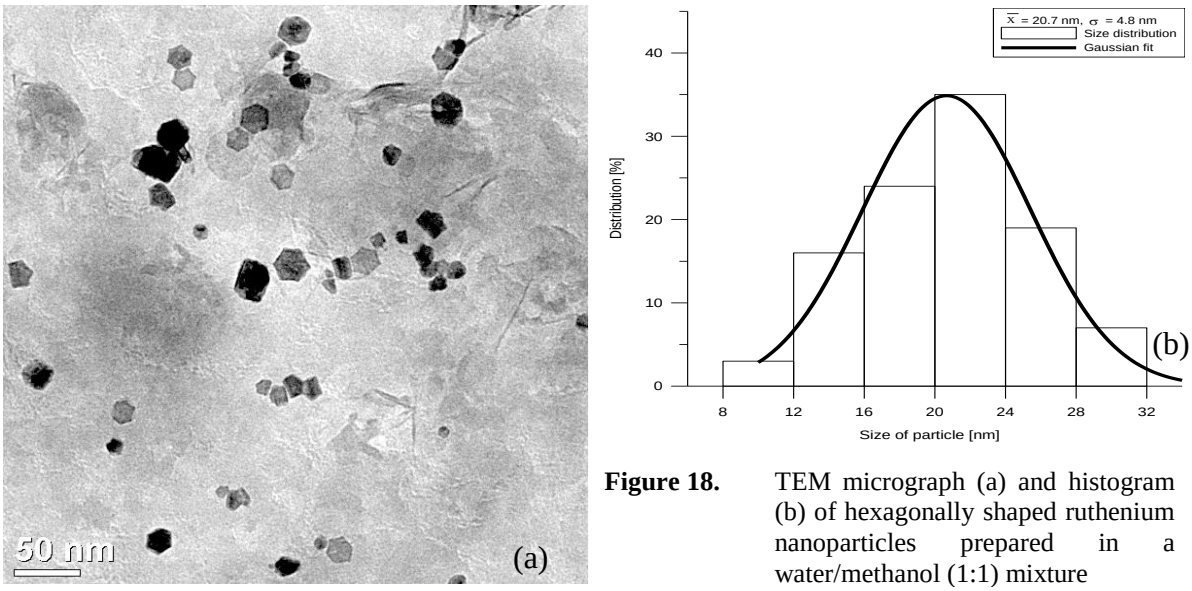

Figure 18. TEM micrograph (a) and histogram (b) of hexagonally shaped ruthenium nanoparticles prepared in a water/methanol (1:1) mixture

The reduction of **56** with molecular hydrogen in different alcohols was studied as well. The TEM micrographs in these cases reveal the black hectorite **57** to contain smaller ruthenium nanoparticles as those observed in aqueous media, see Fig. 19.

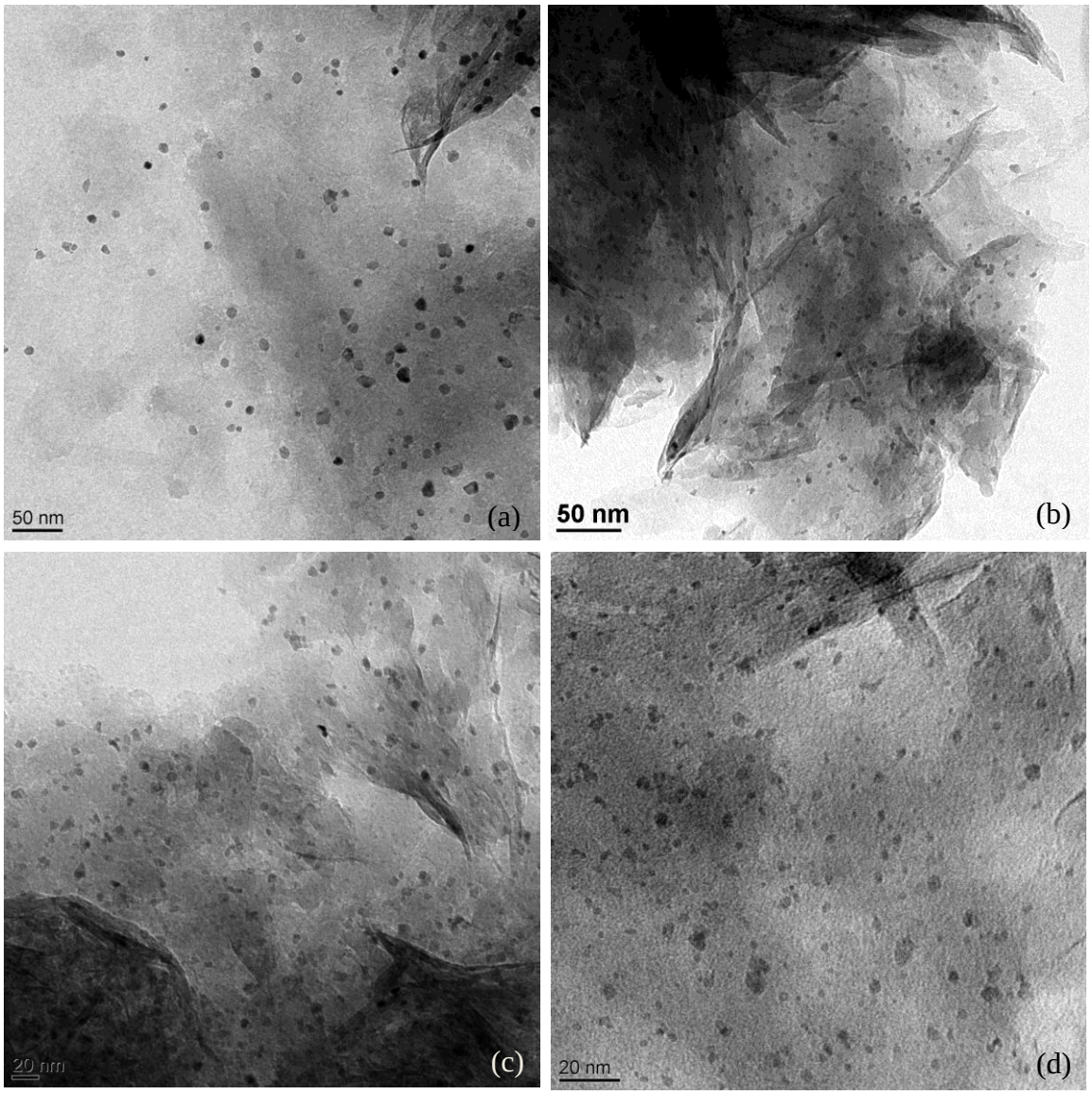

Figure 19. TEM micrographs of hectorite-stabilized ruthenium nanoparticles prepared from H_2 reduction of yellow ruthenium(II)-modified hectorite **56** in different alcohols: methanol (a), ethanol (b), 2-propanol (c), 2-butanol (d)

When **56** is reduced in primary alcohols, well separated particles are observed, the average size ranging from 9.4 nm (ethanol) to 12.3 nm (1-propanol) with a fairly wide particle size distribution as shown in the histograms. In the case of 1-butanol, two kinds of particles are observed with an average size of 3 nm and of 26.7 nm. In secondary alcohols, the reduction of **56** with H_2 results in well separated and even smaller particles (Figs. 19 and 20).

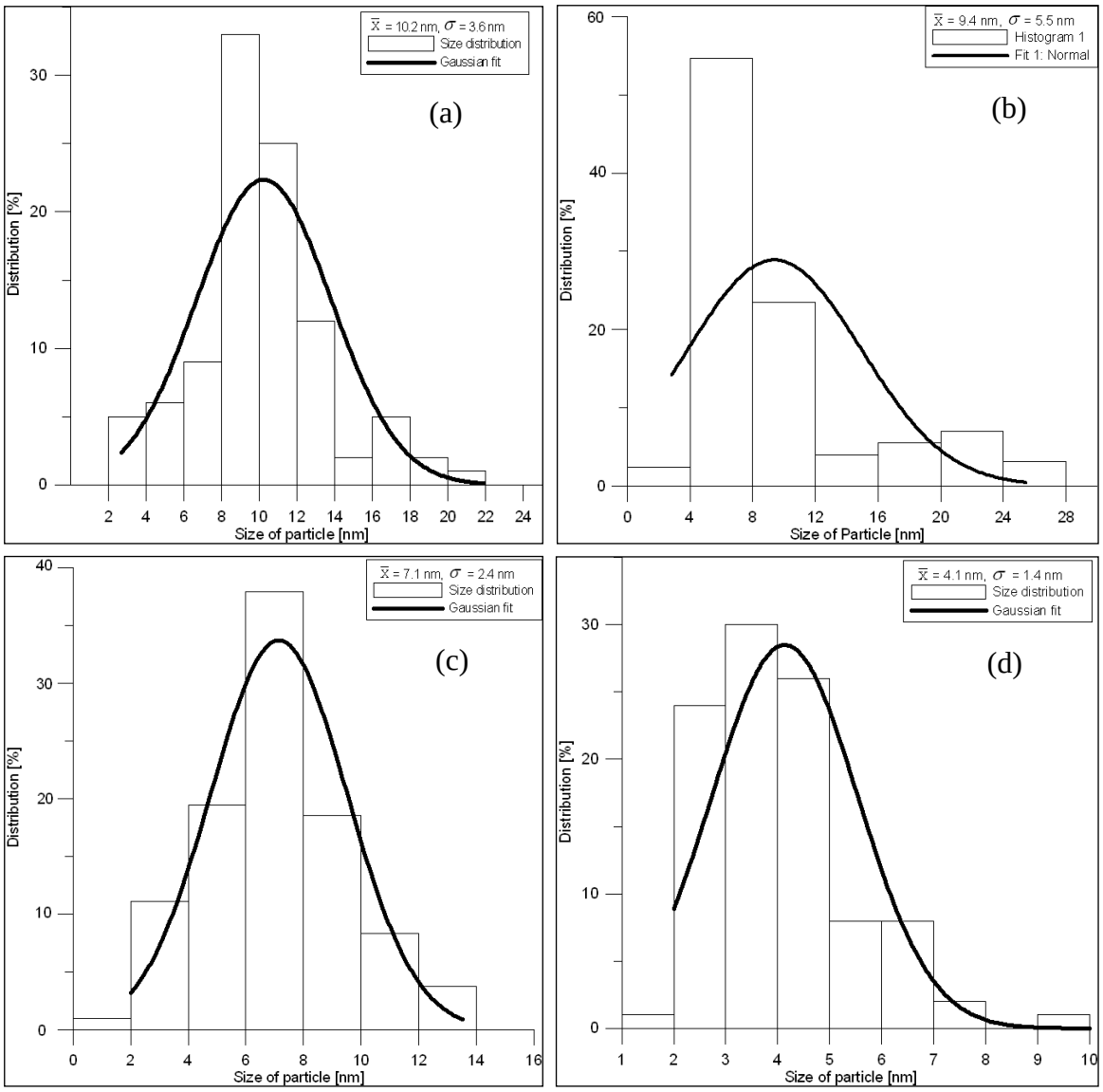

Figure 20. Histograms of hectorite-stabilized ruthenium nanoparticles prepared by H_2 reduction in methanol (a), ethanol (b), 2-propanol (c), 2-butanol (d) showing the particle size distribution

Formation of Hectorite-Stabilized Ru(0) in Refluxing Alcohols

We found out that in refluxing alcohols other than methanol, the Ru(II) complex in **56** is reduced to Ru(0) nanoparticles to give **57** even without hydrogen being present, which shows that, in this case, the alcohol itself functions as reducing agent (Scheme 18). This can be observed very easily by the color change of the refluxing hectorite suspension in various alcohols from yellow to black. In the case of primary alcohols, the refluxing time necessary for completion varies from 96 h (ethanol) to 12 h (1-butanol), indicating that long-chain alcohols are better reducing agents for **56** to **57**. The same applies to secondary alcohols which are, however, less efficient than primary alcohols (67 h for 2-propanol and 24 h for 2-

butanol). Once the reduction is complete, an increased refluxing time has no effect on particle size. However, hectorite-stabilized ruthenium nanoparticles obtained this way tend to aggregate to form clusters of nanoparticles. In every case, the mean particle size is always less than 10 nm with a standard deviation (σ) generally greater than 18% of mean particle size (Figs. 21 and 22).

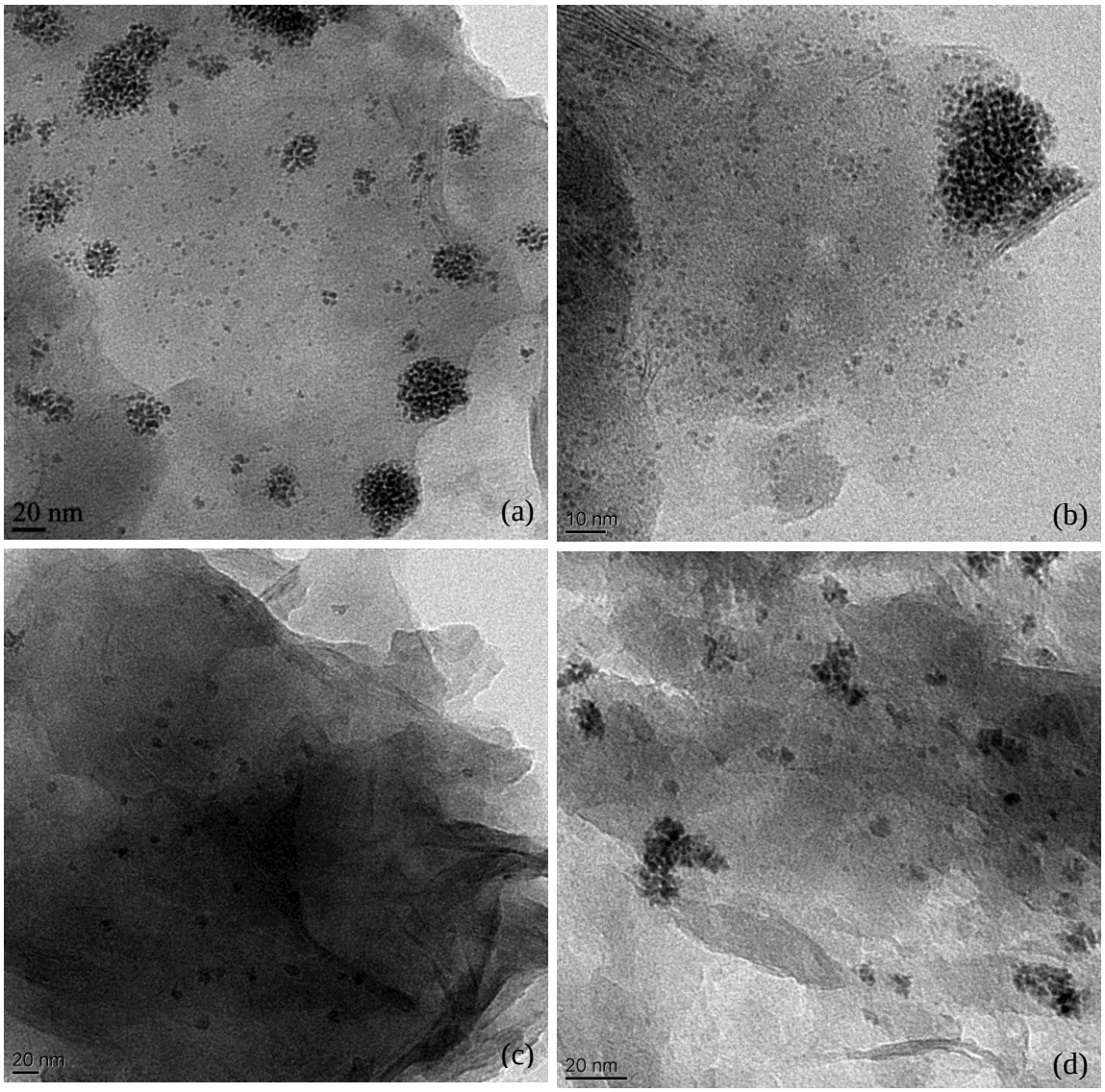

Figure 21. TEM micrographs of hectorite-stabilized ruthenium nanoparticles prepared by the reduction of yellow ruthenium(II)-modified hectorite **56** in different refluxing alcohols without H_2 being present: ethanol (a), 1-propanol (b), 2-propanol (c), 2-butanol (d)

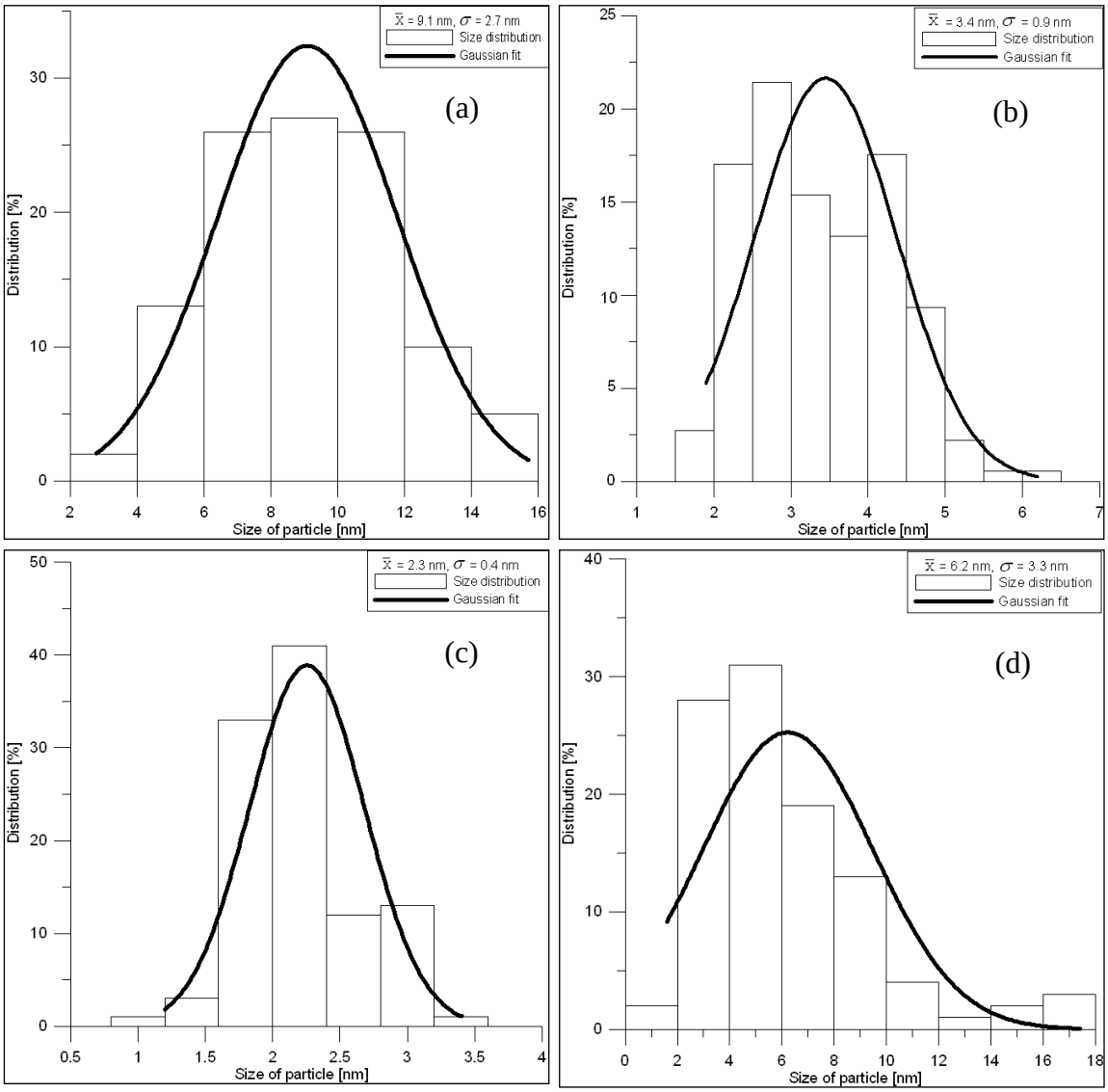

Figure 22. Histograms showing the particle size distribution of hectorite-stabilized ruthenium nanoparticles prepared by the reduction of yellow ruthenium(II)-modified hectorite **56** in different refluxing alcohols without H_2 being present: ethanol (a), 1-propanol (b), 2-propanol (c), 2-butanol (d)

3.2.2 Preparation of Ruthenium Nanoparticles from $[(arene)_2Ru_2(OH)_3]^+$

When an aqueous solution of a dinuclear complex such as $[(C_6H_6)_2Ru_2Cl_4]$, $[(p\text{-}MeC_6H_4Pr^i)_2Ru_2Cl_4]$ and $[(C_6Me_6)_2Ru_2Cl_4]$ is passed through a strongly basic anion exchange resin, all chloro ligands are depleted from the complex as chloride anions. The ^1H NMR spectrum in D_2O solution shows the presence of a single species. A chloride-depleted species, obtained by passing $[(C_6H_6)_2Ru_2Cl_4]$ through strongly basic anion exchange resin, has been isolated and structurally characterized. The X-ray

crystallographic analysis reveals the presence of a new hydroxo- and oxo-bridged complex, $[(C_6H_6)_2Ru_2(OH)_2(O)] \cdot 8H_2O$ (**58**).

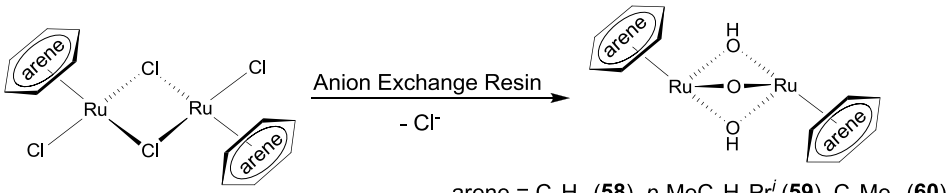

Scheme 19

arene = C_6H_6 (**58**), *p*-$MeC_6H_4Pr^i$ (**59**), C_6Me_6 (**60**)

The analogous complexes $[(p\text{-}MeC_6H_4Pr^i)_2Ru_2(OH)_2O] \cdot nH_2O$ (**59**) and $[(C_6H_6)_2Ru_2(OH)_2(O)] \cdot nH_2O$ (**60**) have also been prepared according to the above mentioned procedure and characterized by ^1H NMR, UV-Vis and IR spectroscopic methods.

*X-Ray Structural Analysis of $[(C_6H_6)_2Ru_2(OH)_2(O)] \cdot 8H_2O$ (**58**)*

Suitable crystals were obtained as yellow hexagonal plates by slow evaporation of aqueous solution. The molecule possesses mirror symmetry and crystallizes as an octa-hydrate. There is evidence that some of the C-atoms in one of the aromatic rings (atoms C5-C8) undergo considerable thermal motion. Attempts to split these atoms did not improve the situation. The OH^- anion appears to be disordered with a water molecule in a position related by the mirror symmetry of the structure. It was not possible to locate a hydrogen atom on bridging oxygen O2. The average bond lengths for the bridging hydroxyl groups (Ru-O1) in this cation is 2.1 Å, which is very close to that of an already reported $[(C_6H_6)_2Ru_2(OH)_3]^+$ cation.[138] However, the bond length for bridging oxygen (Ru-O2) is relatively small (2.05 Å). The metal distance between two ruthenium atoms (Ru1-Ru2) is 2.95 Å, just slightly outside the distance of a metal-metal bond.

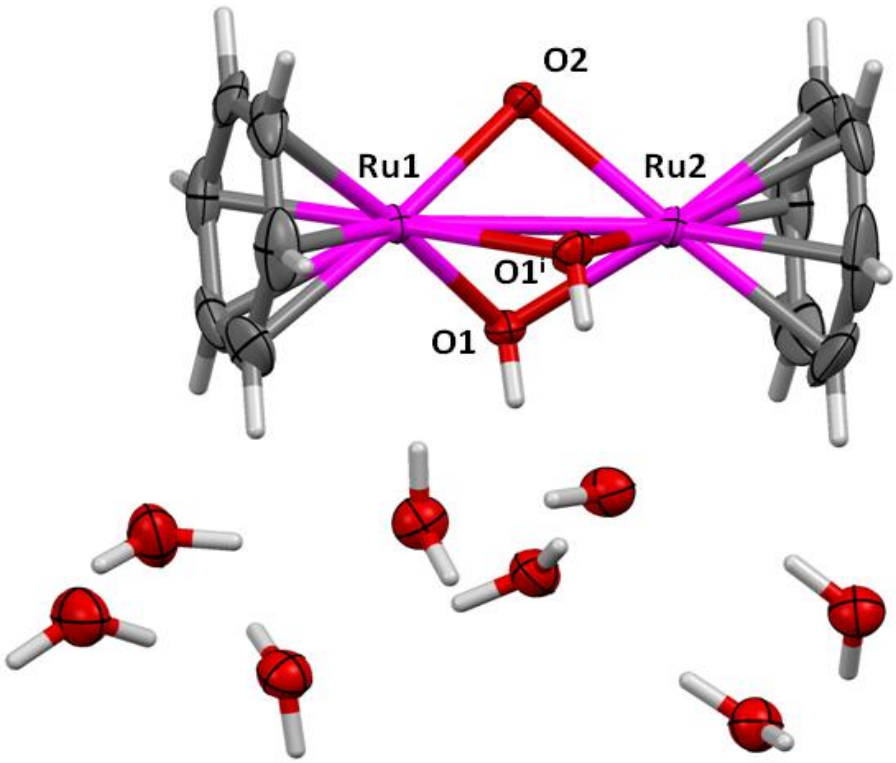

Figure 23. A view of the molecular structure of $[(C_6H_6)_2Ru_2(OH)_2O] \cdot 8H_2O$ with partial numbering scheme and displacement ellipsoids drawn at the 50% probability level [symmetry code: (i) x, -y+1/2, z]

Table 9. Selected bond lengths (Å) and angles (°) for **58**

Bond lengths (Å)		**Angles (°)**	
Ru(1)-Ru(2)	2.950(6)	Ru(1)-Ru(2)-O(2)	43.98(8)
Ru(1)-O(1)	2.095(2)	Ru(2)-Ru(1)-O(1)	45.36(5)
Ru(1)-O(2)	2.050(3)	O(1)-Ru(1)-O(2)	74.83(8)
Ru(2)-O(1)	2.099(2)	O(1)-Ru(2)-O(2)	74.76(8)
Ru(2)-O(2)	2.049(3)	O(1)-Ru(2)-O(1)	76.17(8)
		Ru(1)-O(1)-Ru(2)	89.42(8)
		Ru(1)-O(2)-Ru(2)	92.08(1)

When the yellow solution of these dimeric complexes, obtained from anion exchange resin, is added to white sodium hectorite (**55**), they intercalate into the solid, replacing the appropriate amount of sodium cations, to give the yellow ruthenium(II)-modified hectorites. Inductively coupled plasma-optical emission

spectroscopy (ICP-OES) analysis of these yellow hectorites shows 27 – 32 mg Ru / g of the yellow hectorites which means that these complexes replaced ~ 70% of sodium cations present in hectorite. It may be assumed that the neutral oxodi-μ-dihydroxobis[(η-arene)ruthenium(II)] complex dissolves in water (pH > 9) with protonation of the oxo bridge gives the cationic trihhydroxo-bridge complexes (**61** – **63**). These cations can be intercalated into hectorite by cationic sodium exchange. The same mechanism has already been reported in which treatment of the phenoxo-bridged $[(C_6H_6)_2Ru_2(OC_6H_5)_3]^+$ cation with excess of water at room temperature gives the $[(C_6H_6)_2Ru_2(OH)_3]^+$ cation.[138]

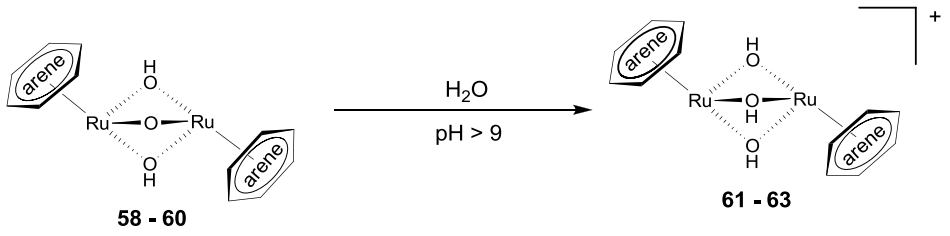

Scheme 20

The hectorite materials obtained (**64** – **66**) react with hydrogen under pressure (50 bar) at 100 °C by reduction of the corresponding tri-μ-hydroxobis[(η-arene)ruthenium(II)] cation to give the black ruthenium(0)-modified hectorites **67** – **69** (Scheme 21).

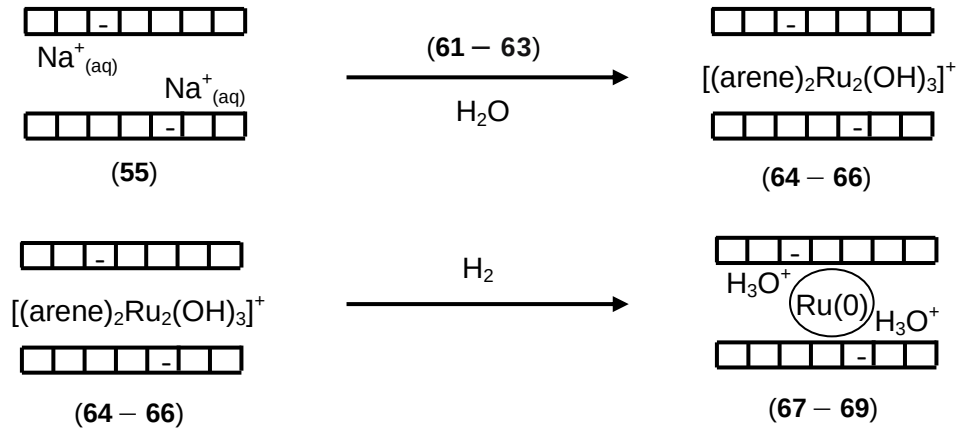

Scheme 21. Ion exchange of Na^+ cations in sodium hectorite **55** (white) against $[(arene)_2Ru_2(OH)_3]^+$ cations to give ruthenium(II)-modified hectorites **64** – **66** (yellow) and reduction of $[(arene)_2Ru_2(OH)_3]^+$ in **64** – **66** by molecular hydrogen give ruthenium nanoparticles in the ruthenium(0)-containing hectorite **67** – **69**

The size distribution of the ruthenium(0) nanoparticles in **67** – **69** was studied by transmission electron microscopy (TEM). The micrographs show particles varying from 1 to 24 nm depending on the nature of the arene substituent in tri-μ-hydroxobis[(η-arene)ruthenium(II)] cation used to prepare **64** – **66**. At the edges of superimposed silicate layers nanoparticles are visible, the lighter tone of which is typical for intercalated particles. The mean particle size and standard deviation (σ) were estimated from image analysis of *ca.* 100 particles at least.

*Formation of Hectorite-Stabilized-Ru(0) Nanoparticles Using $[(C_6H_6)_2Ru_2(OH)_3]^+$ (**67**)*

When a yellow solution of $[(C_6H_6)_2Ru_2(OH)_3]^+$ (**61**), obtained by passing $[(C_6H_6)_2Ru_2Cl_4]$ through a strongly basic anion exchange resin, is added to white sodium hectorite (**55**), cations intercalate into the solid, replacing the appropriate amount of sodium cations, to give the yellow ruthenium(II)-modified hectorite **64**. ICP-OES analysis of this yellow hectorite shows the presence of 32.2 mg Ru / g of **64**. This material, which can be dried and stored in air, reacts with hydrogen under pressure (50 bar) at 100 °C by reduction of $[(C_6H_6)_2Ru_2(OH)_3]^+$ to give the black ruthenium(0)-modified hectorite **67** (Scheme 21). The ruthenium loading of the black hectorite **67** was assumed to be 3.2 wt%, based upon the ICP-OES analysis of Ru for yellow ruthenium(II)-modified hectorite **64**.

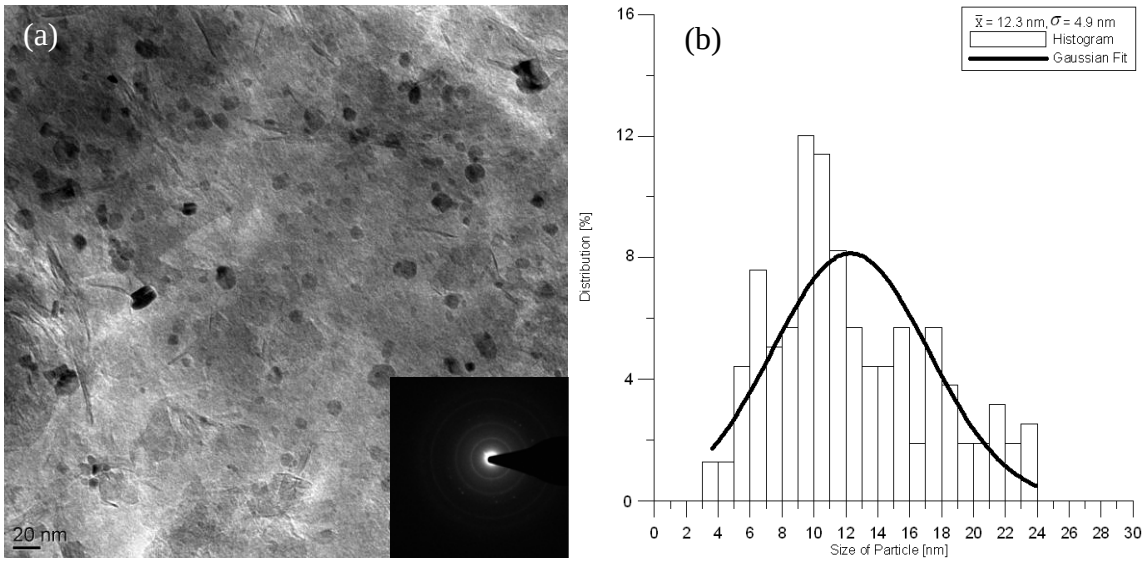

Figure 24. TEM micrograph with SAED (**a**) and histogram (**b**) showing size distribution of ruthenium(0) nanoparticles in **67** prepared from H_2 reduction of $[(C_6H_6)_2Ru_2(OH)_3]^+$ containing yellow ruthenium (II)-modified hectorite **64** in ethanol

The TEM analysis of this material shows the presence of ruthenium nanoparticles intercalated in hectorite, the nanoparticles having mean size of 12.3 nm with a wide range of size distribution (σ = 4.9), see Fig. 24. Fine rings in selected-area-electron-diffraction (SAED) pattern show that these nanoparticles are crystalline in nature.

*Formation of Hectorite-Stabilized-Ru(0) Nanoparticles Using [(p-$MeC_6H_4{}^iPr)_2Ru_2(OH)_3]^+$ (**68**)*

When a yellow solution of $[(p\text{-}MeC_6H_4{}^iPr)_2Ru_2(OH)_3]^+$ (**62**), obtained by passing $[(p\text{-}MeC_6H_4{}^iPr)_2Ru_2Cl_4]$ through a strongly basic anion exchange resin, is added to white sodium hectorite (**55**), cations intercalate into the solid, replacing the appropriate amount of sodium cations, to give the yellow ruthenium(II)-modified hectorite **65**. ICP-OES analysis of this yellow hectorite shows the presence of 31.8 mg Ru / g of **65**. This material, which can be dried and stored in air, reacts with hydrogen under pressure (50 bar) at 100 °C by reduction of $[(p\text{-}MeC_6H_4{}^iPr)_2Ru_2(OH)_3]^+$ to give the black ruthenium(0)-modified hectorite **68** (Scheme 21).

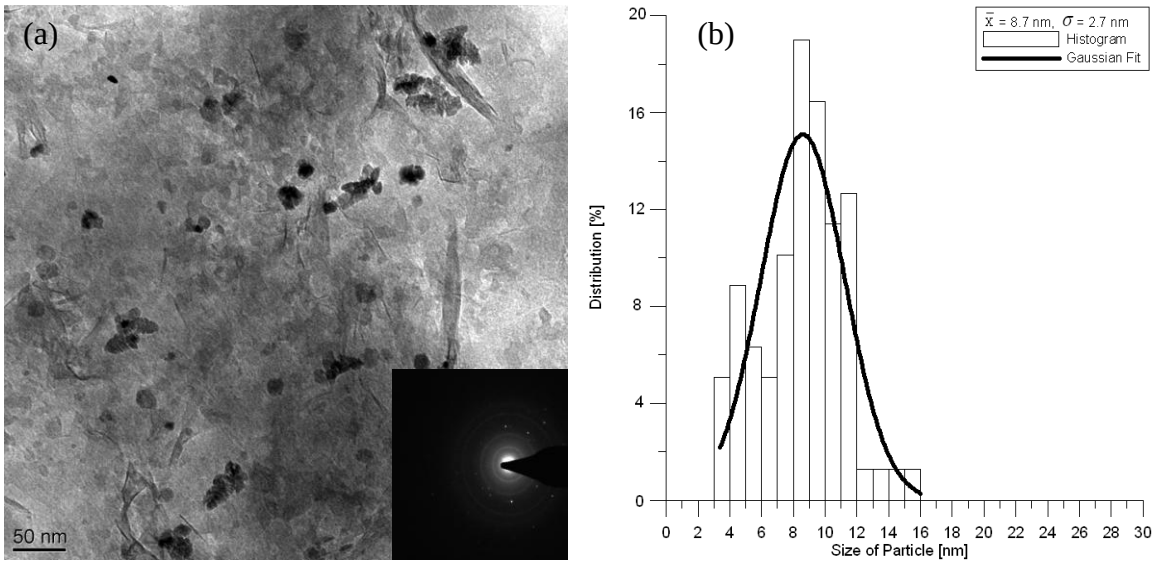

Figure 25. TEM micrograph (**a**) and histogram (**b**) showing size distribution of ruthenium(0) nanoparticles in **68** prepared from H_2 reduction of $[(p\text{-}MeC_6H_4{}^iPr)_2Ru_2(OH)_3]^+$ containing yellow ruthenium (II)-modified hectorite **65** in ethanol

The TEM analysis of this material shows the presence of aggregated ruthenium nanoparticles intercalated in hectorite, the nanoparticles having mean size of 8.7 nm with a wide range of size distribution (σ = 2.7), see Fig. 25.

*Formation of Hectorite-Stabilized-Ru(0) Nanoparticles Using $[(C_6Me_6)_2Ru_2(OH)_3]^+$ (**69**)*

When a yellow solution of $[(C_6Me_6)_2Ru_2(OH)_3]^+$ (**63**), obtained by passing $[(C_6Me_6)_2Ru_2Cl_4]$ through a strongly basic anion exchange resin, is added to white sodium hectorite (**55**), cations intercalate into the solid, replacing the appropriate amount of sodium cations, to give the yellow ruthenium(II)-modified hectorite **66**. ICP-OES analysis of this yellow hectorite shows the presence of 27.1 mg Ru / g of **66**, relatively less than those discussed previously. This material, which is highly sensitive to air and should be stored under inert atmosphere, reacts with hydrogen under pressure (50 bar) at 100 °C by reduction of $[(C_6Me_6)_2Ru_2(OH)_3]^+$ to give the black ruthenium(0)-modified hectorite **69** (Scheme 21). The ruthenium loading of the black hectorite **69** was assumed to be 2.7 wt%, based upon the ICP-OES analysis of Ru for yellow ruthenium(II)-modified hectorite **66**.

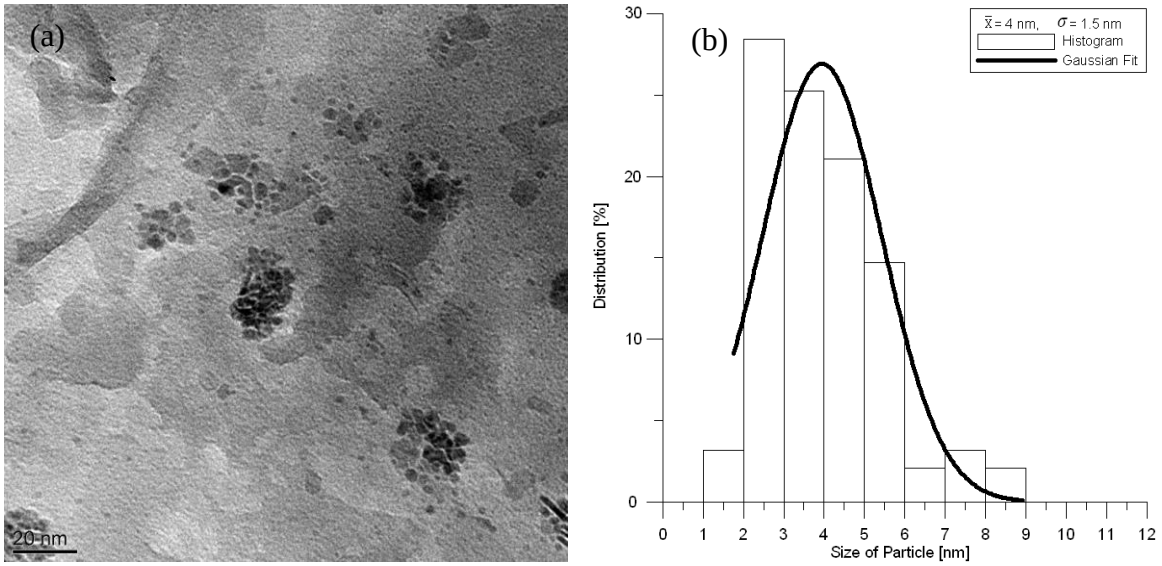

Figure 26. TEM micrograph (**a**) and histogram (**b**) showing size distribution of ruthenium(0) nanoparticles in **69** prepared from H_2 reduction of $[(C_6H_6)_2Ru_2(OH)_3]^+$ containing yellow ruthenium (II)-modified hectorite **66** in ethanol

The TEM analysis of this material shows the presence of clusters of small ruthenium nanoparticles intercalated in hectorite, the nanoparticles having mean size of 4 nm with a relatively narrow range of size distribution (σ = 2.7), see Fig. 26.

An overall comparison of particle size distribution of ruthenium nanoparticles obtained in the above mentioned experiments is shown in Figure 27. It is evident from this figure that the reduction of $[(C_6H_6)_2Ru_2(OH)_3]^+$ in **64** gives large nanoparticles with a

wide range of size distribution. However, small nanoparticles with narrow size distribution can be obtained by the reduction of $[(C_6Me_6)_2Ru_2(OH)_3]^+$ containing **66**. In conclusion, growth of ruthenium nanoparticles in hectorite can be easily controlled by changing the nature of arene substituent in these organometallic complexes.

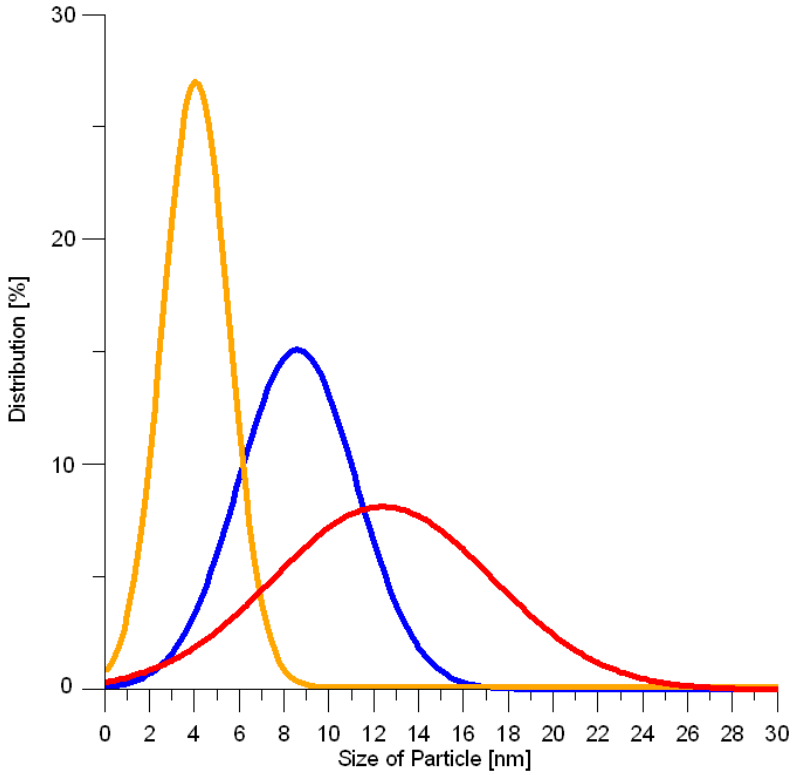

Figure 27. Comparison of Ru nanoparticles size distribution in the hectorites **67** (——), **68** (——) and **69** (——)

The yellow ruthenium(II)-modified hectorite **66** containing $[(C_6Me_6)_2Ru_2(OH)_3]^+$ (**63**) is highly sensitive to air, it turns green upon exposure to air, probably due to the oxidation of the ruthenium centers. This material **66** must be stored under nitrogen.

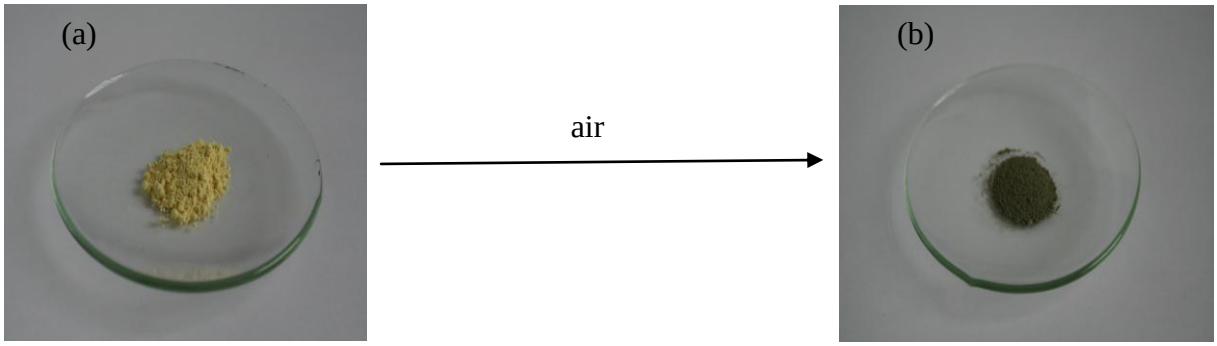

Figure 28. Freshly prepared hectorite **66**, containing $[(C_6Me_6)_2Ru_2(OH)_3]^+$ which is yellow (a) and green material obtained by exposure to air **70** (b)

This green hectorite material also reacts with hydrogen under pressure (50 bar) at 100 °C to give a black ruthenium(0)-modified hectorite **71**. The TEM analysis of this material shows the presence of small-sized, highly-dispersed ruthenium nanoparticles intercalated in hectorite, the nanoparticles having a mean size of 2 nm with a narrow range of size distribution ($\sigma = 0.7$), see Fig. 29.

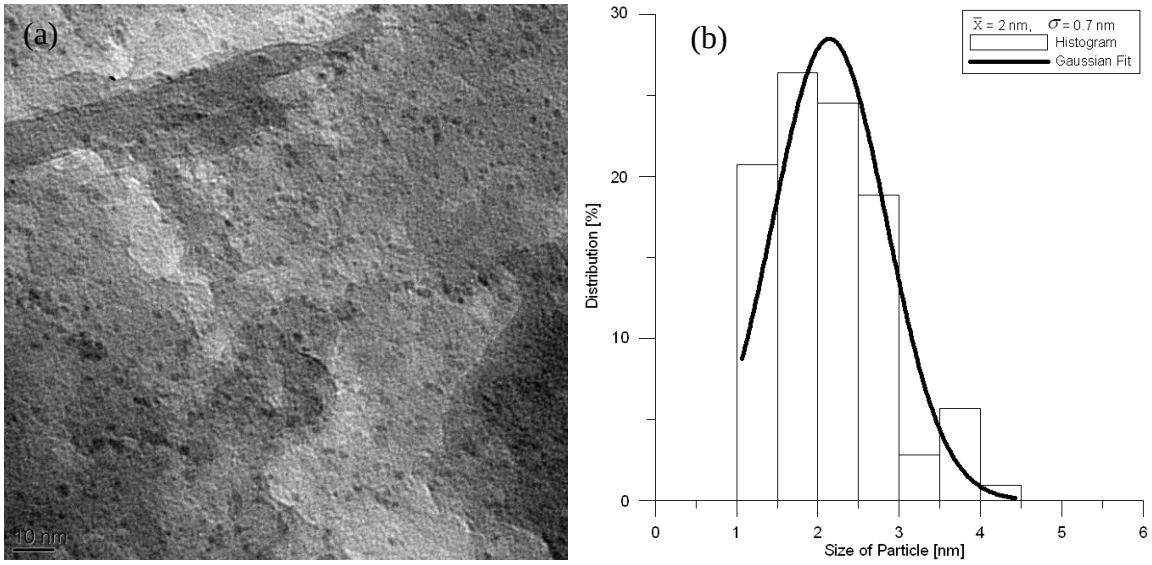

Figure 29. TEM micrograph (**a**) and histogram (**b**) showing size distribution of ruthenium(0) nanoparticles in **71** prepared from H_2 reduction of green hectorite **70** in ethanol

The nanoparticles obtained by the reduction of green hectorite **70** are even smaller than those observed by the reduction of yellow hectorite **66** containing $[(C_6Me_6)_2Ru_2(OH)_3]^+$. Moreover, the Gaussian fit is sharper with a narrower size distribution ($\sigma = 0.7$), which means that these particles are monodispersed.

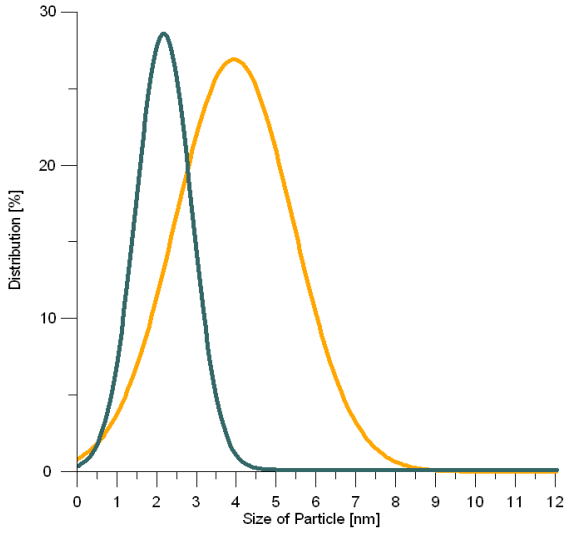

Figure 30. Comparison of Ru nanoparticle size distribution obtained by the reduction of $[(C_6Me_6)_2Ru_2(OH)_3]^+$ containing yellow hectorite **66** (——) and oxidized green hectorite **70** (——)

3.3 Ruthenium Nanoparticles Supported by Montmorillonite, Mesoporous Silicas and Zeolites

3.3.1 Montmorillonite-Supported Ruthenium Nanoparticles

Montmorillonite is, just like hectorite, a naturally occurring clay belonging to smectite family. Both clays have the same cation exchange capacity (1.0 meq/g) but different structural and swelling properties. Montmorillonite is a dioctahedral, aluminium based clay[79,81] in which the sodium cations in the interlaminar space can easily be exchanged in water by other water-soluble organic, inorganic or organometallic cations.

*Preparation of Ruthenium Nanoparticles Supported by Montmorillonite **74***

When a yellow solution, obtained from dissolving the dinuclear complex $[(C_6H_6)RuCl_2]_2$ in water after adjusting the pH to 8 by NaOH, is added to white sodium montmorillonite **72**, the main hydrolysis product $[(C_6H_6)Ru(H_2O)_3]^{2+}$ intercalates into the solid, replacing the appropriate amount of sodium cations, to give the yellow ruthenium(II)-modified montmorillonite **73**. This material, which can be dried and

stored in air, reacts with hydrogen under pressure (50 bar) at 100 °C by reduction of $[(C_6H_6)Ru(H_2O)_3]^{2+}$ to give the black ruthenium(0)-modified montmorillonite **74**. The ruthenium loading of the black montmorillonite **74** was assumed to be 3.2 wt%, based upon the the molar ratio of $[(C_6H_6)RuCl_2]_2$ used in **73**.

3.3.2 Zeolite-Supported Ruthenium Nanoparticles

Zeolites are robust alumino silicate minerals and are considered promising as a support for metallic nanoparticles.[139] They are porous materials with a pore size usually less than 10 nm. Zeolites are well known for molecular shape selectivity during a catalytic reaction.[140] Two faujasite zeolites *viz.* Y-type and ultrastable Y-type (USY) zeolites were selected for the intercalation of $[(C_6H_6)Ru(H_2O)_3]^{2+}$ complexes and generation of zeolite-supported ruthenium nanoparticles for catalytic studies. These zeolites possess high surface area 660 m^2 / g having pore diameter in the range of 0.74 – 1.3 nm. Compared to USY-type zeolite (3.90 meq / g), Y-type zeolite has huge cation exchange capacity (5.34 meq / g), thus allowing the dispersion of large amount of catalytically active components.

*Preparation of Ruthenium Nanoparticles Supported by Y-Type Zeolite **77***

When a yellow solution, obtained from dissolving the dinuclear complex $[(C_6H_6)RuCl_2]_2$ in water after adjusting the pH to 8 by NaOH, is added to NH_4-Y zeolite **75**, the main hydrolysis product $[(C_6H_6)Ru(H_2O)_3]^{2+}$ adsorbs into the zeolite channels, replacing the appropriate amount of ammonium cations, to give the yellow ruthenium(II)-modified Y-type zeolite **76**. ICP-OES analysis shows 81.4 mg of ruthenium loading per gram of **76**. This material, which can be dried and stored in air, reacts with hydrogen under pressure (50 bar) at 100 °C by reduction of $[(C_6H_6)Ru(H_2O)_3]^{2+}$ to give the black ruthenium(0)-modified Y-zeolite **77**. The ruthenium loading of the black Y-zeolite **23** was assumed to be 8.1 wt%, based upon the ICP-OES analysis of **76**.

*Preparation of Ruthenium Nanoparticles Supported by USY-Type Zeolite **80***

When a yellow solution, obtained from dissolving the dinuclear complex $[(C_6H_6)RuCl_2]_2$ in water after adjusting the pH to 8 by NaOH, is added to NH_4-USY zeolite **78**, the main hydrolysis product $[(C_6H_6)Ru(H_2O)_3]^{2+}$ adsorbs into the zeolite channels, replacing the appropriate amount of ammonium cations, to give the yellow ruthenium(II)-modified USY-type zeolite **79**. ICP-OES analysis shows 70.9 mg of ruthenium loading per gram of **79**. This material, which can be dried and stored in air, reacts with hydrogen under pressure (50 bar) at 100 °C by reduction of $[(C_6H_6)Ru(H_2O)_3]^{2+}$ to give the black ruthenium(0)-modified USY-zeolite **78**. The ruthenium loading of the black USY-zeolite **80** was assumed to be 7.1 wt%, based upon the ICP-OES analysis of **79**.

3.3.3 Silica-Supported Ruthenium Nanoparticles

Two types of silicas *viz.* GRACE SP-1522 and SBA-15 were selected for the intercalation of $[(C_6H_6)Ru(H_2O)_3]^{2+}$ complex and generation of silica-supported ruthenium nanoparticles. Compared to SP-1522 silica, SBA-15 is highly ordered mesoporous silica with pore size of 6.8 nm and huge surface area (785 m^2g^{-1}), allowing the dispersion of large amount of catalytically active components. SBA-15 has honey-comb like structure containing disconnected channel-like pores.[141] These pores help the diffusion of molecules during catalytic processes. These properties make SBA-15 a promising candidate as catalyst support and therefore one of the most attractive silica host material for nanoparticles.[142]

*Preparation of Ruthenium Nanoparticles Supported by SP-1522 Silica **83***

When a yellow solution obtained, from dissolving the dinuclear complex $[(C_6H_6)RuCl_2]_2$ in water after adjusting the pH to 8 by NaOH, is added to GRACE SP-1522 silica **81**, the main hydrolysis product $[(C_6H_6)Ru(H_2O)_3]^{2+}$ adsorbs into silica pores to give the yellow ruthenium(II)-modified SP-1522 silica **82**. ICP-OES analysis shows 39.1 mg of ruthenium loading per gram of **82**. This material, which is sensitive to air and should be stored under N_2 atmosphere, reacts with hydrogen under pressure (50 bar) at 100 °C by reduction of $[(C_6H_6)Ru(H_2O)_3]^{2+}$ to give the black ruthenium(0)-modified SP-1522 silica

83. The ruthenium loading of the black SP-1522 silica **83** was assumed to be 3.9 wt%, based upon the ICP-OES analysis of **82**.

*Preparation of Ruthenium Nanoparticles Supported by SBA-15 Silica **86***

When a yellow solution, obtained from dissolving the dinuclear complex $[(C_6H_6)RuCl_2]_2$ in water after adjusting the pH to 8 by NaOH, is added to SBA-15 silica **84**, the main hydrolysis product $[(C_6H_6)Ru(H_2O)_3]^{2+}$ adsorbs into silica pores to give the yellow ruthenium(II)-modified SBA-15 silica **85**. ICP-OES analysis shows 47.1 mg of ruthenium loading per gram of **85**. This material, which is sensitive to air and should be stored under N_2 atmosphere, reacts with hydrogen under pressure (50 bar) at 100 °C by reduction of $[(C_6H_6)Ru(H_2O)_3]^{2+}$ to give the black ruthenium(0)-modified SBA-15 silica **86**. The ruthenium loading of the black SBA-15 silica **86** was assumed to be 4.7 wt%, based upon the ICP-OES analysis of **85**.

3.4 Hydrogenation of Arenes Catalyzed by Ruthenium Nanoparticles

Arene hydrogenation catalysis has been a fascinating area of research since many decades.[143] Hydrogenated aromatic products such as cyclohexane are industrially important intermediates. Annually, millions of tons of cyclohexane are produced by this route for adipic acid synthesis, which is used in polymer (nylon, resin), pharmaceutical and food industry.[144] Moreover, growing demand and stricter environmental legislations also insist for cleaner fuels, thus necessitating the removal of toxic benzene and polyaromatic contents in diesel.[145] Lower aromatic contents also enhance the fuel quality by improving its cetane number.[146] Therefore, the development of an efficient catalyst for the hydrogenation of arenes is a demanding task.

Traditionally, such hydrogenations are usually performed under harsh reaction conditions.[147] For example, industrial processes for benzene hydrogenation include either a liquid phase processes employing Raney-Ni (170 – 230 °C, 20 – 40 bar H_2)[148] or vapour phase processes using noble metals (> 400 °C, 30 bar H_2)[149] or Ziegler-type catalysts doped with Ni or Co salts (180 °C, 7 bar H_2).[150]

During the last decades, extensive efforts have been devoted to develop a competent, practically feasible and energy efficient catalyst for arene hydrogenation. A brief look over

the research work which appeared during the last five years shows that the supported noble metal nanoparticles are being thoroughly studied to realize the dream of an efficient and practically viable catalyst for such hydrogenations at mild conditions. Recently, several articles reported the hydrogenation of arenes especially neat benzene catalyzed by supported metal nanoparticles under mild reaction conditions ($\leq$ 25 °C, $\leq$ 3 bar H_2) with modest turnover frequencies upto ~ 1000 h^{-1}.[125,145] Currently, Zahmakiran *et al.* were able to provoke solventless hydrogenation of neat benzene at a rate of 5420 h^{-1} using Ru(0) nanoclusters stabilized by Y-type nanozeolite framework under the above mentioned mild reaction conditions.[125] Jacinto *et al.* hydrogenated benzene and toluene at 75 °C and 6 bar hydrogen using supported Pt(0) nanoparticles, turnover frequencies being 1111 and 662 h^{-1} respectively.[151] Rhodium especially activated on carbon-supported Rh(0), is considered the best option for arene hydrogenation as compared to other supported transition metal catalysts.[152] For example, Motoyama *et al.* efficiently catalyzed the benzene hydrogenation using CNT-supported Rh(0) with a turnover frequency of 7750 h^{-1} under 4 bar H_2 pressure at 75 °C.[152] Yoon *et al.* reported the solventless hydrogenation of benzene using Pd – Rh/CNT system at room temperature and 10 bar H_2 with a TOF being 593 h^{-1}.[153] Dyson group used polymer-stabilized rhodium nanoparticles for toluene hydrogenation (95 – 97 % conversion) at 60 °C and 20 bar H_2 for 2 h.[154] Recently, Vanglis *et al.* achieved an exceptionally high catalytic activity (TOF > 204000 h^{-1}) using water-soluble Rh/TPPTS complexes at 80 bar H_2 pressure and 130 °C, turnover frequency being calculated as per mole of hydrogenated C=C units of benzene per mole of Rh per hour.[149] In spite of excellent activity of rhodium towards arene hydrogenation, the recycling of expensive rhodium catalysts is limited due to facile sintering and leaching of metallic rhodium.[155]

Supported ruthenium catalysts are also being studied extensively and several papers have been published during this time. For example, Sharma *et al.* achieved the complete conversion of benzene into cyclohexane within 2 hours using ruthenium containing hydrotalcite clay at 120 °C and 60 bar H_2 pressure.[146] Boricha *et al.* used montmorillonite-supported Ru(0) at 100 °C and 34.5 bar H_2.[156] Marquardt *et al.* reported a turnover frequency of 1570 h^{-1} using graphene-supported Ru(0) at 4 bar H_2 and 75 °C.[157] Rossi *et al.* calculated a turnover frequency of 3550 h^{-1} for benzene hydrogenation under mild reaction conditions (75 °C, 4 bar H_2) using Ru(0) nanoparticles stabilized by imidazolium ionic liquids.[64c] Our group has recently reported that hectorite-supported Ru(0) nanoparticles are also efficient catalyst

for such hydrogenations under mild conditions (50°C, 50 bar H_2) with turnover frequencies being 6531 and 3550 h^{-1} for benzene and toluene respectively.[34a,34c]

In this section, a detailed study for the hydrogenation of arenes (benzene and toluene) over the supported-ruthenium nanoparticles is being presented. The triaqua cationic complex $[(C_6H_6)Ru(H_2O)_3]^{2+}$ was used as precursor of ruthenium nanoparticles. Different support materials such as zeolites (Y and USY type), silicas (SBA-15 and SP-1522) and layered clays (hectorite and montmorillonite) were evaluated with a special emphasis to hectorite-supported ruthenium nanoparticles which proved to be relatively the best choice for such hydrogenations.

3.4.1 Arene Hydrogenation Catalyzed by Ruthenium Nanoparticles in Layered Clays

The hectorite-supported ruthenium nanoparticles **57**, and the montmorillonite-supported ruthenium nanoparticles **74** have been used as catalysts for the hydrogenation of benzene and toluene. Both hectorite and montmorillonite have different swelling properties, hectorite being known for its exceptional swelling (35 times higher).

*Hydrogenation of Benzene Catalyzed by Ru Nanoparticles in Hectorite **57***

Ruthenium nanoparticles intercalated in hectorite are highly active hydrogenation catalysts: Ruthenium(0)-containing hectorite **57** efficiently reduces even benzene to give cyclohexane under mild conditions (50 °C). However, the catalytic activity of **57** crucially depends on the way how the ruthenium(0)-containing hectorite **57** is prepared and conditioned as well as on the solvent used for benzene hydrogenation.

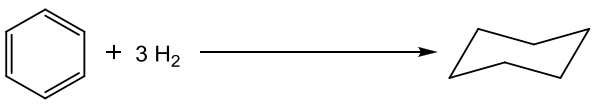

The catalytic activity of the various Ru(0)-hectorite **57** samples obtained by different synthesis and conditioning for the hydrogenation of benzene was studied in various alcohols or in water under a hydrogen pressure of 50 bar at 50 °C. It turned out that ethanol is by far the best solvent for catalytic benzene hydrogenation (Table 10).

Table 10. Benzene hydrogenation using Ru(0)-hectorite **57** prepared by reduction of Ru(II)-hectorite **56** with H_2

Medium for catalyst preparation	Mean particle size (nm)	Solvent for catalytic reaction	Reaction time (h)	Conversion (%)	Activity TOF (h^{-1})[a]
H_2O	38	H_2O	0.5	63	3670
		EtOH	2.2	56	839
H_2O/MeOH (1:1)	21	H_2O/MeOH (1:1)	1.1	71	1874
		EtOH	1.7	39	883
MeOH	10	MeOH	1.9	47	893
		EtOH	0.3	46	5060
EtOH	9	EtOH	0.2	38	6531
Pr^nOH	12	Pr^nOH	1.3	64	1553
		EtOH	0.5	39	3278
Pr^iOH	7	Pr^iOH	0.3	34	4753
		EtOH	0.3	60	5732
Bu^nOH	3 and 27	Bu^nOH	1.4	56	1354
		EtOH	0.6	70	3508
Bu^iOH	4	Bu^iOH	0.4	41	4125
		EtOH	0.2	18	5564

[a]TOF, turnover frequency was calculated as moles of converted benzene per mol Ru per hour

Otherwise, no clear correlation between the catalytic activity and the size nor the shape of the ruthenium(0) nanoparticles intercalated in hectorite can be established. The way how **57** is prepared and conditioned is much more important than particle size and shape. Thus, the Ru(0)-hectorite **57** obtained by reduction of **56** in refluxing alcohols (in the absence of hydrogen) is almost inactive in the original alcohol and become only slightly active after being transferred to ethanol (Table 11).

Table 11. Benzene hydrogenation using Ru(0)-hectorite **57** prepared by reduction of Ru(II)-hectorite **56** in refluxing alcohols

Medium for catalyst preparation	Mean particle size (nm)	Solvent for catalytic reaction	Reaction time (h)	Conversion (%)	Activity TOF (h^{-1})[a]
EtOH	3	EtOH	4.7	34	301
Pr^nOH	2	Pr^nOH	72	0	0
		EtOH	3.2	53	564
Pr^iOH	9	Pr^iOH	72	0	0
		EtOH	57	21	20
Bu^nOH	4	Bu^nOH	182	14	5
		EtOH	2.6	53	684
Bu^iOH	6	Bu^iOH	3.1	37	479
		EtOH	6.9	35	208

[a]TOF, turnover frequency was calculated as moles of converted benzene per mol Ru per hour

By contrast, the Ru(0)-hectorites **57** prepared by reduction of **56** with H_2 in ethanol or other alcohols are more or less catalytically active in the original reaction medium and become even more active if transferred to ethanol, whatever the size (mean values varying from 3 to 27 nm) of the ruthenium nanoparticles is (Table 11). The highest catalytic activity is observed with **57** being prepared with H_2 in ethanol (TOF 6531 h^{-1}). This suggests that the highly active ruthenium nanoparticles (made by H_2 reduction of **56**) contain hydrogen adsorbed at the surface or in the interior.

A special case is the large and medium-sized hexagonally shaped ruthenium-nanoparticles obtained in hectorite by reduction of **56** with molecular hydrogen in water or in aqueous methanol. Despite their regular shapes and sizes, they are quite active for benzene hydrogenation in an aqueous system (TOF 3670 h^{-1} in H_2O or 1874 h^{-1} in H_2O/MeOH, 1:1), but their activity drops sharply by transferring them to ethanol (Table 11). A possible explanation might be that the hexagonal nanoparticles exclusively obtained in the presence of water contain water or hydroxyl groups at the surface which may be blocked or replaced by alcohols.

*Hydrogenation of Toluene Catalyzed by Ru Nanoparticles in Hectorite **57***

The catalytic activity of the Ru(0)-hectorite **57** for the hydrogenation of toluene was studied under a hydrogen pressure of 50 bar at 50 °C. It turned out that ethanol is by far the best solvent for catalytic toluene hydrogenation (Table 12).

Table 12. Toluene hydrogenation using Ru(0)-hectorite **57** prepared by reduction of Ru(II)-hectorite **56** with H_2

Medium for catalyst preparation	Solvent for catalytic reaction	Reaction time (h)	Conversion (%)	Activity TOF (h^{-1})[a]
EtOH	EtOH	-	-	3550
No Solvent	No Solvent	0.5	61	1760

[a]TOF, turnover frequency was calculated as moles of converted benzene per mol Ru per hour

*Hydrogenation of Benzene and Toluene Catalyzed by Ru Nanoparticles in Montmorillonite **74***

The catalytic activity of the Ru(0)-montmorillonite **74** samples for the hydrogenation of benzene and toluene was studied under a hydrogen pressure of 50 bar at 50 °C. It turned out that ethanol is by far the best solvent for catalytic benzene hydrogenation (Table 13).

Table 13. Benzene hydrogenation using Ru(0)-montmorillonite **74** prepared by reduction of Ru(II)-montmorillonite **73** with H_2

Medium for catalyst preparation	Solvent for catalytic reaction	Reaction time (h)	Conversion (%)	Activity TOF (h^{-1})[a]
EtOH	EtOH	20	38	1327
H_2O	H_2O	0.8	37	1543
No Solvent	No Solvent	4.8	28	204

[a]TOF, turnover frequency was calculated as moles of converted benzene per mol Ru per hour

Table 14. Toluene hydrogenation using Ru(0)-montmorillonite **74** prepared by reduction of Ru(II)-montmorillonite **73** with H_2

Medium for catalyst preparation	Solvent for catalytic reaction	Reaction time (h)	Conversion (%)	Activity TOF (h^{-1})[a]
EtOH	EtOH	17	50	86
H_2O	H_2O	16	58	104
No Solvent	No Solvent	18	61	102

[a]TOF, turnover frequency was calculated as moles of converted benzene per mol Ru per hour

3.4.2 Arene Hydrogenation Catalyzed by Ruthenium Nanoparticles in Zeolites

The catalytic activity of the Ru(0)-zeolite (Y- and USY-type) samples for the hydrogenation of benzene and toluene was studied under a hydrogen pressure of 50 bar at 50 °C. It turned out that water is by far the best solvent for catalytic benzene hydrogenation for USY- zeolite supported ruthenium nanoparticles (Table 15). However, Ru(0)-zeolite system proved to be relatively inefficient as compared to Ru(0)-hectorite.

Table 15. Arene hydrogenation using Ru(0)-Y zeolite **77** prepared by reduction of Ru(II)-Y zeolite **76** with H_2

Medium for catalyst preparation	Substrate	Solvent for catalytic reaction	Reaction time (h)	Conversion (%)	Activity TOF (h^{-1})[a]
EtOH	Benzene	EtOH	5.0	26	72
H_2O	Benzene	H_2O	0.6	46	999
No Solvent	Benzene	No Solvent	5.3	6.1	16
EtOH	Toluene	EtOH	48	40	10
H_2O	Toluene	H_2O	22	50	26
No Solvent	Toluene	No Solvent	4.6	40	101

[a]TOF, turnover frequency was calculated as moles of converted benzene per mol Ru per hour

Table 16. Arene hydrogenation using Ru(0)-USY zeolite **80** prepared by reduction of Ru(II)-USY zeolite **79** with H_2

Medium for catalyst preparation	Substrate	Solvent for catalytic reaction	Reaction time (h)	Conversion (%)	Activity TOF (h^{-1})[a]
EtOH	Benzene	EtOH	1.9	25	202
H_2O	Benzene	H_2O	0.5	43	1469
No Solvent	Benzene	No Solvent	4.2	29	111
EtOH	Toluene	EtOH	41	37	12
H_2O	Toluene	H_2O	16	59	49
No Solvent	Toluene	No Solvent	5	47	125

[a]TOF, turnover frequency was calculated as moles of converted benzene per mol Ru per hour

3.4.3 Arene Hydrogenation Catalyzed by Ruthenium Nanoparticles in Silicas

The catalytic activity of the Ru(0)-silica (SP-1522 and SBA-15) samples for the hydrogenation of benzene and toluene was studied at 50 °C under a hydrogen pressure of 50 bar. SP-1522 supported Ru(0) was able to efficiently catalyze the toluene hydrogenation under solventless conditions at a rate of 4169 h^{-1} (Table 17). However, Ru(0)-silica system proved to be relatively inefficient for benzene hydrogenation.

Table 17. Arene hydrogenation using Ru(0)-SP-1522 silica **83** prepared by reduction of Ru(II)-SP-1522 silica **82** with H_2

Medium for catalyst preparation	Substrate	Solvent for catalytic reaction	Reaction time (h)	Conversion (%)	Activity TOF (h^{-1})[a]
EtOH	Benzene	EtOH	0.6	29	1423
H_2O	Benzene	H_2O	0.3	37	3392
No Solvent	Benzene	No Solvent	3.8	58	447
EtOH	Toluene	EtOH	17	43	608
H_2O	Toluene	H_2O	2.0	56	668
No Solvent	Toluene	No Solvent	3.7	64	4169

[a]TOF, turnover frequency was calculated as moles of converted benzene per mol Ru per hour

Table 18. Arene hydrogenation using Ru(0)-SBA-15 silica **86** prepared by reduction of Ru(II)-SBA-15 silica **85** with H_2

Medium for catalyst preparation	Substrate	Solvent for catalytic reaction	Reaction time (h)	Conversion (%)	Activity TOF (h^{-1})[a]
EtOH	Benzene	EtOH	5	26	123
H_2O	Benzene	H_2O	12	37	736
Solventless	Benzene	No Solvent	0.8	89	2566
EtOH	Toluene	EtOH	0.8	65	1634
H_2O	Toluene	H_2O	16	63	92
Solventless	Toluene	No Solvent	21	58	55

[a]TOF, turnover frequency was calculated as moles of converted benzene per mol Ru per hour

In conclusion, silica- and zeolite-supported Ru(0) are found to be relatively inefficient probably due to high cations exchange capacity of these materials. Huge quantities of $[(C_6H_6)Ru(H_2O)_3]^{2+}$ cation intercalate in these materials, which result in large agglomerates of Ru(0) upon H_2 reduction. The size of these agglomerates was found to be 50 – 100 nm. The best results are obtained with hectorite-supported ruthenium nanoparticles.

3.5 Hydrogenation of Furfuryl Alcohol Catalyzed by Ruthenium Nanoparticles in Hectorite

The hydrogenation of furfuryl alcohol (FA) to give tetrahydrofurfuryl alcohol (THFA) is of great importance. It is an environmentally acceptable green solvent which is biodegradable with low toxicity.[158] This green solvent has an octane number of 83 and it is also being investigated for use as an additive in "clean" fuels, allowing diesel and ethanol to be mixed.[159-161] Furfural, THFA's parent compound, is derived from agricultural waste biomass such as rice hulls, corn-cobs and sugarcane bagasse. Thus, THFA is manufactured from renewable sources, which make it a preferred choice for fine chemical synthesis, pharmaceutical formulations, coatings and paint stripper applications.[162]

This great potential of THFA focused our attention on the hydrogenation of FA, but little information is available in this regard. A brief literature survey shows that nickel-based catalysts (alloys or Raney-nickel, promoted or supported) are generally used for this reaction. With these catalysts, the yields are generally high, but the reaction is not very selective. Moreover, drastic pressure and temperature conditions are required. Noble metals (Pd, Pt and Rh) supported catalysts are less efficient than Ni-supported catalysts.[163-168]

Ruthenium nanoparticles intercalated in hectorite are shown to be highly active and selective catalysts for this reaction: Ruthenium(0)-containing hectorite **57** efficiently reduces FA to give THFA under mild conditions, the formation of the usual side-product 2,5-bis(trimethyleneoxy)-1,4-dioxane being avoided.

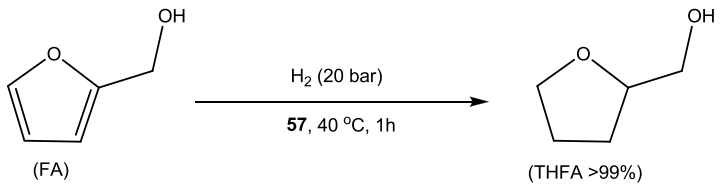

However, the catalytic activity of **57** crucially depends on the way how the ruthenium(0)-containing hectorite **57** is prepared and conditioned as well as on the solvent used for FA hydrogenation. The effects of various factors on the course of FA hydrogenation were evaluated in order to determine suitable conditions for maximum FA conversion and highest possible selectivity towards THFA.

3.5.1 Influence of the Various Solvents on Catalyst Behavior

Solvents are known to have a significant effect on the rate of catalytic hydrogenation. The effect of solvent is attributed to various factors, which include solubility of hydrogen, thermodynamic interaction of solvent with reactant and product, competitive adsorption of solvent, etc.[169] Yellow hectorite **56** was reduced in 10 mL of different polar solvents (Fig. 31a) under a pressure of hydrogen (50 bar) at 100 °C for 14 h. The hydrogenation of FA was evaluated by adding 1mL of FA under a pressure of hydrogen (25 bar) at 50 °C for 2h while stirring vigorously. The effect of various solvents on FA hydrogenation is shown in Fig. 31a. Methanol resulted in a maximum FA conversion and in the highest yield of THFA. The use of other alcohols as solvent decreased the yield. In non alcoholic solvents, the catalyst was almost inactive. This high yield in alcoholic solvents, especially in methanol, may be attributed to an increase in the concentration of dissolved hydrogen and therefore to an increase in the general reaction rate.[163,170-171]

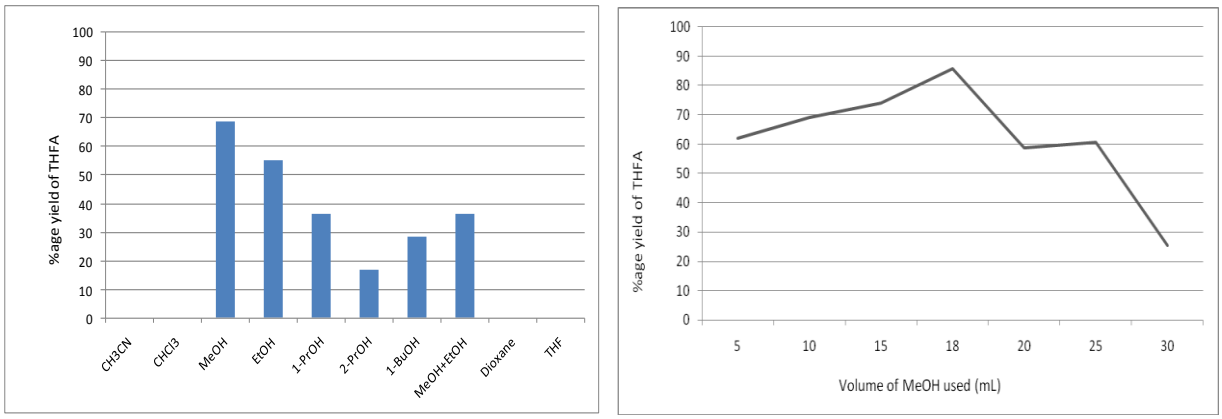

Fig. 31 Effect of different solvents on FA hydrogenation (**a**) Effect of different volumes of MeOH on FA hydrogenation (**b**)

3.5.2 Influence of the Solvent Volume on the Catalyst Performance

In order to find the optimal volume of methanol for the hydrogenation of FA, the ruthenium(0) nanoparticles in **57** were obtained by reducing yellow hectorite **56** in different volumes (mL) of methanol (Fig. 31b) under a pressure of hydrogen (50 bar) at 100 °C for 14 h. Hydrogenation of FA was done by adding 1mL of FA under a pressure of hydrogen (25 bar) at 50 °C for 2h while stirring vigorously. The optimal volume of methanol for the highest

yield of THFA was found to be 18 mL. For further experiments, this volume of methanol was used to prepare ruthenium (0) nanoparticles in **57**.

3.5.3 Influence of Pressure and Temperature on the Catalyst Performance

The effect of reaction temperature was studied in the range of 40 – 60 °C with different hydrogenation partial pressures (Fig. 32). It was observed that reaction temperature has a pronounced effect on the catalytic behavior of the ruthenium(0) nanoparticles in **57** as evident from the graphical representation of experimental results. When yellow hectorite **56** was reduced in MeOH (18 mL) under a pressure of hydrogen (50 bar) at 100 °C for 14 h, a black suspension of the ruthenium(0) nanoparticles **57** in methanol was obtained. For the hydrogenation of FA (1 mL) over these ruthenium(0) nanoparticles, the optimal conditions found were 40 °C under 20 bar hydrogen partial pressure.

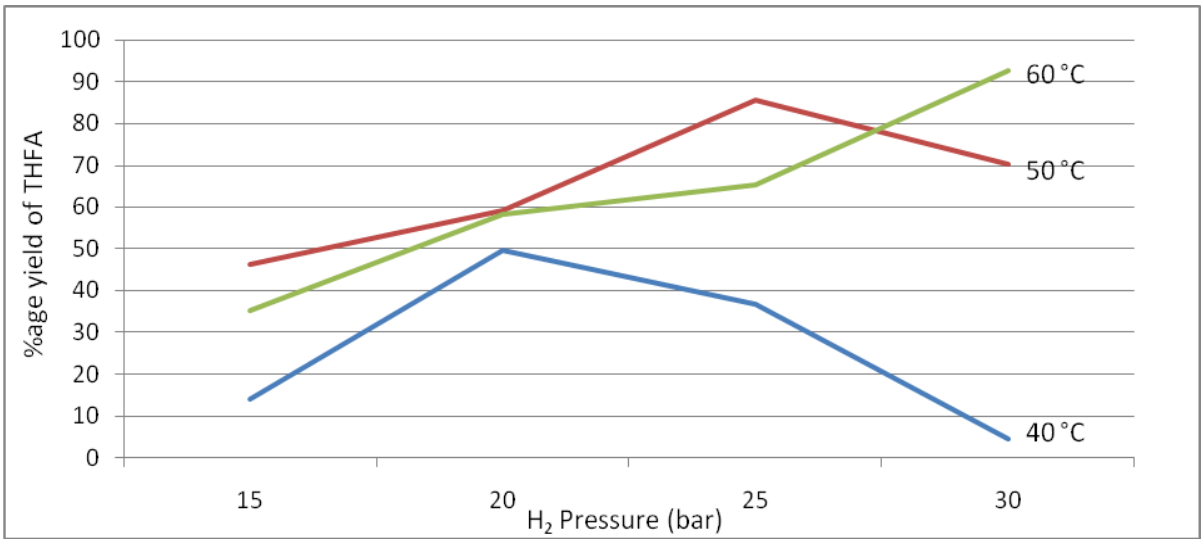

Figure 32. Effect of pressure and temperature on FA hydrogenation

3.5.4 Evaluation of Selectivity and Activity

The hydrogenation of FA was done by using **57**, obtained by reduction of **56** in methanol (18 mL) under a pressure of hydrogen (50 bar) at 100 °C for 14 h. GC-MS analysis shows complete conversion of FA (100 %) into THFA. The commercial production of THFA by the hydrogenation of FA over Ni-based catalysts usually results in the formation of a number of by-products attributable to hydrogenolysis[172] or hydrolytic ring cleavage.[173] In

practice, these are separated by fractional distillation, being recovered as a low-boiling fore-run and a high-boiling residue. Formation of by-products such as 2,5-bis(trimethyleneoxy)-1,4-dioxane, is a common problem during catalytic FA hydrogenation.[174] However, these side-reactions do not occur during the catalytic hydrogenation of FA over **57**, and only traces of 1,2-pentandiol was observed. The overall selectivity of **57** towards THFA was >99%. The turnover number was determined by adding 0.2 mL of FA after regular intervals (1 h), until the catalyst became almost inactive, the total volume of substrate added being 2 mL (Table 19).

Table 19. Furfuryl alcohol hydrogenation using Ru(0)-hectorite **57** in methanol by adding fresh substrate each hour

Cat. Run	FA Conversion (%)	Time (h)	TON	THFA Selectivity (%)
1	100	1	144	100
2	100	1	142	98.7
3	100	1	143	99.6
4	100	1	144	99.8
5	100	1	144	99.8
6	100	1	144	99.9
7	100	1	142	98.9
8	100	1	142	98.6
9	94.8	1	136	99.3
10	100	2	142	98.7

The size distribution of the ruthenium(0) nanoparticles in **57** was studied by transmission electron microscopy. The mean particle size of ruthenium(0) nanoparticles in **57** was found to be ~ 4 nm having σ > 25% of the mean particle size (Fig. 33).

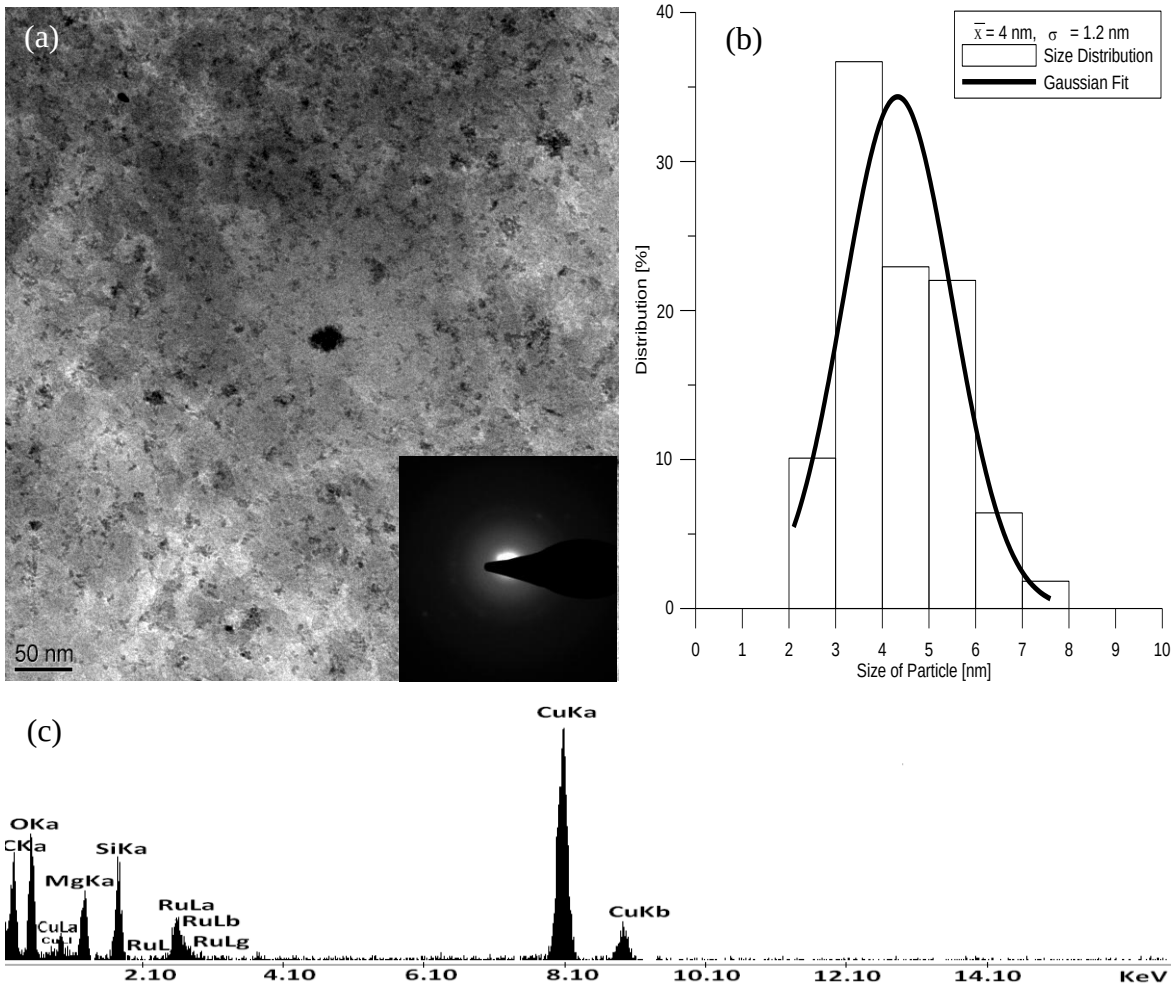

Figure 33. TEM micrograph with SAED (**a**) histogram (**b**) and EDS analysis (**c**) of ruthenium(0) nanoparticles in **57** prepared by reduction of **56** in methanol (18 mL) at 100 °C under 50 bar H_2

3.5.5 Recycling and Regeneration

Once the ruthenium nanoparticles became inactive, the ruthenium(0)-hectorite **57** was recycled by washing three times with methanol (3x18 mL). The recycled ruthenium(0)-hectorite **57** regained their activity by transforming FA into THFA selectively (selectivity upto 100%). However, a decrease in TOF was observed for these recycled nanoparticles as evident from time of reaction (see Table 20).

Table 20. Furfuryl alcohol hydrogenation using recycled Ru(0)-hectorite **57**

Cat. Run	FA Conversion (%)	Time (h)	TON	THFA Selectivity (%)
1	100	2	142	98.7
2	100	2	144	100
3	100	2	144	100

It was also observed that presence of air during the catalytic reaction results in a loss of activity and selectivity. But this inactive catalyst can be regenerated by reacting the thoroughly washed suspension of recycled ruthenium(0)-hectorite **57** in a magnetically stirred stainless-steel autoclave (volume 100 mL) with H_2 (50 bar) at 100 °C for 14 h in methanol (18 mL). This regenerated ruthenium(0)-containing hectorite **57** was also able to selectively produce THFA with a selectivity upto 100% (Table 21).

Table 21. Furfuryl alcohol hydrogenation using regenerated Ru(0)-hectorite **57**

Cat. Run	FA Conversion (%)	Time (h)	TON	THFA Selectivity (%)
1	100	2	144	100
2	100	2	143	99.1
3	100	2	143	99.6

Transmission electron microscopy (TEM) images of these recycled and regenerated ruthenium(0) nanoparticles in **57** show particles varying from 2 to 18 nm (Fig. 19 and 20). These nanoparticles are still crystalline in nature with an average size of 6 nm ($\sigma = 2$) and 9 nm ($\sigma = 3$) respectively. Thus decrease in TOF can be attributed to decrease in overall surface

area of these recycled ruthenium nanoparticles as evident from an increase in particle size during the course of catalytic reactions.

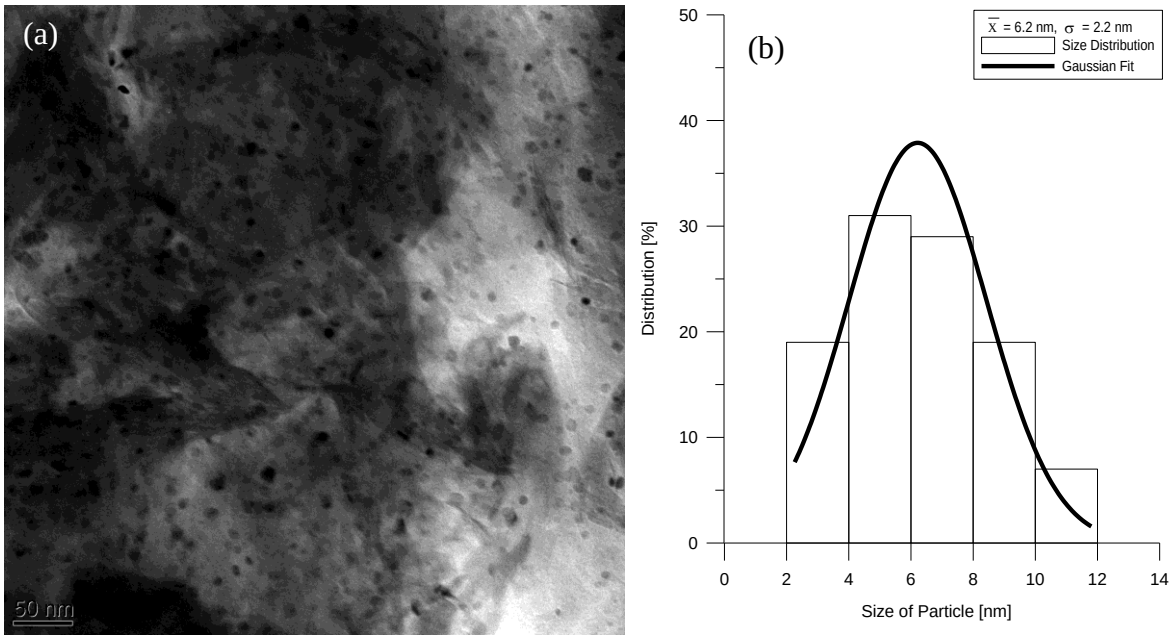

Figure 34. TEM micrograph (**a**) histogram (**b**) of recycled ruthenium(0) nanoparticles in **57**

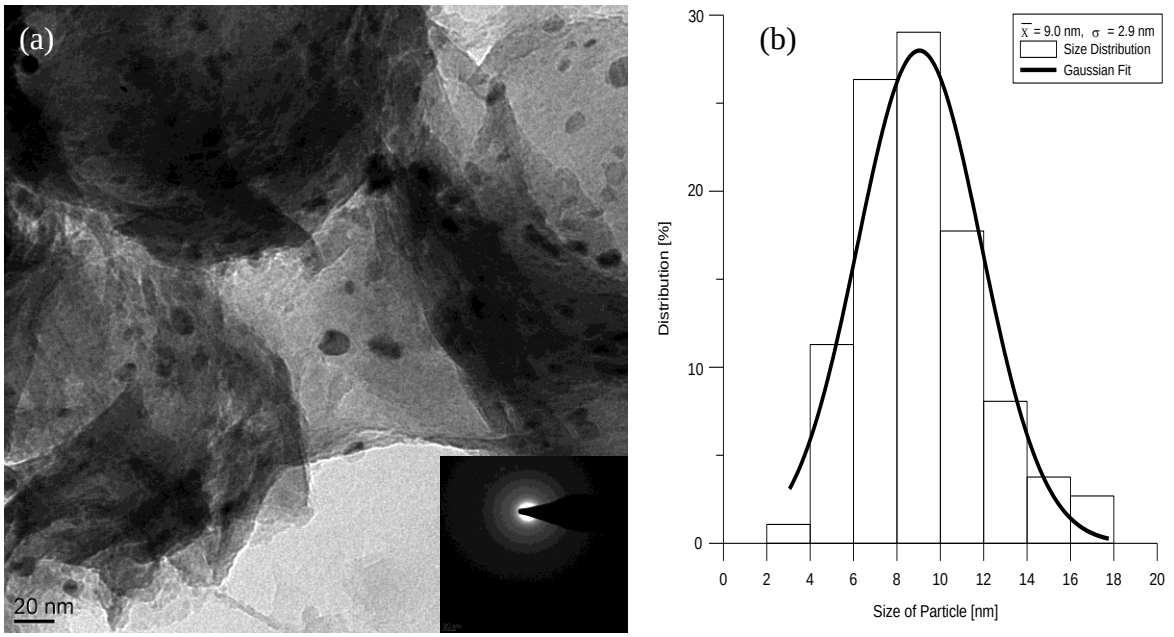

Figure 35. TEM micrograph with SAED (**a**) histogram (**b**) of ruthenium(0) nanoparticles in **57** after regeneration

In conclusion, ruthenium nanoparticles intercalated in hectorite are found to efficiently catalyze the hydrogenation of FA at low temperatures. The best results were obtained at 40 °C

under a hydrogen pressure of 20 bar (conversion 100%, selectivity > 99%, TOF = 177, TON = 1423). Hectorite-supported ruthenium nanoparticles can be recycled and regenerated.

3.6 Selective C=C Hydrogenation of α,β-Unsaturated Ketones Catalyzed by Ruthenium Nanoparticles intercalated in Hectorite

Chemoselective hydrogenation of α,β-unsaturated carbonyl compounds is useful in the preparation of fine chemicals, flavours, hardening of fats, pharmaceutical manufacturing processes and in the synthesis of various organic intermediates and solvents.[175] The selectivity of the reaction is a problem and requires specific reaction conditions and catalyst systems. In heterogeneous catalysts, the effect of metal-support interaction also plays an important role in determining the selectivity of the reaction.[176] Therefore, the design of nanocomposites consisting of functional metals and adequate matrices is a challenge for the fabrication of recyclable catalysts. Highly active metallic nanoparticles must be stabilized by a suitable support in order to prevent aggregation to bulk metal.[123] Hectorite is a naturally occurring clay, belonging to the smectite family of layered minerals. These materials are composed of individual platelets containing a metal oxide center sandwiched between two silicon dioxide outer layers.[177] Included in this group of minerals are sodium hectorite, bentonite (montmorillonite), saponite, vermiculite, kenyaite, volkonskoite, sepiolite, beidellite, magadiite, nontronite and sauconite. Of these, hectorite is the most important one because of its exceptional swelling properties. It can be defined as layers of negatively charged two dimensional silicate sheets held together by cationic species in the interlaminar space, which are susceptible to ion exchange. [34b,34c,178,179] Ruthenium-supported hectorite obtained by ion exchange has been reported by Shimazu *et al.* using $[Ru(NH_3)_6]^{2+}$ cations[180] and by our group using $[(C_6H_6)Ru(H_2O)_3]^{2+}$ cations[34a,34c] or $[(C_6H_6)_4Ru_4H_4]^{2+}$ cations[135] for the intercalation. These materials show high catalytic activity for the hydrogenation of olefins[180] and of aromatic compounds.[34a,34c] Recently, we reported the highly selective low-temperature hydrogenation of furfuryl alcohol to tetrahydrofurfuryl alcohol catalyzed by hectorite-supported nanoparticles.[181]

The hydrogenation of α,β-unsaturated ketones implies either the olefinic C=C bond or the carbonyl C=O bond, or both of them. In addition, side reactions have to be considered as well.[176] Supported metals such as platinum, rhodium, ruthenium, gold, nickel, aluminum, copper and iron are reported to be active for the hydrogenation of α,β-unsaturated ketones.[182]

However, in most cases the selectivity for C=C bond hydrogenation is only high at low conversion.[183,184] Therefore, palladium is conventionally used to selectively reduce C=C bond in unsaturated carbonyl compounds.[184,185] Complex metal hydrides such as potassium triphenylborohydride and lithium aluminum hydride-copper(I) iodide also show a good selectivity (upto 99 %) for olefinic bond hydrogenation in both cyclic and acyclic enones, but they result in the production of substantial amounts of waste.[186] Some organometallic complexes are also highly selective towards the hydrogenation of C=C bond in α,β-unsaturated ketones under milder conditions.[187] These complexes are sensitive to permanent deactivation and show all disadvantages of homogeneous catalysts. Metal-free approaches towards such hydrogenations are almost futile with 75% selectivity towards saturated ketones.[188]

We have been interested in the influence of increasing steric hindrance at the C=C bond of α,β-unsaturated ketones on the selectivity of the hydrogenation using our hectorite-supported nano-ruthenium as catalyst. Therefore, 3-buten-2-one, 3-penten-2-one and 4-methyl-3-penten-2-one have been studied. Of these three substrates, 4-methyl-3-penten-2-one is the most important industrial precursor; it is also called mesityl oxide which, upon selective hydrogenation, gives methyl isobutyl ketone. Methyl isobutyl ketone is an important commercial solvent with a reported world consumption of 295 thousand metric tons in 2007.[189]

Traditionally, methyl isobutyl ketone is manufactured via a three-step process in which acetone condensation gives diacetone alcohol which readily dehydrates into mesityl oxide. The olefinic C=C bond in mesityl oxide is then selectively hydrogenated to methyl isobutyl ketone avoiding further C=O reduction into methyl isobutyl carbinol.

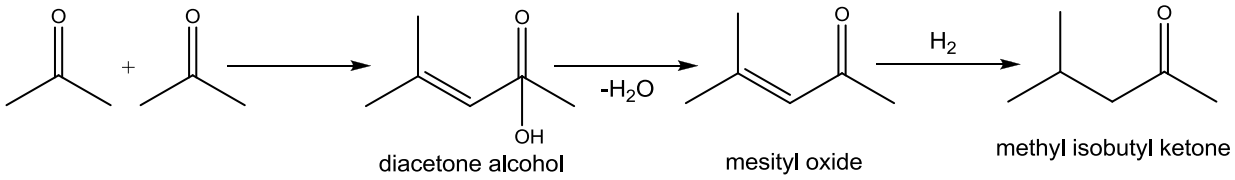

Scheme 22

Methyl isobutyl ketone production may also be achieved by using a bifunctional catalyst to facilitate all three reaction steps in a single step. A 20 – 60 % conversion of acetone with 30 – 90 % selectivity for methyl isobutyl ketone is observed for these single-step processes under harsh reaction conditions (80 – 160 °C, 10 – 100 bar H_2).[175b,190] Thus, the methyl isobutyl ketone concentration in the effluent is typically less than 30 wt%

necessitating further purification steps.[175b] The large-scale production of methyl isobutyl ketone still follows a three-step route[191] involving mesityl oxide hydrogenation into methyl isobutyl ketone at 150-200 °C and 3-10 bar H_2 using Cu or Ni catalysts[192] or, alternatively, on a supported palladium catalyst at 80-220 °C.[185d-185f] It is therefore desirable to find alternative green processes which produce methyl isobutyl ketone under mild reaction conditions. Metallic ruthenium nanoparticles intercalated in hectorite are promising as catalysts, since they can be easily handled and recycled.

Here, we report ruthenium nanoparticles (~7 nm) intercalated in hectorite to be a highly productive (conversion 100%, turnover number 765 – 91800) and highly selective (selectivity > 99.9 %) reusable catalyst for the hydrogenation of various industrially important α, β-unsaturated ketones under mild conditions (ethanol solution, 35 °C, 1-10 bar H_2). To the best of our knowledge, such a high selectivity with a complete conversion of mesityl oxide into methyl isobutyl ketone at mild conditions has never been reported in the published literature, except for a sodium hydride containing complex reducing agent of the type NaH – *t*-AmONa – $Ni(OAc)_2$, but giving only a turnover number of 20.[186e]

3.6.1 Preparation of the Catalyst

A freshly prepared suspension (5 mL) of ruthenium(0)-containing hectorite **57** was prepared for selective hydrogenation. The ruthenium loading of the black hectorite **57** was assumed to be 3.2 wt%, based upon the molar ratio of $[(C_6H_6)Ru(H_2O)_3]^{2+}$ used (corresponding to 75% of the experimentally determined cation exchange capacity of **55**), and the presence of metallic ruthenium was proven by its typical reflections in the X-ray diffraction pattern. The size distribution of the ruthenium(0) nanoparticles in **57** was studied by transmission electron microscopy. The micrographs show particles of a size up to 18 nm. At the edges of superimposed silicate layers nanoparticles are visible, the lighter tone of which is typical for intercalated particles. The mean particle size and standard deviation (σ) were estimated from image analysis of *ca.* 500 particles at least.

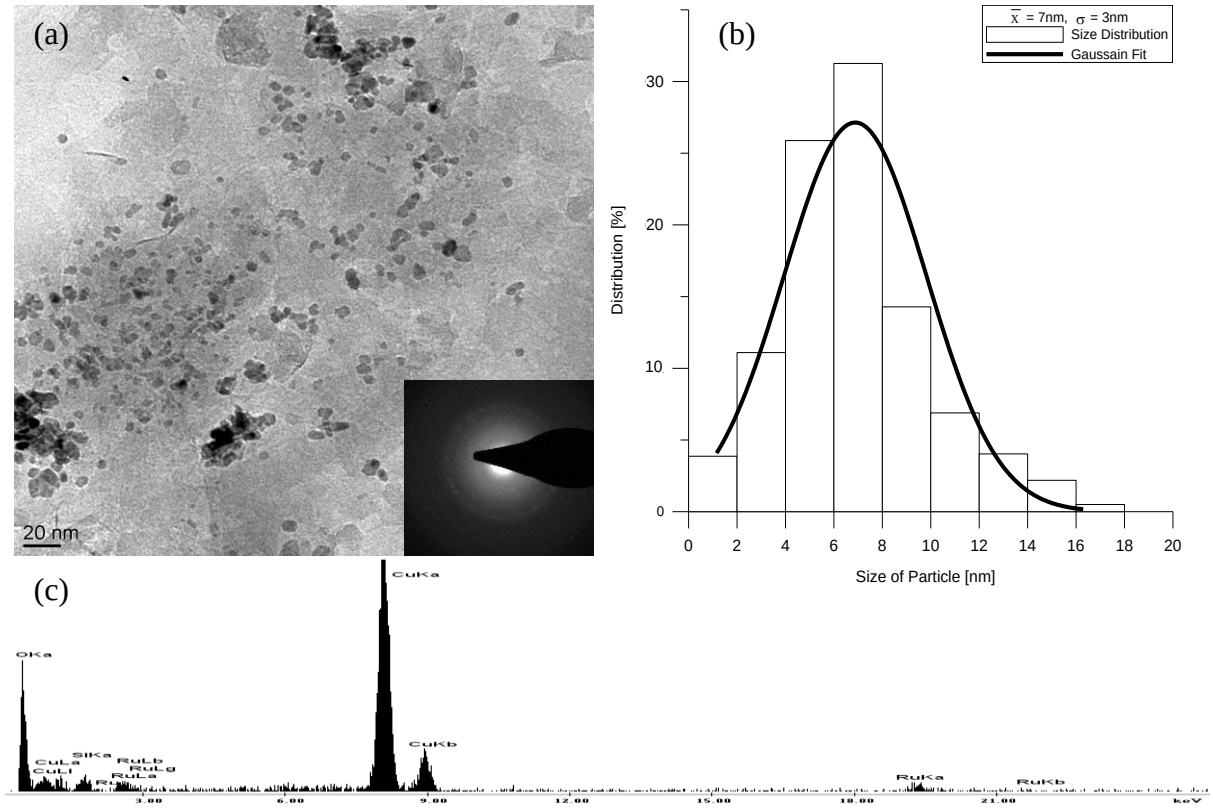

Figure 36. TEM micrograph with SAED (**a**) histogram (**b**) and EDAX analysis (**c**) of ruthenium(0) nanoparticles in **57** prepared by reduction of **56** in ethanol (5 mL) at 100 °C under 50 bar H_2

A comparison of the diffractogram for ruthenium(0)-containing hectorite **57** with the powder pattern of sodium-containing hectorite **55** and ruthenium(II)-containing hectorite **56** is shown in Fig. 37. The d-spacing value (d001 = 17.8 Å) is significantly higher for 3 than that of 1 (d001 = 13.32 Å). The ruthenium(II)-containing hectorite 2 also shows a slight shift (d001 = 14.08 Å) as compared to that of 1. Peaks of the Ru phase are not observed, which is presumably due to the low concentration of Ru nano-crystallites, the peaks of which being hidden by the high hectorite background.

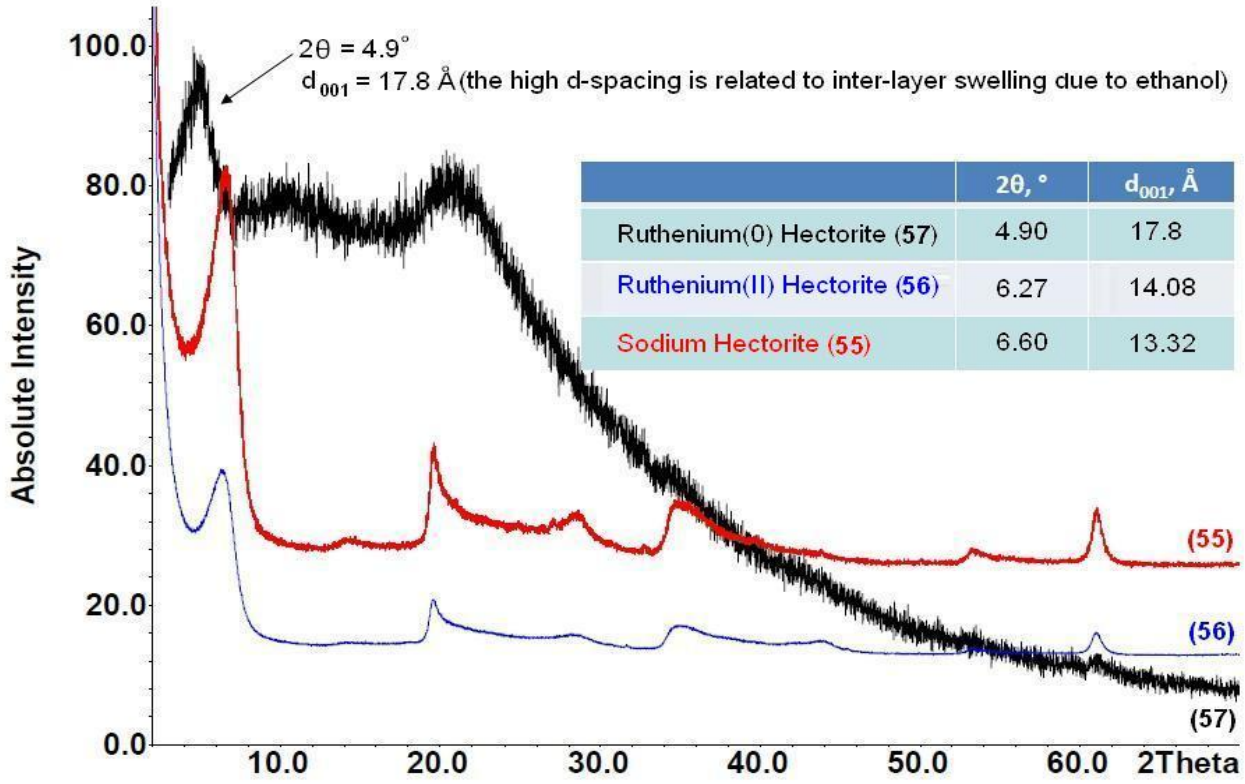

Figure 37. XRD pattern for sodium-containing hectorite **55**, ruthenium(II)-containing hectorite **56** and Ru(0)-containing hectorite **57**

3.6.2 Catalytic Reaction

These ruthenium nanoparticles intercalated in hectorite are highly active and selective hydrogenation catalysts: Ruthenium(0)-containing hectorite **57** efficiently reduces different α, β-unsaturated ketones to give saturated ketones under mild conditions, the formation of the alcohols (saturated and unsaturated) being avoided.

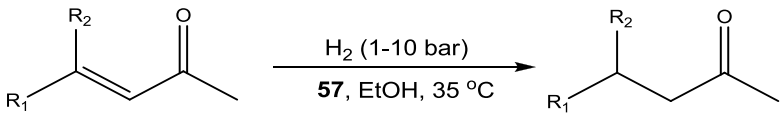

Scheme 23

Table 22. Selective hydrogenation of different α,β-unsaturated ketones by metallic ruthenium nanoparticles intercalated in hectorite.

Substrate	Pressure (bar)	Temp (°C)	Time[a] (h)	Conversion (%)	Selectivity (%)	TOF[b] (h^{-1})	TON[c]
3-buten-2-one	1	35	2	100	>99.9	822	765
3-penten-2-one	7	35	1	100	>99.9	1254	3825
4-methyl-3-penten-2-one	10	35	1	100	>99.9	1212	91800

[a]Time required for 100% conversion of 12.2 mmol unsaturated ketones into saturated ketones, [b]Turnover frequency calculated as moles of saturated ketone per mol ruthenium per hour for 12.2 mmol substrate hydrogenation after 25 minutes, [c]Total turn over number (until the catalyst loses its selectivity or activity).

The highly productive reduction of mesityl oxide to methyl isobutyl ketone by hectorite-supported ruthenium nanoparticles is striking, especially, since no traces of further C=O reduction (methyl isobutyl carbinol) observed. This highly selective C=C bond hydrogenation is also observed for other α,β-unsaturated ketones. Low catalyst loading is capable of reducing only the olefinic double bond. Molar ratio of converted substrate to catalyst decreased in the order 4-methyl-3-penten2-one > 3-penten-2-one > 3-buten-2-one in the direction of decreasing steric hinderance. The increasing steric hinderance in the substrate requires increased hydrogen pressure : while 3-buten-2-one is hydrogenated under 1 bar hydrogen pressure, for 3-penten-2-one a hydrogen pressure of 7 bar is required, and for the bulkiest substrate 4-methyl-3-penten-2-one 10 bar. However, the selectivity for C=C bond hydrogenation is not reduced by the high pressure (Table 22). It is likely that the absence of bulky substituents on the conjugated C=C double bond of 3-buten-2-one favors stable adsorption of the product on catalytic sites. The high selectivity for the C=C bond hydrogenation of these α,β-unsaturated ketones can be tentatively attributed to the activation of the C=C bond by the metal-support interaction.[193] It can be assumed that hectorite probably modifies the electronic properties of ruthenium which in turn leads to an increase in the hydrogenation selectivity for the C=C bond. Thus, the specific hydrogenation tendency of α,β-unsaturated ketones can be interpreted in terms of an exclusive adsorption of C=C bonds at the surface of these nanoparticles. The same metal-support effect was observed in the highly selective C=C bond hydrogenation of furfuryl alcohol by hectorite-supported ruthenium nanoparticles.[181]

Ruthenium nanoparticles intercalated in hectorite are found to efficiently catalyze the hydrogenation of α,β-unsaturated ketones at mild conditions. The best results were obtained at 35 °C under a constant hydrogen pressure of 1-10 bar (conversion 100 %, selectivity > 99.9 %). Surprisingly, an exceptionally high catalytic activity is observed in the case of mesityl oxide hydrogenation. Methyl isobutyl ketone is produced in high yield with essentially all of mesityl oxide converted to methyl isobutyl ketone, and further hydrogenation of methyl isobutyl ketone does not occur. Hectorite-supported ruthenium nanoparticles can be recycled and reused.

3.7 Selective C=O Hydrogenation of α,β-Unsaturated Ketones Catalyzed by Ruthenium Nanoparticles Intercalated in Hectorite

Selective hydrogenation of the carbon-oxygen bond in α,β-unsaturated carbonyl compounds is a synthetic challenge, since the C=C bond reduction is thermodynamically more favorable (35 kJ mol^{-1}) than the C=O bond reduction.[194] This problem becomes even more complicated by the presence of an aromatic substituent in such systems due to a possible ring hydrogenation.[176] Moreover, the transformation of unsaturated ketones into unsaturated alcohols is more difficult than that of unsaturated aldehydes, because ketones are sterically more hindered.[195] In addition, the "promoter effect" to enhance the selectivity is also absent in case of unsaturated ketones.[196]

In a pioneering study, Szöllosi *et al.* evaluated the potential of different metals such as Pt, Pd, Rh, Ru, Cu and Ni supported on silica for the selective hydrogenation of α,β-unsaturated ketones.[197] Later on, von Arx *et al.* were able to attain chemoselectivities >90 % for a sterically hindered C=O bond in ketoisophoron over alumina-supported Pt and Pd catalysts.[198] Such a remarkable selectivity might be attributed to steric effects,[194b,176] because the presence of bulky substituents at the olefinic double bond presumably hampers its adsorption at catalytic sites.[193] Milone *et al.* and Mertens *et al.* showed that unsaturated alcohols can be obtained from different α,β-unsaturated ketones with a selectivity higher than 60 % at a conversion of 90 % using a gold catalyst.[196,199] Recently, Wang *et al.* also used gold supported on mesostructured CeO_2 to hydrogenate *trans*-4-phenyl-3-penten-2-one at 100 °C with 63% selectivity for the unsaturated alcohol.[200] However, in spite of extensive studies, efforts to selectively hydrogenate α,β-unsaturated ketones to give the corresponding unsaturated alcohols by molecular hydrogen have not been very successful.[199a, 200]

Thus, the synthesis of unsaturated alcohols is mainly achieved with hazardous metal hydrides such as $LiAlH_4$ and $NaBH_4$,[201] silicon hydrides[202] or by transfer hydrogenation[196a,203] including Meerwein-Ponndorf-Verley-type reduction methods.[204] Homogeneous transition metal catalysts show sometimes high selectivity,[205] but such complexes are often inefficient or have limited reusability.[206] Moreover, the separation of these complexes from the reaction mixture is very difficult.[207] Thus, the development of a highly selective, easily recoverable and recyclable heterogeneous catalyst for the hydrogenation of unsaturated ketones remains a demanding task,[194a] because unsaturated alcohols are important intermediates used in the production of fine chemicals, pharmaceuticals, perfumery and food processing industries.[208]

3.7.1 Preparation of the Catalyst

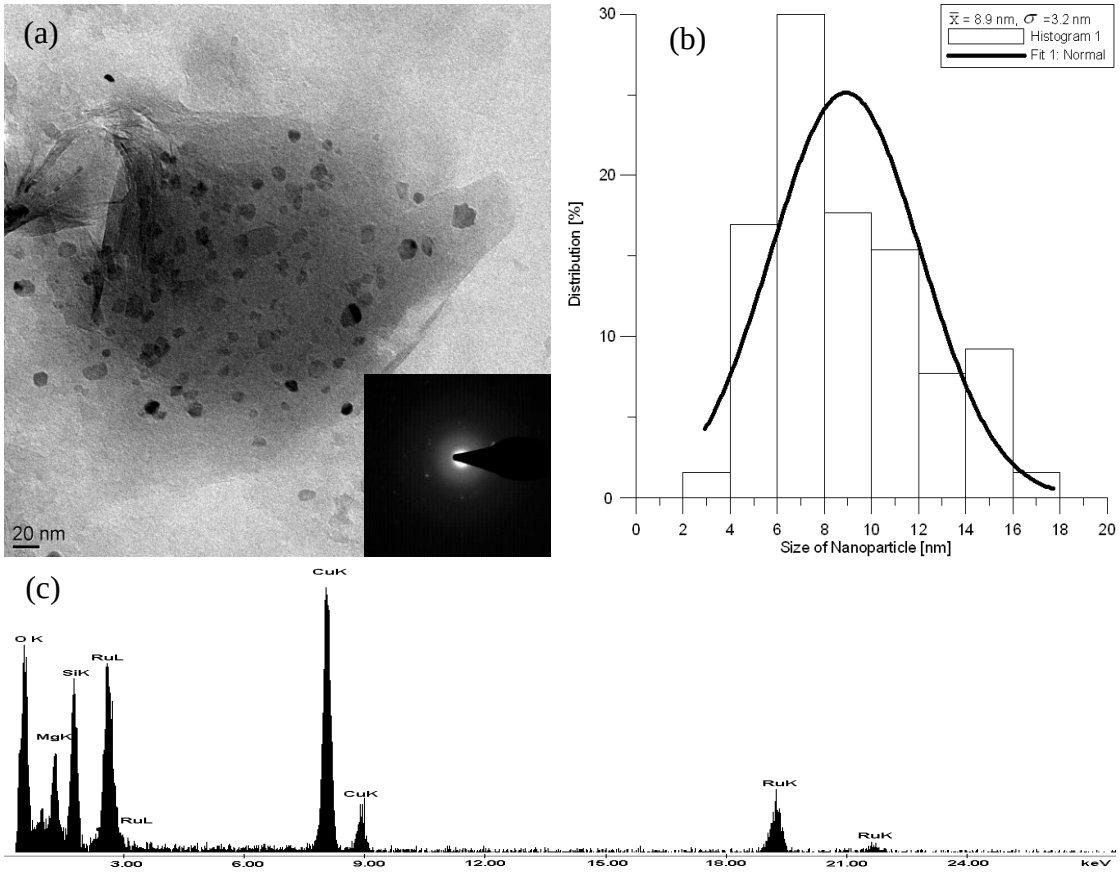

Figure 38. TEM micrograph with SAED (**a**) histogram (**b**) and EDAX analysis (**c**) of ruthenium(0) nanoparticles in **57** prepared by reduction of **56** in ethanol (10 mL) at 100 °C under 50 bar H_2

A freshly prepared suspension (10 mL) of ruthenium(0)-containing hectorite **57** was prepared for selective hydrogenation. The size distribution of the ruthenium(0) nanoparticles

in **57** was studied by transmission electron microscopy (TEM). The initial micrograph analysis shows particles of a size ranging from 2 to 18 nm. At the edges of superimposed silicate layers nanoparticles are visible, the lighter tone of which is typical for intercalated particles. The mean particle size and standard deviation (σ) were estimated from image analysis of *ca.* 100 particles at least.

3.7.2 Catalytic Reaction

These ruthenium nanoparticles intercalated in hectorite are highly active and selective hydrogenation catalysts: Ruthenium(0)-containing hectorite **57** efficiently reduces C=O bond of an unconstrained α, β-unsaturated ketone to give unsaturated alcohol under mild conditions, the formation of the ketones and saturated alcohols being avoided.

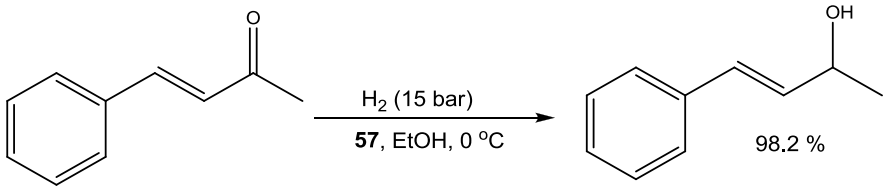

Scheme 24

The high selectivity for the C=O bond hydrogenation of *trans*-4-phenyl-3-penten-2-one can be attributed to the activation of the C=O bond due to metal-support interaction, presumably provoked by an excessive use of solvent (50 mL EtOH) and low temperature. It can be anticipated that a 100 % selectivity for unsaturated alcohol in this case can be attained by further increasing the volume of solvent and decreasing the reaction temperature up to -10 °C.

Ruthenium nanoparticles intercalated in hectorite are found to efficiently catalyze the hydrogenation of α,β-unsaturated ketones at mild conditions. The best results were obtained at 0 °C under a constant hydrogen pressure of 15 bar (conversion 100 %, selectivity 98.2 %, initial turnover number 751). The remaining 1.8 % are totally hydrogenated product *viz.* 4-cyclohexylbutan-2-ol.

4

Ruthenium Nanoparticles Supported on Magnetite Cores

4.1 State of the Art: Superparamagnetic Core-Shell Nanoparticles

In chemical technology heterogeneous catalysts are usually preferred, because separation, recovery and recycling of the catalyst are relatively easy.[209] However, in liquid-phase batch reactions, the separation of the catalyst from the reaction products is still problematic.[210] Therefore, environmentally friendly and cost-effective, robust, easily recoverable and cleanly reusable catalysts would be highly desirable[82] to ensure minimum loss, enhance their lifetime and minimize the consumption of auxiliary substances used in achieving separations.[210]

Recently, the use of magnetic materials as catalyst support has attracted much attention,[82] because solid catalysts with magnetic properties can efficiently be separated from the reaction mixture by applying an external magnetic field.[211] This green and sustainable approach has many advantages over traditional time- and solvent-consuming processes, since it is a fast, economical and environmentally acceptable way of product separation and catalyst recycling.[210]

Superparamagnetic nanoparticles are such materials with high surface area.[212] They can be easily dispersed in solution, because they are intrinsically non-magnetic and therefore show no tendency to aggregate in solution.[209] On the other hand, these nanoparticles can be

recovered easily from the reaction mixture by applying an external magnetic field, thus offering better handling properties.[210]

4.2 Superparamagnetic Nanoparticles Containing a Magnetite Core and a Metallic Ruthenium Shell

Nano-sized magnetite (Fe_3O_4) is prepared by the co-precipitation method,[96,213a] adding the aqueous solution of a 1 : 2 mixture of $FeCl_2$ and $FeCl_3$ to ammonia (0.7 M), followed by vigorous stirring. The black Fe_3O_4 nanoparticles thus obtained are sensitive to air and must be handled in an inert atmosphere.[214] NH_4^+ cations adsorbed at the surface of these particles are partially exchanged against Na^+ by adjusting the pH to 10 using NaOH (2M).[213b] The Fe_3O_4 nanoparticles containing Na^+ and NH_4^+ at their surface are isolated from the solution by magnetic decantation and further used without washing with water.

$$Fe^{2+}_{(aq)} + 2\,Fe^{3+}_{(aq)} + 8\,OH^-_{(aq)} \longrightarrow Fe_3O_{4(s)} + 4\,H_2O_{(l)}$$

When the yellow solution obtained by dissolving the dinuclear complex $[(C_6H_6)RuCl_2]_2$ in water is added to magnetite nanoparticles described above, the main hydrolysis product $[(C_6H_6)Ru(H_2O)_3]^{2+}$ adsorbs on the surface of nano-sized Fe_3O_4, replacing the appropriate amount of counter ions, to give the ruthenium(II)-modified magnetite **87**. This material is isolated by magnetic decantation, washed with deoxygenated water and dried under vacuum. Inductively coupled plasma–optical emission spectroscopy (ICP–OES) analysis of this material shows a ruthenium loading of 0.074 mmol per gram of Fe_3O_4. Fourier transform infrared (FT-IR) spectrum indicates the presence of an absorption band at 576 cm^{-1} that can be assigned to Fe–O vibrations of bulk Fe_3O_4.[215]

Ruthenium(II)-modified magnetite **87** reacts with hydrogen under pressure (50 bar) at 100 °C in n-BuOH by reduction of the adsorbed $[(C_6H_6)Ru(H_2O)_3]^{2+}$ species to metallic ruthenium to give core-shell-type Fe_3O_4/Ru nanoparticles **88** (Scheme 25), in a similar way as hectorite-supported ruthenium nanoparticles are prepared.[34a,34c,181]

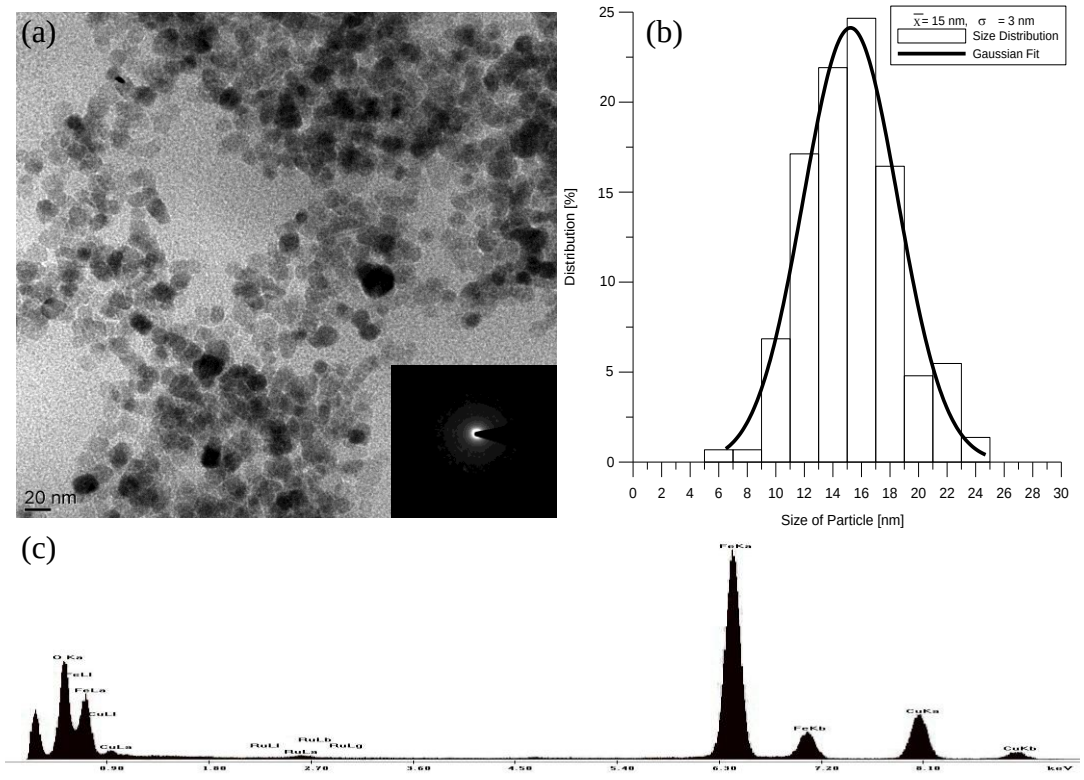

Figure 39. TEM micrograph with SAED (**a**) histogram (**b**) and EDAX analysis (**c**) of core-shell-type Fe_3O_4/Ru nanoparticles **88**

Fig. 39 shows the TEM micrograph of **88**. The size distribution of the ruthenium(0) nanoparticles was studied by transmission electron microscopy (TEM). The mean particle size was calculated by using the equation:[120]

$$\bar{d} = \sum n_i d_i / n_i$$

Where $\bar{d}$ is the mean particle size, d_i is the individual particle size and n is the total number of particles measured. Some aggregation of the nanoparticles were observed, presumably because n-BuOH is not very effective in preventing the aggregation of these particles. However, n-BuOH favors the substrate accessibility to catalytically active sites on the nanoparticles.[216] The micrographs show particles varying from 5 to 25 nm, the average particle size being 15 nm, which is close to the boundary between superparamagnetic and single domains. The mean particle size and standard deviation (σ) were estimated from image analysis of *ca.* 100 particles at least. The presence of ruthenium was inferred from energy dispersive X-ray spectroscopic (EDAX) analysis, which was further confirmed by inductively coupled plasma optical emission spectroscopy (ICP-OES).

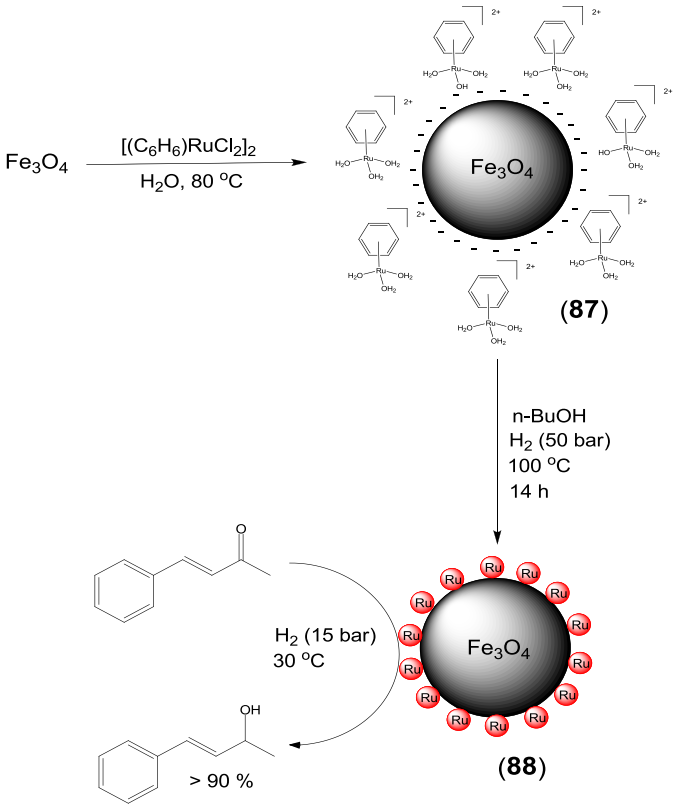

Scheme 25. Synthesis of superparamagnetic core-shell-typeFe_3O_4/Ru nanoparticles and their catalytic action

The X-ray powder diffraction (WAXS) of Ru(0)-modified magnetite **88** nanoparticles is shown below (Fig. 40). The average crystallite size of 14.4 nm was estimated by applying Scherrer formula[217] on the full widths at half maximum (0.89) of the strongest (100 %) reflection, the value of 2θ being 35.59˚.

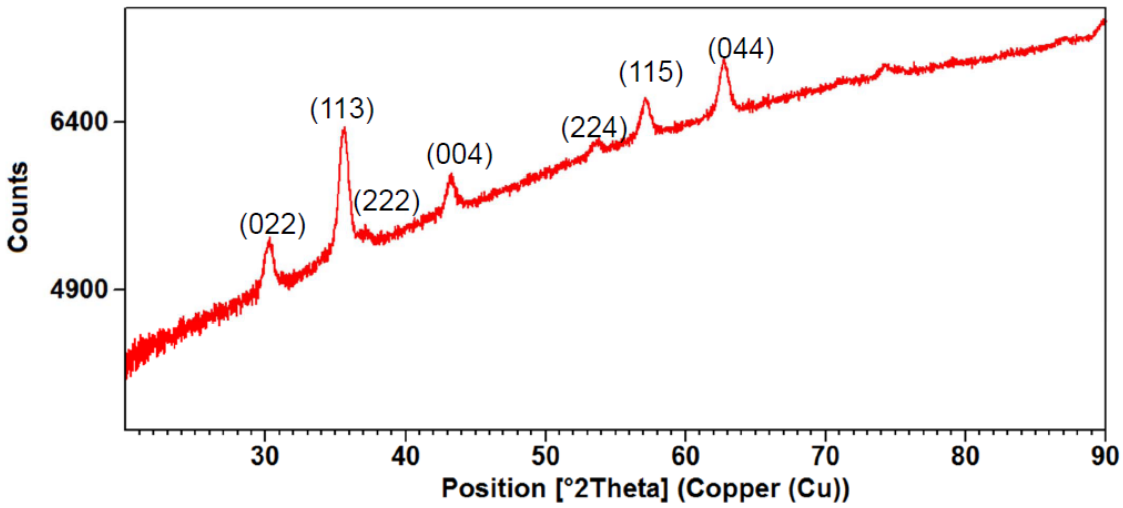

Figure 40. Wide Angle X-ray Scattering (WAXS) of Ru(0)-modified magnetite **88** nanoparticles

Fig. 41 shows the magnetization curves for ruthenium(II)-modified magnetite nanoparticles **87** and Ru(0)-modified magnetite **88** nanoparticles measured at room temperature. These modified nanoparticles have a saturation magnetization (σ_s) of 62.4 and 69.6 emu/g, respectively. These values are slightly smaller than that of bulk magnetite (92 emu/g), which is consistent with the presence of surface coatings with ruthenium.[218] At low magnetic field, the hysteresis loops of these nanoparticles (insets of Fig. 41) indicate low coercivity and almost zero remnance, suggesting the particles to exhibit superparamagnetic behavior. The slightly opened loop can be attributed to particles with grain size larger than *ca.* 20 nm which still can carry a remnant magnetization during the measurement duration of 100 ms.

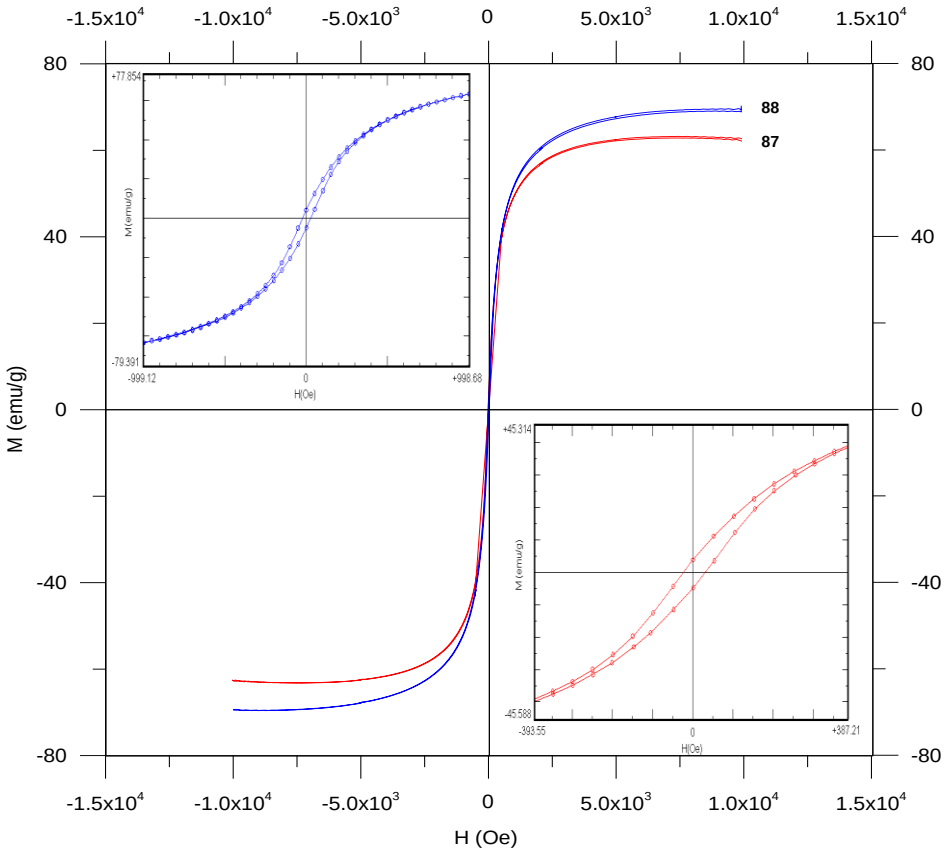

Figure 41. Magnetization curves for **87** (——) and **88** (——) measured at 300 K. The insets show magnified hysteresis loops at low magnetic fields highlighting the coercivity and remanance of particles. These particles exhibit predominantly superparamagnetic behavior with some blocked, single-domain particles

4.3 Hydrogenation of α,β-Unsaturated Ketones Catalyzed by Fe_3O_4/Ru Nanoparticles: Selective Reduction of the Carbon-Oxygen Bond

The core-shell-type Fe_3O_4/Ru nanoparticles **88** which are intrinsically non-magnetic can be readily dispersed in n-BuOH and easily recovered by applying an external magnetic field (Fig. 42). They are highly active and selective hydrogenation catalyst, converting *trans*-4-phenyl-3-penten-2-one under hydrogen into 4-phenylbutan-2-ol, avoiding the formation of saturated products (Scheme 26).

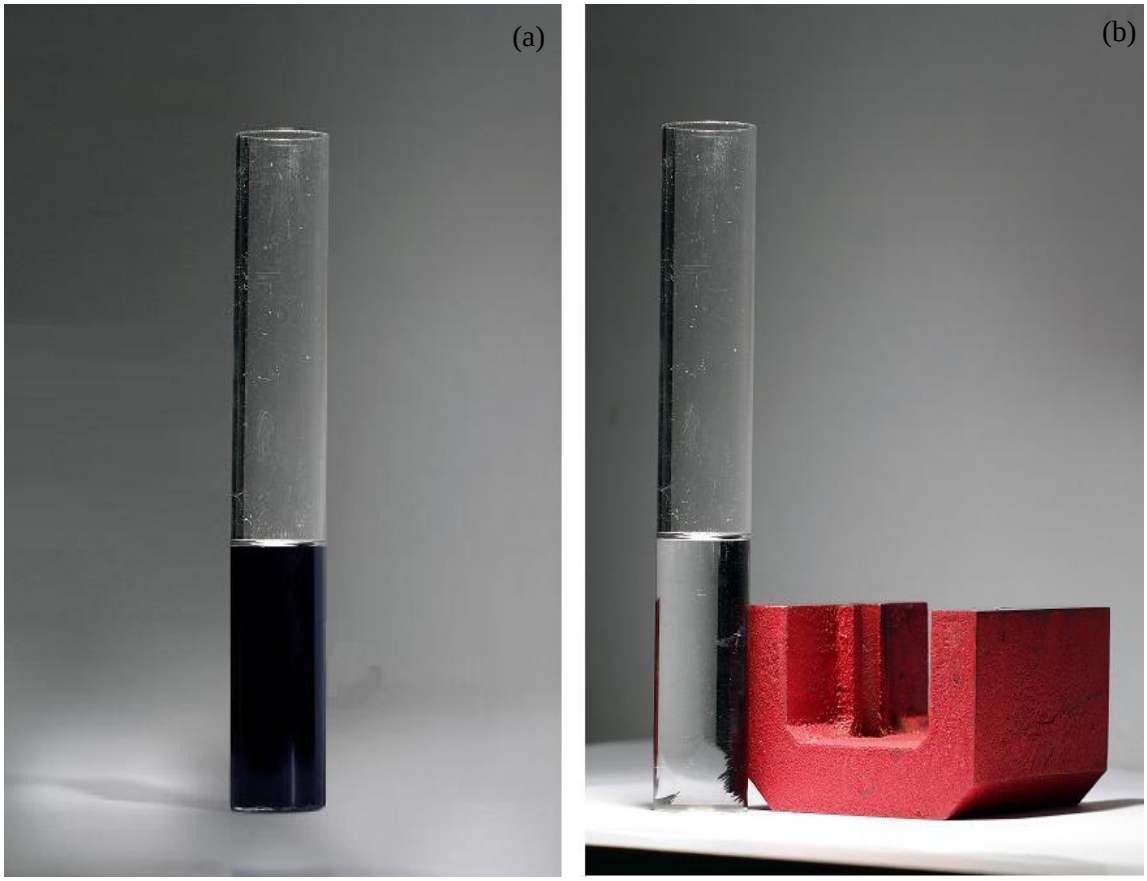

Figure 42. Superparamagnetic core-shell-type Fe_3O_4/Ru nanoparticles dispersed in n-BuOH (a) and placed on the glass wall by an external magnet (b)

This highly selective reduction of unconstrained α,β-unsaturated ketone is striking, especially, since no aromatic ring hydrogenation was observed. Thus, the catalyst is capable of reducing C=O bond selectively. The catalytic reaction was followed by gas chromatography coupled to mass detector (GC-MS). The products were separated on an apolar column and were identified by their retention time and mass spectrum using electron impact (EI) ionization method.

The hydrogenation of *trans*-4-phenyl-3-penten-2-one was done by using **88** freshly prepared by the reduction of **87** in n-BuOH (20 mL) under a pressure of hydrogen (50 bar) at 100 °C for 14 h. GC-MS shows complete conversion of substrate (100 %). The overall selectivity of **88** towards unsaturated alcohol was > 90 %, presumably due to mild reaction conditions and catalyst-support interaction. The turnover number was determined by adding 12.2 mmol (1.78 g) of *trans*-4-phenyl-3-penten-2-one after regular intervals, until the catalyst became almost inactive, the total mass of substrate added being 5.34 g (Table 23).

Table 23. *trans*-4-phenyl-3-penten-2-one hydrogenation using Fe_3O_4/Ru nanoparticles in n-butanol by adding fresh substrate at regular intervals

Cat. Run [a]	Conversion (%)	Time (h)	S. A. (%)[b]	U. A. (%)[c]
1	100	8	8.3	91.7
2	100	8	5.4	94.6
3	100	24	12.9	87.1

[a]12.2 mmol of substrate used for each catalytic run [b] Saturated alcohol [c] Unsaturated alcohol

Table 24 shows the time dependence of the catalytic hydrogenation during first run, which is linear before saturation (Fig. 43).

Table 24. *trans*-4-phenyl-3-penten-2-one hydrogenation using Fe_3O_4/Ru nanoparticles in n-butanol

Time	Conversion (%)	Unsaturated Alcohol (%)	Unsaturated Alcohol Selectivity (%)
1	15.2	14.3	94.1
2	32.4	30.9	95.4
3	49.3	46.8	94.9
4	69.0	63.1	91.5
5	88.0	79.5	90.3
6	98.8	89.7	90.8
7	100	92.8	92.8

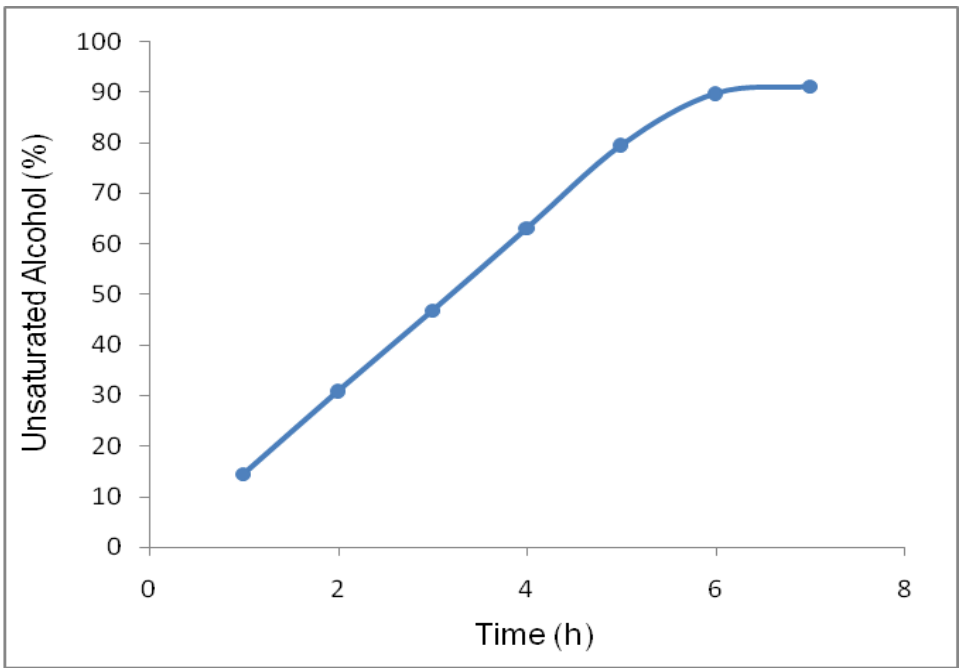

Figure 43. Time dependence of the *trans*-4-phenyl-3-penten-2-one hydrogenation catalyzed by the Ru(0)-coated magnetite **88**

A schematic representation of the reaction pathway (Scheme 26) shows the reaction to undergo path A and not path B, because no traces of 4-phenylbutan-2-one were observed during GC-MS analysis of the reaction mixtures taken over the reaction times. It may be assumed that the saturated alcohol 4-phenylbutan-2-ol is essentially obtained by the further reduction of the unsaturated alcohol 4-phenyl-3-buten-2-ol. Interestingly, no traces of 4-cyclohexylbutan-2-one and 4-cyclohexylbutan-2-ol were observed, suggesting that **88** is unable to catalyze aromatic ring hydrogenation under the reaction conditions.

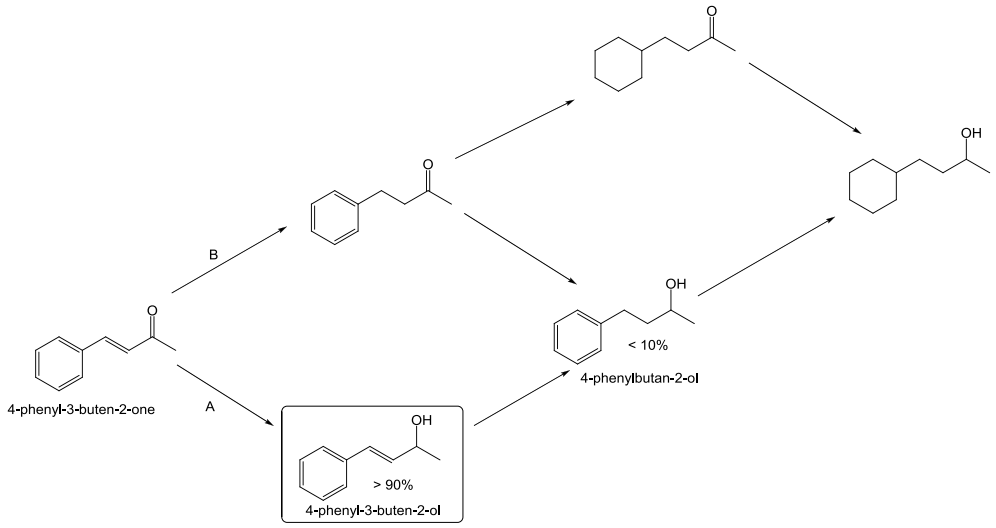

Scheme 26. Selective hydrogenation of *trans*-4-phenyl-3-buten-2-one and possible reaction pathway

The nanoparticles **88** can be recovered and reused, however, after three catalytic runs, aggregation was observed (Fig. 44). The high selectivity for the C=O bond hydrogenation can be tentatively attributed to the activation of the C=O bond by the metal-support interaction. It can be assumed that magnetite probably modifies the electronic properties of ruthenium, which in turn, leads to an increase in the hydrogenation selectivity for the C=O bond. Thus, the specific hydrogenation tendency of *trans*-4-phenyl-3-penten-2-one can be interpreted in terms of an exclusive adsorption of C=O bonds at the surface of the nanoparticles.[193a]

In order to determine the amount of ruthenium leaching, the combined washings of three consecutive runs are analyzed by ICP-OES. As there was no iron peak in the spectrum, which could interfere with the ruthenium signals, the ruthenium quantity could be calculated

without applying any correction. The leaching observed was around 4.1 % with respect to original ruthenium loading after three catalytic runs.

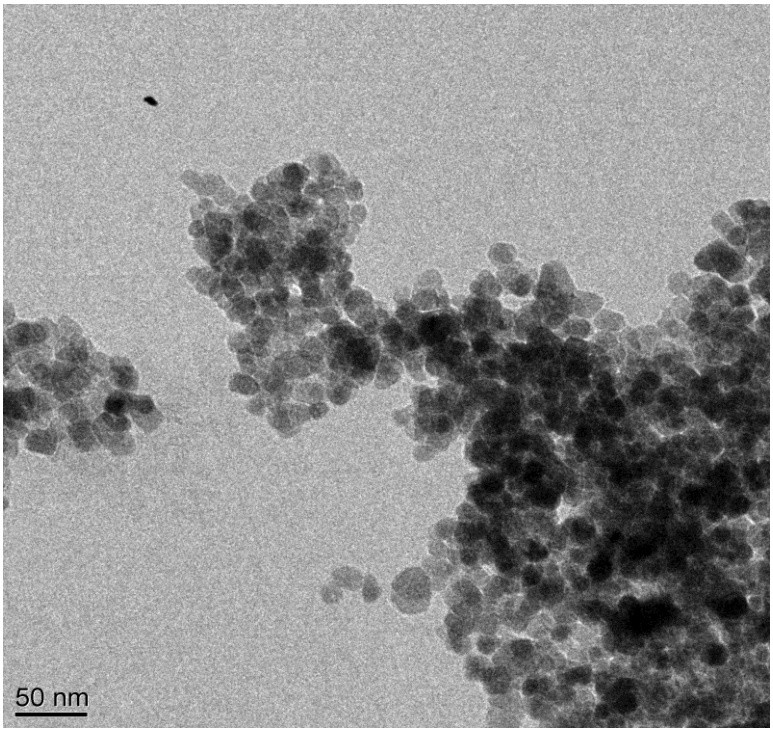

Figure 43. TEM micrograph of **88** after three catalytic runs

In summary, we have prepared novel core-shell-type Fe_3O_4/Ru nanoparticles, which show a remarkable catalytic activity for the selective hydrogenation of C=O bond in an unconstrained α,β-unsaturated ketone viz. *trans*-4-phenyl-3-penten-2-one. These environment friendly superparamagnetic nanoparticles can be easily dispersed due to intrinsically non-magnetic nature and readily recycled and reused by magnetic decantation.

5

Conclusions and Perspectives

The present work deals with the preparation of ruthenium nanoparticles using an organometallic approach. In the first part, the synthesis of ruthenium nanoparticles stabilized by mesogenic isonicotinic ester ligands is presented in view of an organization of nanoparticles in organic mesophases. However, it was not possible to obtain mesomorphous ruthenium nanoparticles in this way. On the other hand, the ruthenium nanoparticles thus obtained as well as their organometallic precursors show high anticancer activity towards human ovarian cancer cell lines. Thus, the synthesis of long-chain isonicotinic ester ligands and their arene ruthenium complexes allowed us to develop a new generation of anticancer agents.

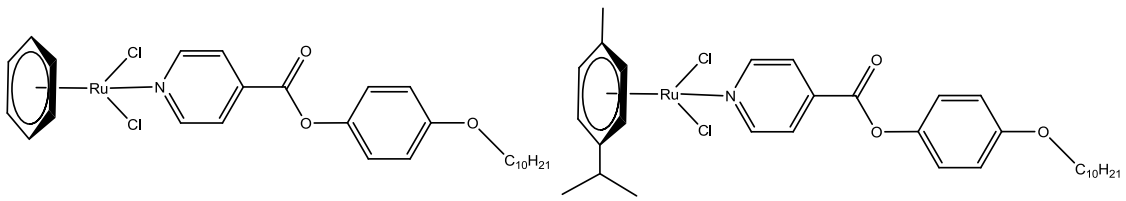

This new series of arene ruthenium complexes containing long-chain isonicotinic ester ligands show cytotoxic activities comparable to cisplatin or superior to cisplatin in the cancer cell lines A2780 and cisplatin-resistant cell line A2780cisR, which is remarkable, especially for such structurally different compounds. The promising results for

these complexes necessitate further *in vivo* studies. It would be desirable to extend this series of highly cytotoxic arene ruthenium complexes in order to find the most active arene ruthenium complexes. This series can be easily extended by further functionalization of the terminal CH_3 in the long-chain isonicotinic ester ligand **5**. For example, the introduction of a terminal COOH group in such ligands may help improve the aqueous solubility of ligand, while provoking some sort of hydrogen bonding inside the tumor cells, which might be helpful in addition to aquation of chloro ligands in arene ruthenium complexes.

In the second part, silicate-supported ruthenium nanoparticles were presented, with a special emphasis on ruthenium nanoparticles intercalated in hectorite. Size- and shape-selective preparation of hectorite-supported ruthenium nanoparticles was achieved by using either molecular hydrogen or solvothermal reduction route employing different organo-metallic precursors.

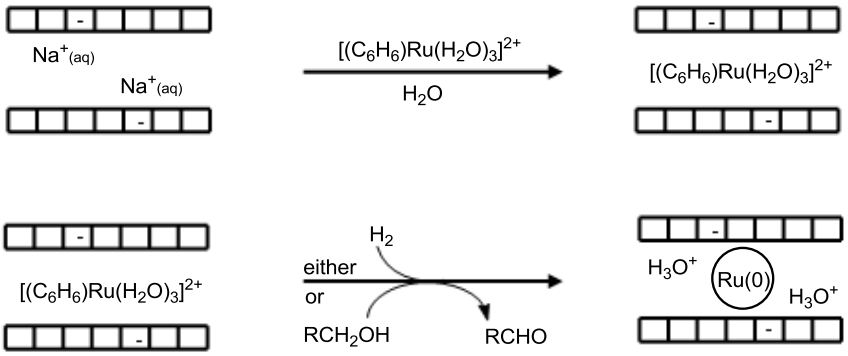

The catalytic efficiency of these nanoparticles was evaluated for different arenes, furfuryl alcohol and α,β-unsaturated ketones. Hectorite-supported ruthenium nanoparticles were found to be promising hydrogenation catalysts. It was observed that the modification of intercalated particles size and reaction conditions tune the catalytic activity for chemo-selective reactions. For example, these nanoparticles preferentially reduce the C=C olefinic bond in α,β-unsaturated ketones at 35 °C. Surprisingly, an exceptionally high catalytic activity was observed in the case of mesityl oxide hydrogenation with an overall turnover number of 91800. Methyl isobutyl ketone was produced in high yield with essentially all of mesityl oxide converted to methyl isobutyl ketone, and further hydrogenation of methyl isobutyl

ketone did not occur. However, a change in the particle size resulted in a high selectivity towards C=O bond of α,β-unsaturated ketones, if an excess of solvent was used at low temperatures. A selectivity > 98 % for an unconstrained α,β-unsaturated ketone *viz. trans*-4-phenyl-3-penten-2-one was observed at 0 °C. This kind of selectivity is unique for a heterogeneous catalyst, especially, when the C=C olefinic bond in the α, β-unsaturated moiety is not sterically hindered.

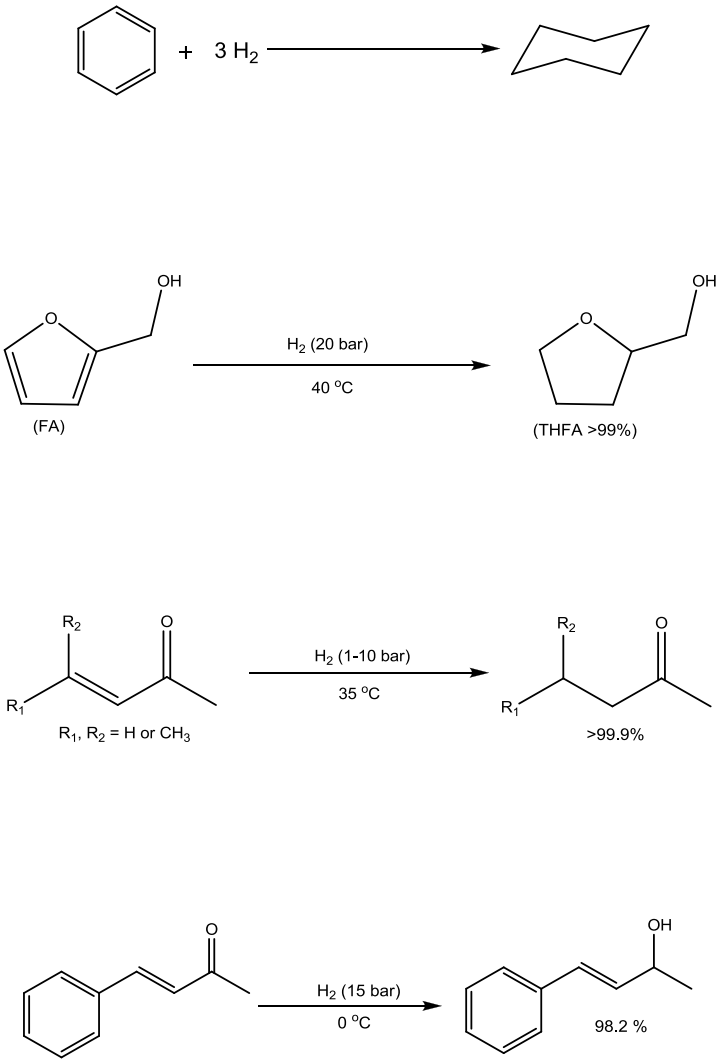

These promising results during the selective hydrogenation of different substrates opened new perspectives to be explored for the hectorite-stabilized ruthenium nanoparticles in other industrially important catalytic reactions.

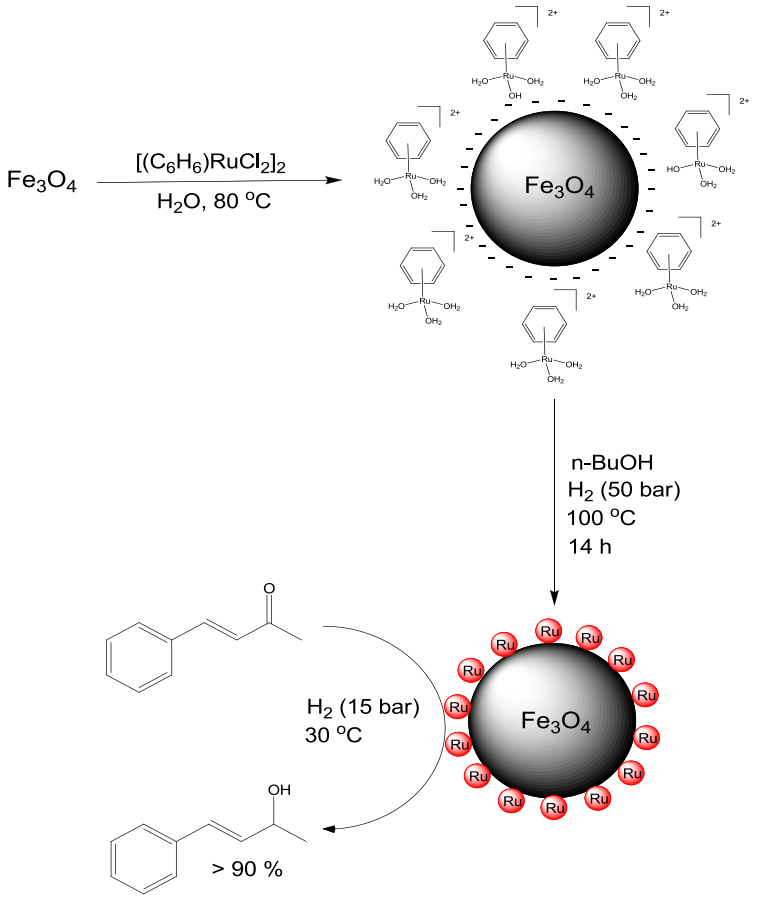

In the last part, superparamagnetic core-shell-type Fe_3O_4/Ru nanoparticles (particle size ~ 15 nm) synthesized by co-precipitation, adsorption and reduction methods were presented. Their catalytic efficiency was evaluated towards selective C=O hydrogenation in an unconstrained α,β-unsaturated ketone. These new Fe_3O_4/Ru nanoparticles presented a green and sustainable approach towards catalyst separation from reaction mixture, as they can be efficiently separated from the reaction mixture by applying an external magnetic field. Superparamagnetic Fe_3O_4 nanoparticles may also be used as support for arene ruthenium complexes containing long-chain isonicotinic ester ligands. This strategy could help targeting cancer tumors selectively by localizing and activating cytotoxic Fe_3O_4 nanoparticles with the help of an external magnetic field.

6

Experimental Section

Experimental Details – Chapter 2

Cytotoxicity test (MTT assay)

Cytotoxicity was determined by the group of Prof. P. J. Dyson in EPFL Lausanne using the MTT assay (MTT = 3-(4,5-dimethyl-2-thiazolyl)-2,5-diphenyl-2H-tetrazolium bromide). Cells were seeded in 96-well plates as monolayers with 100 µl of cell solution (approximately 20,000 cells) per well and preincubated for 24 h in medium supplemeted with 10% FCS (Fetal Calf Serum). Compounds were added as DMSO solutions and serially diluted to the appropriate concentration (to give a final DMSO concentration of 0.5%). The concentration of the nanoparticle solutions used in the cytotoxicity assays was based on the concentration of ruthenium in the precursor present in the solution used to prepare the nanoparticles and assuming quantitative conversion. 100 µl of drug solution was added to each well and the plates were incubated for another 72 h. Subsequently, MTT (5 mg/ml solution in phosphate buffered saline) was added to the cells and the plates were incubated for a further 2 h. The culture medium was aspirated, and the purple formazan crystals formed by the mitochondrial dehydrogenase activity of vital cells were dissolved in DMSO. The optical density, directly proportional to the number of surviving cells, was quantified at 540 nm using a multiwell plate reader and

the fraction of surviving cells was calculated from the absorbance of untreated control cells. Evaluation was based on means from 2 independent experiments, each comprising 3 microcultures per concentration level.

Preparaton of the Ligand ***L*** ^{1} ***(4)***

4-Benzyloxyphenol (3 g, 15 mmol) and aqueous potassium hydroxide (0.84 g, 15 mmol in 30 mL water) were stirred in ethanol (125 mL). Then octyl bromide (15 mmol) was added drop wise and the mixture was refluxed overnight. The next day, water and ethanol were removed under reduced pressure. Dichloromethane (100 mL) was added to the residue. Insoluble potassium bromide was discarded off via filtration. The filtrate was purified by flash chromatography using dichloromethane as mobile phase. The solvent was then removed by evaporation under reduced pressure in order to get a brown residue of 1-(benzyloxy)-4-(octyloxy)benzene, yield: 3.2 g, 68%. ^{1}H NMR (400 MHz, *CDCl*$_3$) δ ppm 7.48-7.35 (m, 5H, C_6H_5), 6.91 (d, ^3J = 9 Hz, 2H, C_6H_4), 6.84 (d, ^3J = 9 Hz, 2H, C_6H_4), 5.01 (s, 2H, CCH_2), 3.91 (t, ^3J = 7 Hz, 2H, OCH_2), 1.75 (p, ^3J = 7 Hz, 2H, CH_2), 1.45 (m, 2H, CH_2), 1.28 (m, 8H, $(CH_2)_4$), 0.89 (t, ^3J = 7 Hz, 3H, CH_3).

1-(Benzyloxy)-4-(octyloxy)benzene (3.2 g, 10.2 mmol) was deprotected using 10% Pd/C (0.4 mol eq) in a CH_2Cl_2/EtOH mixture (9:1). The above mentioned mixture was stirred overnight under H_2 pressure (4 bar) at room temperature. The next day, Pd/C was removed by filtration and the solvents were evaporated under reduced pressure in order to get a pale-white residue of 4-octyloxyphenol, yield: 2.1 g, 91%. ^{1}H NMR (400 MHz, *CDCl*$_3$) δ ppm 6.77 (m, 4H, C_6H_4), 4.57 (s, 1H, OH), 3.98 (t, ^3J = 7 Hz, 2H, OCH_2), 1.75 (p, ^3J = 7 Hz, 2H, CH_2), 1.44 (m, 2H, CH_2), 1.28 (m, 8H, $(CH_2)_4$), 0.89 (t, ^3J = 7 Hz, 3H, CH_3).

4-Octyloxyphenol (1.26 g, 5.7 mmol) and Et_3N (0.8 mL) were dissolved in CH_2Cl_2 (100 mL). Isonicotinoyl chloride hydrochloride (1.06 g, 5.09 mmol) was then added. The reaction mixture was stirred overnight at room temperature. The precipitate was were filtered off and discarded, and the solution was evaporated to dryness under reduced pressure. The yellow residue obtained was recrystallized several times from ethanol to give a white product *viz.* 4-(octyloxy)phenyl isonicotinate, yield: 1.04 g, 56%. IR (KBr, cm^{-1}): 3436(m), 2917(s, νCH_2CH_3), 1736(s, νCOO), 1513(s, νCN_{py}), 1290(m), 1253(m), 1206(m), 1102(m), 818(m), 753(m), 700(m). ^{1}H NMR (400 MHz, *CDCl*$_3$) δ ppm 8.87 (d, *J* = 6 Hz, 2H, NC_5H_4), 8.01 (d, ^3J = 6 Hz, 2H, NC_5H_4), 7.13 (d, ^3J = 9 Hz, 2H, C_6H_4), 6.95 (d, ^3J = 9 Hz, 2H, C_6H_4), 3.98 (t, ^3J = 7 Hz, 2H, OCH_2), 1.83 (m, 2H, CH_2), 1.46-1.30 (m, 10H, $(CH_2)_5$), 0.91 (t, ^3J = 7 Hz, 3H,

CH_3) ppm. $^{13}C(^1H)$ NMR (100 MHz, $CDCl_3$): δ = 164.1 (1C, C=O), 157.2 (1C, C–O), 150.8 (1C, NCH), 143.7 (1C, C–O), 136.9 (1C, C_{py}), 123.0 (1C, CH_{py}), 122.0 (1C, CH), 115.1 (1C, CH), 68.4 (1C, OCH_2), 31.7-22.6 (6C, $(CH_2)_6$), 14.1 (1C, CH_3) ppm. MS (ESI) *m/z*: 327 $[M+H]^+$.

Preparation of the Ligand ***L²(32)***

4'-Cyanobiphenyl-4-yl 4-(10-hydroxydecyloxy)benzoate (0.1 g, 0.21 mmol) and triethylamine (0.021 g, 0.21 mmol) were dissolved in CH_2Cl_2 (100 mL) and isonicotinoyl chloride hydrochloride (0.09 g, 0.63 mmol) was added. The reaction mixture was stirred overnight at room temperature. The precipitate formed was filtered off and discarded and the solution was evaporated to dryness. The yellow residue obtained was recrystallized several times from ethanol to give a white product, yield: 0.104 g, 85%. (Found: C, 74.87; H, 6.36; N, 4.76. Calc. for $C_{36}H_{36}N_2O_5$ (*M* = 576): C, 74.98; H, 6.29; N, 4.86%). IR (KBr, cm^{-1}): 2920(m), 2223(w, νCN), 1723(s, νCOO), 1604(s), 1493(m), 1255(s), 1162(s). ^1H NMR (400 MHz, *CDCl₃*) δ ppm 8.89 (d, ^3J = 6 Hz, 2H, NC_6H_4), 8.17 (d, ^3J = 9 Hz, 2H, OC_6H_4COO), 7.86 (d, ^3J = 6 Hz, 2H, NC_6H_4), 7.75 (d, ^3J = 8 Hz, 2H, C_6H_4CN), 7.70 (d, ^3J = 8 Hz, 2H, C_6H_4CN), 7.65 (d, ^3J = 9 Hz, 2H, OC_6H_4), 7.34 (d, ^3J = 9 Hz, 2H, OC_6H_4), 6.99 (d, ^3J = 9 Hz, 2H, OC_6H_4COO), 4.36 (t, ^3J = 7 Hz, 2H, OCH_2), 4.05 (t, ^3J = 7 Hz, 2H, CH_2COO), 1.81 (m, 4H, $(CH_2)_2$), 1.54-1.32 (m, 12H, $(CH_2)_6$). MS (ESI) *m/z*: 599.3 $[M+Na]^+$. UV-Vis (CH_2Cl_2): λ_{max} 278 (220124), 228 (56183) nm.

Preparation of the Ligand ***L³(39)***

10-Bromodecanol was synthesized by reported procedures.[118] A typical procedure for the synthesis of 10-bromodecanol is as follows: 1,10-decandiol (25 g, 0.14 mol) and 48 % HBR solution (125 mL, 2.2 mol) in 380 mL ligroin were distilled in a liquid-liquid extractor. After 3 days, the organic layer was separated. Solvent was then removed by evaporation under reduced pressure in order to get a dark brown oily residue of 10-bromodecanol, yield: 22.9 g, 67.1 %. ^1H NMR (400 MHz, *CDCl₃*) δ ppm 3.64 (t, ^3J =4 Hz, 2H, CH_2Br), 3.41 (t, ^3J = 4 Hz, 2H, CH_2OH), 1.88 (p, ^3J = 8 Hz, 2H, CH_2), 1.59 (p, ^3J = 8 Hz, 2H, CH_2), 1.52-1.29 (m, 12H, $(CH_2)_6$).

A mixture of 4-benzyloxyphenol (5.0 g, 21 mmol), potassium carbonate (5.6 g, 41 mmol) and 18-crown-6 ether (0.2 g, 0.7 mmol) was stirred in dry acetone (125 mL) for 30 minutes at room temperature. Then, 1-bromodecanol (2.8g, 14 mmol) in acetone (25) was added

dropwise. This mixture was refluxed under inert atmosphere. After four days, the product was filtered off and the solvent was removed by evaporation under reduced pressure. The product was further purified by CH_2Cl_2/H_2O extraction followed by recrystallization in isopropanol which affords a light brown product *viz.* 10-(4-(benzyloxy)phenoxy)decanol, yield: 4.46 g, 88.9%. ^{1}H NMR (400 MHz, *CDCl$_3$*) δ ppm 7.43-7.31 (m, 5H, C_6H_5), 6.91 (d, ^3J = 9 Hz, 2H, C_6H_4), 6.84 (d, ^3J = 9 Hz, 2H, C_6H_4), 5.01 (s, 2H, $C_6H_5CH_2O$), 3.91 (t, ^3J = 6 Hz, 2H, OCH_2), 3.66 (m, 2H, CH_2OH), 1.78 (p, ^3J = 7 Hz, 2H, CH_2), 1.60 (p, ^3J = 7 Hz, 2H, CH_2), 1.44-1.31 (m, 12H, $(CH_2)_6$).

10-(4-(Benzyloxy)phenoxy)decanol (0.21 g, 0.6 mmol) was deprotected using 10% Pd/C (0.4 mol eq) in a CH_2Cl_2/EtOH mixture (9:1). The above mentioned mixture was stirred overnight under H_2 pressure (4 bar) at room temperature. The next day, Pd/C was removed by filtration and the solvents were evaporated under reduced pressure in order to get off the white residue of 4-(10-hydroxydecyloxy)phenol, yield: 0.15 g, 95.4 %. ^{1}H NMR (400 MHz, *CDCl$_3$*) δ ppm 6.77 (m, 4H, C_6H_4), 4.48 (s, 1H, OH), 3.91 (t, ^3J = 6, 2H, OCH_2), 3.67 (m, 2H, CH_2OH), 1.76 (p, ^3J = 6 Hz, 2H, CH_2), 1.58 (m, 2H, CH_2), 1.48-1.21 (m, 12H, $(CH_2)_6$).

4-(10-Hydroxydecyloxy)phenol (0.15 g, 0.6 mmol) and Et_3N (0.08 mL) were dissolved in $CHCl_3$ (20 mL). Isonicotinoyl chloride hydrochloride (0.1 g, 0.6 mmol) was then added. The reaction mixture was stirred overnight at room temperature. The yellow precipitate was filtered off and discarded, and the solution was evaporated to dryness. The yellow residue obtained was recrystallized several times from ethanol to give a white product *viz.* 4-(10-hydroxydecyloxy)phenyl isonicotinate **39**, yield: 1.04 g, 61.4 %. (Found: C, 71.05; H, 7.95; N, 3.78. Calc. for $C_{22}H_{29}NO_4$ (*M* = 371.48): C, 71.13; H, 7.87; N, 3.77%). IR (KBr, cm^{-1}): 3466(s), 2930(s), 1637(s, νCOO), 1514(w), 1207(w), 1103(w), 1616(m). ^{1}H NMR (400 MHz, *CDCl$_3$*) δ ppm 8.86 (s, 2H, NC_5H_4), 8.03 (d, ^3J = 5 Hz, 2H, NC_5H_4), 7.13 (d, ^3J = 9 Hz, 2H, C_6H_4), 6.95 (d, ^3J = 9 Hz, 2H, C_6H_4), 3.98 (t, ^3J = 7 Hz, 2H, OCH_2), 3.66 (t, ^3J = 7 Hz, 2H, CH_2OH), 1.83 (p, ^3J = 7 Hz, 2H, CH_2), 1.9 (p, ^3J = 7 Hz, 2H, CH_2), 1.46-1.30 (m, 12H, $(CH_2)_6$). MS (ESI) *m/z*: 372.4 $[M+H]^+$.

Synthesis of 4,4´-disubstituted-2,2´-bipyridine and 5,5´-disubstituted-2,2´-bipyridine Containing Long Alkyl Chain Ligands

4,4´-Bis(bromomethyl)-2,2´-bipyridine, 5,5´-bis(bromomethyl)-2,2´-bipyridin and 4-decyloxyphenol were synthesized by reported procedures.[121,122]

Synthesis of the Ligand ***L*** ^{4} ***(44)***

4-Decyloxyphenol (0.15g, 0.6 mmol) and aqueous potassium hydroxide (0.036 g, 0.6 mmol) were mixed and stirred in hot ethanol (50 mL). Then, 5,5´-bis(bromomethyl)-2,2´-bipyridin (0.1 g, 0.3 mmol) was added drop wise and the mixture was refluxed overnight. The next day, water and ethanol were removed under reduced pressure and dichloromethane (100 mL) was added to the residue. Insoluble potassium bromide was discarded off via filtration. Solvent was removed by evaporation under reduced pressure to give a white residue, which was further purified by re-crystallization in ethanol in order to afford a white product, yield: 0.183 g, 91.5 %. (Found: C, 77.43; H, 8.87; N, 4.13. Calc. for $C_{44}H_{60}N_2O_4$ (*M* = 680.97): C, 77.61; H, 8.88; N, 4.11%). IR (KBr, cm^{-1}): 3413(s), 2919(s), 1617(m), 1509(s), 1231(s), 1031(s), 826(s), 620(m). ^{1}H NMR (400 MHz, *CDCl*$_3$) δ ppm 8.70 (d, ^{3}J = 5 Hz, 2H, NCH_{py}), 8.49 (s, 2H, $NCCH_{py}$), 7.46 (d, ^{3}J = 4 Hz, 2H, CH_{py}), 6.92 (d, ^{3}J = 9 Hz, 4H, C_6H_4), 6.85 (d, ^{3}J = 9 Hz, 4H, C_6H_4), 5.14 (s, 4H, CH_2O_{py}), 3.92 (t, ^{3}J = 6 Hz, 4H, CH_2O), 1.79 (p, ^{3}J = 7 Hz, 4H, CH_2), 1.44-1.27 (m, 28H, $(CH_2)_7$), 0.90 (t, ^{3}J = 7 Hz, 6H, CH_3). MS (ESI) *m/z*: 681.6 $[M+H]^+$.

Synthesis of the Ligand ***L*** ^{5} ***(52)***

A mixture of 4-decyloxyphenol (1.62 g, 6.5 mmol), potassium carbonate (1.79 g, 13 mmol) and $18C_6$ crown ether (0.06 g, 0.2 mmol) was stirred in acetonitrile (80 mL) for 30 minutes at room temperature. Then, 4,4´-bis(bromomethyl)-2,2´-bipyridin (0.74 g, 2.2 mmol) was added. This mixture was refluxed under an inert atmosphere. After four days, the precipitate was filtered off and the filtrate was discarded. The brown precipitate was further purified by CH_2Cl_2/H_2O extraction followed by flash chromatography using $CHCl_3$/EtOH (16:1) which affords a white product. yield: 1.11 g, 75.2 %. (Found: C, 74.60; H, 8.98; N, 3.97. Calc. for $C_{44}H_{60}N_2O_4 \cdot 0.4\ CH_2Cl_2$ (*M* = 714.93): C, 74.59; H, 8.57; N, 3.92%). IR (KBr, cm^{-1}): 3435(s), 1634(m), 1510(w), 1240(w), 520(w). ^{1}H NMR (400 MHz, *CDCl*$_3$) δ ppm 8.72 (s, 2H, NCH), 8.43 (d, ^{3}J = 8 Hz, 2H, NCCH), 7.91 (d, ^{3}J = 8 Hz, 2H, CCH), 6.93 (m, 4H, C_6H_4), 6.85 (m, 4H, C_6H_4), 5.09 (s, 4H, CH_2O_{py}), 3.92 (t, *J* = 7 Hz, 4H, CH_2O), 1.79 (p, ^{3}J = 7 Hz, 4H, CH_2), 1.44-1.27 (m, 28H, $(CH_2)_7$), (t, ^{3}J = 6 Hz, 6H, CH_3) ppm. MS (ESI) *m/z*: 681.5 $[M+H]^+$.

Preparation of the Complexes [(arene)Ru(L)Cl$_2$*]*

A mixture of the appropriate [(arene)Ru_2Cl_4] dimer and 2 equivalents of the ligand **L**^{1} or **L**^{2} or **L**^{3} in CH_2Cl_2 solution (25 mL) was stirred for 3 h at room temperature. The

solvent was then removed under reduced pressure, and the residue was re-dissolved in EtOH (30 mL). Then the solvent was evaporated to dryness, and the final product was collected and dried *in vacuo*.

[(*p*-MeC$_6$H$_4$Pr^i)Ru(L^1)Cl$_2$] (**9**): Yield: 0.0816 g, > 99%. (Found: C, 52.59; H, 5.08; N, 2.54. Calc. for $C_{24}H_{27}NO_3Cl_2Ru$ (*M* = 549.46): C, 52.46; H, 4.95; N, 2.55%). ^{1}H NMR (400 MHz, *CDCl$_3$*) δ ppm 9.32 (d, ^3J = 5 Hz, 2H, NC_5H_4), 7.99 (d, ^3J = 5 Hz, 2H, NC_5H_4), 7.12 (d, ^3J = 8 Hz, 2H, C_6H_4), 6.95 (d, ^3J = 8 Hz, 2H, C_6H_4), 5.48 (d, ^3J = 6 Hz, 2H, RuC_6H_4), 5.26 (d, ^3J = 6 Hz, 2H, RuC_6H_4), 4.05 (q, ^3J = 6 Hz, 2H, OCH_2), 3.05-2.98 (m, 1H, CH), 2.13 (s, 3H, CH_3), 1.63-1.20 (m, 9H, $CH(CH_3)_2$ and CH_3).

[(*p*-MeC$_6$H$_4$Pr^i)Ru(L^1)Cl$_2$] (**10**): Yield: 0.0908 g, > 99%. (Found: C, 53.79; H, 5.50; N, 2.41. Calc. for $C_{26}H_{31}NO_3Cl_2Ru \cdot 0.05\ CH_2Cl_2$ (*M* = 581.75): C, 53.78; H, 5.39; N, 2.41. ^{1}H NMR (400 MHz, *CDCl$_3$*) δ ppm 9.32 (d, ^3J = 5 Hz, 2H, NC_5H_4), 7.99 (d, ^3J = 5 Hz, 2H, NC_5H_4), 7.12 (d, ^3J = 8 Hz, 2H, C_6H_4), 6.95 (d, ^3J = 8 Hz, 2H, C_6H_4), 5.48 (d, ^3J = 6 Hz, 2H, RuC_6H_4), 5.26 (d, ^3J = 6 Hz, 2H, RuC_6H_4), 4.05 (t, ^3J = 6 Hz, 2H, OCH_2), 3.05-2.98 (m, 1H, CH), 2.13 (s, 3H, CH_3), 1.81 (p, ^3J = 6 Hz, 2H, CH_2), 1.49 (m, 2H, CH_2), 1.34 (d, ^3J = 7 Hz, 6H, $(CH_3)_2$), 1.00 (t, ^3J = 7 Hz, 3H, CH_3).

[(*p*-MeC$_6$H$_4$Pr^i)Ru(L^1)Cl$_2$] (**11**): Yield: 0.0964 g, > 99%. (Found: C, 55.75; H, 5.85; N, 2.34. Calc. for $C_{28}H_{35}NO_3Cl_2Ru$ (*M* = 605.56): C, 55.54; H, 5.83; N, 2.31%). ^{1}H NMR (400 MHz, *CDCl$_3$*) δ ppm 9.32 (d, ^3J = 5 Hz, 2H, NC_5H_4), 7.99 (d, ^3J = 5 Hz, 2H, NC_5H_4), 7.12 (d, ^3J = 8 Hz, 2H, C_6H_4), 6.95 (d, ^3J = 8 Hz, 2H, C_6H_4), 5.48 (d, ^3J = 6 Hz, 2H, RuC_6H_4), 5.26 (d, ^3J = 6 Hz, 2H, RuC_6H_4), 3.96 (t, ^3J = 6 Hz, 2H, OCH_2), 3.03-2.95 (m, 1H, CH), 2.13 (s, 3H, CH_3), 1.81 (p, ^3J = 6 Hz, 2H, CH_2), 1.47 (m, 2H, CH_2), 1.34 (m, 10H, $(CH_3)_2$ and C_2H_4), 0.95 (t, ^3J = 16 Hz, 3H, CH_3).

[(*p*-MeC$_6$H$_4$Pr^i)Ru(L^1)Cl$_2$] (**12**): Yield: 0.1052 g, > 99%. (Found: C, 57.08; H, 6.23; N, 2.23. Calc. for $C_{30}H_{39}NO_3Cl_2Ru$ (*M* = 633.62): C, 56.87; H, 6.20; N, 2.21%). ^{1}H NMR (400 MHz, *CDCl$_3$*) δ ppm 9.32 (d, ^3J = 5 Hz, 2H, NC_5H_4), 7.99 (d, ^3J = 5 Hz, 2H, NC_5H_4), 7.12 (d, ^3J = 8 Hz, 2H, C_6H_4), 6.95 (d, ^3J = 8 Hz, 2H, C_6H_4), 5.49 (d, ^3J = 6 Hz, 2H, RuC_6H_4), 5.26 (d, ^3J = 6 Hz, 2H, RuC_6H_4), 3.98 (t, *J* = 6 Hz, 2H, OCH_2), 3.03-2.95 (m, 1H, CH), 2.13 (s, 3H, CH_3), 1.83 (p, ^3J = 6 Hz, 2H, CH_2), 1.47 (m, 2H, CH_2), 1.34 (m, 14H, $(CH_3)_2$ and C_4H_8), 0.91 (t, ^3J = 7 Hz, 3H, CH_3). MS(ESI) *m/z*: 565.1 [M+MeOH].

[(C_6H_6)Ru(L^1)Cl_2] (**13**): Yield: 0.363 g, > 99%. (Found: C, 55.03; H, 5.83; N, 2.25. Calc. for $C_{28}H_{35}Cl_2NO_3Ru \cdot 0.1\ CH_2Cl_2$ (*M* = 613.5): C, 54.96; H, 5.78; N, 2.28%). IR (KBr, cm^{-1}): 2925(m), 1747(m, νCOO), 1631(m), 1505(m), 1277(w), 1192(m). ^{1}H NMR (400 MHz, *CD_2Cl_2*) δ ppm 9.31 (d, ^3J = 6 Hz, 2H, NC_5H_4), 8.00 (d, ^3J = 6 Hz, 2H, NC_5H_4), 7.11 (d, ^3J = 9 Hz, 2H, C_6H_4), 6.92 (d, ^3J = 9 Hz, 2H, C_6H_4), 5.65 (s, 6H, C_6H_6), 3.95 (t, ^3J = 7 Hz, 2H, OCH_2), 1.76 (m, 2H, CH_2), 1.46-1.26 (m, 14H, $(CH_2)_7$), 0.86 (t, ^3J = 7 Hz, 3H, CH_3). MS (ESI) *m/z*: 452.9 $[(M-\{C_6H_4O(CH_2)_9CH_3\})+Me_2CO+Na]^+$, 391$[(M-\{C_6H_4OC_{10}H_{21}\})+H_2O+H]^+$. UV-Vis ($CH_2Cl_2$): λ_{max} 337 (4308), 276 (6671), 230 (21465) nm.

[(*p*-$MeC_6H_4Pr^i$)Ru(L^1)Cl_2] (**14**): Yield: 0.324 g, > 99%. (Found: C, 58.17; H, 6.57; N, 2.06. Calc. for $C_{32}H_{43}Cl_2NO_3Ru$ (*M* = 661.17): C, 58.09; H, 6.55; N, 2.12%). IR (KBr, cm^{-1}): 2925(m), 1745(m, νCOO), 1631(m), 1505(m), 1250(m), 1187(m). ^{1}H NMR (400 MHz, *$CDCl_3$*) δ ppm 9.31 (d, ^3J = 6 Hz, 2H, NC_5H_4), 7.98 (d, ^3J = 6 Hz, 2H, NC_5H_4), 7.11 (d, ^3J = 9 Hz, 2H, C_6H_4), 6.93 (d, ^3J = 9 Hz, 2H, C_6H_4), 5.49 (d, ^3J = 6 Hz, 2H, RuC_6H_4), 5.26 (d, ^3J = 6 Hz, 2H, RuC_6H_4), 3.96 (t, ^3J = 7 Hz, 2H, OCH_2), 3.05-2.98 (m, 1H, CH), 2.13 (s, 3H, CH_3), 1.82-1.75 (m, 2H, CH_2), 1.48-1.28 (m, 18H, $(CH_3)_2$ and C_7H_{14}), 0.87 (t, ^3J = 7 Hz, 3H, CH_3). MS(ESI) *m/z*: 565.0 $[(M-\{OC_{10}H_{21}\})+Me_2CO+H]^+$. UV-Vis ($CH_2Cl_2$): λ_{max} 340 (5135), 275 (6882), 230 (21482) nm.

[(C_6Me_6)Ru(L^1)Cl_2] (**15**): Yield: 0.309 g, > 99%. (Found: C, 59.02; H, 6.84; N, 1.98. Calc. for $C_{34}H_{47}Cl_2NO_3Ru$ (*M* = 689.20): C, 59.21; H, 6.87; N, 2.03%). IR (KBr, cm^{-1}): 2923(s), 1740(s, νCOO), 1631(w), 1502(s), 1275(m), 1184(s). ^{1}H NMR (400 MHz, *$CDCl_3$*) δ ppm 9.08 (d, ^3J = 6 Hz, 2H, NC_5H_4), 7.96 (d, ^3J = 6 Hz, 2H, NC_5H_4), 7.11 (d, ^3J = 9 Hz, 2H, C_6H_4), 6.93 (d, ^3J = 9 Hz, 2H, C_6H_4), 3.96 (t, ^3J = 6 Hz, 2H, OCH_2), 2.02 (s, 18H, $C_6(CH_3)_6$), 1.79 (m, 2H, CH_2), 1.47-1.27 (m, 14H, $(CH_2)_7$), 0.88 (t, ^3J = 7 Hz, 3H, CH_3). MS(ESI) *m/z*: 620.1 $[(M-2Cl)+H]^+$. UV-Vis (CH_2Cl_2): λ_{max} 354 (5349), 277 (6368), 230 (18000) nm.

[(*p*-$MeC_6H_4Pr^i$)Ru(L^1)Cl_2] (**16**): Yield: 0.1087 g, > 99%. (Found: C, 59.27; H, 6.81; N, 2.04. Calc. for $C_{34}H_{47}NO_3Cl_2Ru$ (*M* = 689.73): C, 59.21; H, 6.87; N, 2.03%). ^{1}H NMR (400 MHz, *$CDCl_3$*) δ ppm 9.32 (d, ^3J = 5 Hz, 2H, NC_5H_4), 7.99 (d, ^3J = 5 Hz, 2H, NC_5H_4), 7.12 (d, ^3J = 8 Hz, 2H, C_6H_4), 6.95 (d, ^3J = 8 Hz, 2H, C_6H_4), 5.48 (d, ^3J = 6 Hz, 2H, RuC_6H_4), 5.26 (d, ^3J = 6 Hz, 2H, RuC_6H_4), 3.96 (t, ^3J = 6 Hz, 2H, OCH_2), 3.03-2.95 (m, 1H, CH), 2.13 (s, 3H, CH_3), 1.81 (p, ^3J = 6 Hz, 2H, CH_2), 1.47 (m, 2H, CH_2), 1.34 (m, ^3J = 7 Hz, 22H, $(CH_3)_2$ and C_8H_{16}), 0.88 (t, ^3J = 7 Hz, 3H, CH_3).

[(*p*-MeC$_6$H$_4$Pr^i)Ru(L^1)Cl$_2$] (**17**): Yield: 0.1237 g, > 99%. (Found: C, 60.30; H, 7.08; N, 1.98. Calc. for $C_{36}H_{51}NO_3Cl_2Ru$ (*M* = 717.78): C, 60.24; H, 7.16; N, 1.95%). ^{1}H NMR (400 MHz, *CDCl$_3$*) δ ppm 9.32 (d, ^3J = 5 Hz, 2H, NC_5H_4), 7.99 (d, ^3J = 5 Hz, 2H, NC_5H_4), 7.12 (d, ^3J = 8 Hz, 2H, C_6H_4), 6.95 (d, ^3J = 8 Hz, 2H, C_6H_4), 5.48 (d, ^3J = 5 Hz, 2H, RuC_6H_4), 5.26 (d, ^3J = 5 Hz, 2H, RuC_6H_4), 3.96 (t, ^3J = 6 Hz, 2H, OCH_2), 3.03-2.95 (m, 1H, CH), 2.13 (s, 3H, CH_3), 1.81 (p, ^3J = 6 Hz, 2H, CH_2), 1.47 (m, 2H, CH_2), 1.34 (m, ^3J = 6.8 Hz, 26H, $(CH_3)_2$ and $C_{10}H_{20}$), 0.88 (t, ^3J = 7 Hz, 3H, CH_3).

[(*p*-MeC$_6$H$_4$Pr^i)Ru(L^1)Cl$_2$] (**18**): Yield: 0.1219 g, > 99%. (Found: C, 61.33; H, 7.34; N, 1.89. Calc. for $C_{38}H_{55}NO_3Cl_2Ru$ (*M* = 745.83): C, 61.20; H, 7.43; N, 1.88%). ^{1}H NMR (400 MHz, *CDCl$_3$*) δ ppm 9.32 (d, ^3J = 5 Hz, 2H, NC_5H_4), 7.99 (d, ^3J = 5 Hz, 2H, NC_5H_4), 7.12 (d, ^3J = 8 Hz, 2H, C_6H_4), 6.95 (d, ^3J = 8 Hz, 2H, C_6H_4), 5.48 (d, ^3J = 6 Hz, 2H, RuC_6H_4), 5.26 (d, ^3J = 6 Hz, 2H, RuC_6H_4), 3.96 (t, ^3J = 6 Hz, 2H, OCH_2), 3.03-2.95 (m, 1H, CH), 2.13 (s, 3H, CH_3), 1.81 (p, ^3J = 6 Hz, 2H, CH_2), 1.47 (m, 2H, CH_2), 1.34 (m, ^3J = 7 Hz, 30H, $(CH_3)_2$ and $C_{12}H_{24}$), 0.90 (t, ^3J = 7 Hz, 3H, CH_3).

[(C$_6$H$_6$)Ru(L^2)Cl$_2$] (**33**): Yield: 0.495 g, > 99%. (Found: C, 60.62; H, 5.10; N, 3.29. Calc. for $C_{42}H_{42}Cl_2N_2O_5Ru \cdot 0.1\ CH_2Cl_2$ (*M* = 834.55): C, 60.54; H, 5.09; N, 3.35%). IR (KBr, cm^{-1}): 2927(m), 2225(w, νCN), 1725(s, νCOO), 1603(m), 1254(s), 1160(s). 1H NMR (400 MHz, *CDCl$_3$*) δ ppm 9.28 (d, ^3J = 6 Hz, 2H, NC_6H_4), 8.15 (d, ^3J = 9 Hz, 2H, OC_6H_4COO), 7.85 (d, ^3J = 6 Hz, 2H, NC_6H_4), 7.74 (d, ^3J = 8 Hz, 2H, C_6H_4CN), 7.69 (d, ^3J = 8 Hz, 2H, C_6H_4CN), 7.64 (d, ^3J = 8 Hz, 2H, OC_6H_4), 7.33 (d, ^3J = 8 Hz, 2H, OC_6H_4), 6.98 (d, ^3J = 9 Hz, 2H, OC_6H_4COO), 5.68 (s, 6H, C_6H_6), 4.38 (t, ^3J = 7 Hz, 2H, OCH_2), 4.06 (t, ^3J = 6 Hz, 2H, CH_2COO), 1.86-1.74 (m, 4H, $(CH_2)_2$), 1.50-1.34 (m, 12H, $(CH_2)_6$). MS (ESI): *m/z*: 791.1 $[(M\text{-}Cl]^+$. UV-Vis (CH_2Cl_2): λ_{max} 278 (71012), 229 (28025) nm.

[(*p*-MeC$_6$H$_4$Pr^i)Ru(L^2)Cl$_2$] (**34**): Yield: 0.432 g, > 99%. (Found: C, 62.51; H, 5.80; N, 3.07. Calc. for $C_{46}H_{50}Cl_2N_2O_5Ru$ (*M* = 882.21): C, 62.58; H, 5.71; N, 3.17%). IR (KBr, cm^{-1}): 2927(m), 2227(w, νCN), 1731(s, νCOO), 1606(m), 1261(s), 1168(s). ^{1}H NMR (400 MHz, *CDCl$_3$*) δ ppm 9.23 (d, ^3J = 6 Hz, 2H, NC_6H_4), 8.16 (d, ^3J = 9 Hz, 2H, OC_6H_4COO), 7.84 (d, ^3J = 6 Hz, 2H, NC_6H_4), 7.74 (d, ^3J = 8 Hz, 2H, C_6H_4CN), 7.69 (d, ^3J = 8 Hz, 2H, C_6H_4CN), 7.64 (d, ^3J = 8 Hz, 2H, OC_6H_4), 7.33 (d, ^3J = 9 Hz, 2H, OC_6H_4), 6.99 (d, ^3J = 9 Hz, 2H, OC_6H_4COO), 5.45 (d, ^3J = 6 Hz, 2H, RuC_6H_4), 5.24 (d, ^3J = 6 Hz, 2H, RuC_6H_4), 4.37 (t, ^3J = 7 Hz, 2H, OCH_2), 4.06 (t, ^3J = 6 Hz, 2H, CH_2COO), 3.04-2.95 (m, 1H, CH), 2.10 (s, 3H, CH_3), 1.85-1.76 (m, 4H, $(CH_2)_2$), 1.49-1.31 (m, 18H, $(CH_3)_2$ and $(CH_2)_6$). MS (ESI) *m/z*:

650.9 [(M-{$OC_6H_4COOC_6H_4C_6H_4CN$})+Me_2CO+Na+H]$^+$. UV-Vis (CH_2Cl_2): λ_{max} 334 (4558), 279 (47199), 229 (18313) nm.

[(C_6Me_6)Ru(L^2)Cl_2] (**35**): Yield: 0.408 g, > 99%. (Found: C, 61.30; H, 5.87; N, 2.92. Calc. for $C_{48}H_{54}Cl_2N_2O_5Ru \cdot 0.5\ CH_2Cl_2$ (*M* = 952.22): C, 61.10; H, 5.81; N, 2.94%). IR (KBr, cm^{-1}): 2924(m), 2226(w, νCN), 1722(s, νCOO), 1602(s), 1260(s), 1166(s). ^{1}H NMR (400 MHz, *CDCl*$_3$) δ ppm 9.01 (d, ^3J = 7 Hz, 2H, NC_6H_4), 8.15 (d, ^3J = 9 Hz, 2H, OC_6H_4COO), 7.81 (d, ^3J = 6 Hz, 2H, NC_6H_4), 7.74 (d, ^3J = 8 Hz, 2H, C_6H_4CN), 7.69 (d, ^3J = 8 Hz, 2H, C_6H_4CN), 7.64 (d, ^3J = 8 Hz, 2H, OC_6H_4), 7.33 (d, ^3J = 8 Hz, 2H, OC_6H_4), 6.99 (d, ^3J = 9 Hz, 2H, OC_6H_4COO), 4.36 (t, ^3J = 7 Hz, 2H, OCH_2), 4.05 (t, ^3J = 7 Hz, 2H, CH_2COO), 2.00 (s, 18H, $C_6(CH_3)_6$), 1.85-1.74 (m, 4H, $(CH_2)_2$), 1.50-1.34 (m, 12H, $(CH_2)_6$). MS (ESI) *m/z*: 635.0 [(M-{$C_6H_4COOC_6H_4C_6H_4CN$})+Na]$^+$. UV-Vis (CH_2Cl_2): λ_{max} 349 (4318), 278 (46268), 229 (16888) nm.

[(C_6H_6)Ru(L^3)Cl_2] (**40**): Yield: 0.2536 g, > 99%. IR (KBr, cm^{-1}): 3468(s), 2927(w), 1739(w), 1638(s, νCOO), 1505(w), 1188(w), 1093(w), 616(m). ^{1}H NMR (400 MHz, *CD*$_2$*Cl*$_2$) δ ppm 9.38 (d, ^3J = 7 Hz, 2H, NC_5H_4), 8.01 (d, ^3J = 7 Hz, 2H, NC_5H_4), 7.13 (d, ^3J = 9 Hz, 2H, C_6H_4), 6.95 (d, ^3J = 9 Hz, 2H, C_6H_4), 5.71 (s, 6H, C_6H_6), 3.98 (t, ^3J = 7 Hz, 2H, OCH_2), 3.67 (dt, ^3J = 6 Hz, ^3J = 7 Hz, 2H, CH_2OH), 1.83 (p, ^3J = 7 Hz, 2H, CH_2), 1.59 (p, ^3J = 7 Hz, 2H, CH_2), 1.46-1.32 (m, 14H, $(CH_2)_6$), 1.20 (t, ^3J = 6 Hz, 1H, OH).

[(*p*-$MeC_6H_4Pr^i$)Ru(L^3)Cl_2] (**41**): Yield: 0.2219 g, > 99%. IR (KBr, cm^{-1}): 3412(s), 2927(w), 1742(m), 1637(s, νCOO), 1504(m), 1384(w), 1188(m), 618(m). ^{1}H NMR (400 MHz, *CDCl*$_3$) δ ppm 9.32 (d, ^3J = 6 Hz, 2H, NC_5H_4), 8.00 (d, ^3J = 6 Hz, 2H, NC_5H_4), 7.13 (d, ^3J = 9 Hz, 2H, C_6H_4), 6.95 (d, ^3J = 9 Hz, 2H, C_6H_4), 5.49 (d, ^3J = 6 Hz, 2H, RuC_6H_4), 5.26 (d, ^3J = 6 Hz, 2H, RuC_6H_4), 3.98 (t, ^3J = 6 Hz, 2H, OCH_2), 3.67 (dt, *J* = 6 Hz, ^3J = 6.8 Hz, 2H, CH_2OH), 3.03 (m, 1H, CH), 2.13 (s, 3H, CH_3), 1.81 (p, ^3J = 6 Hz, 2H, CH_2), 1.61 (p, *J* = 7 Hz, 2H, CH_2), 1.48-1.28 (m, 18H, $(CH_3)_2$ and $(CH_3)_6$), 1.22 (t, ^3J = 6 Hz, 1H, OH).

[(C_6Me_6)Ru(L^3)Cl_2] (**42**): Yield: 0.2136 g, > 99%. IR (KBr, cm^{-1}): 3467(s), 2926(w), 1741(w), 1638(s, νCOO), 1189(m), 1093(w), 521(w). ^{1}H NMR (400 MHz, *CDCl*$_3$) δ ppm 9.10 (d, ^3J = 6 Hz, 2H, NC_5H_4), 7.97 (d, ^3J = 6 Hz, 2H, NC_5H_4), 7.13 (d, ^3J = 9 Hz, 2H, C_6H_4), 6.95 (d, ^3J = 9 Hz, 2H, C_6H_4), 3.98 (t, ^3J = 6 Hz, 2H, OCH_2), 3.67 (dt, ^3J = 5 Hz, ^3J = 6 Hz, 2H, CH_2OH), 2.02 (s, 18H, $C_6(CH_3)_6$), 1.79 (p, ^3J = 6 Hz, 2H, CH_2), 1.59 (p, ^3J = 7 Hz, 2H, CH_2), 1.47-1.27 (m, 12H, $(CH_2)_6$), 1.22 (t, ^3J = 5 Hz, 1H, OH).

*Preparation of the Complexes [(arene)Ru(L^1)$_2$Cl]$^+$ (**22** – **24**)*

A mixture of the appropriate [(arene)Ru($\mathbf{L^1}$)Cl_2] complex (**13 – 15**) and 1 equivalent of $AgCF_3SO_3$ in CH_3OH (25 mL) was stirred at room temperature. After 2 h, the mixture was filtered and AgCl discarded off. Then, one equivalent of $\mathbf{L^1}$ was added to the filtrate and stirred overnight at room temperature. The next day, the orange solution was evaporated to dryness under reduced pressure and the final product was collected and dried *in vacuo*.

[(C_6H_6)Ru(L^1)$_2$Cl]CF_3SO_3 ([**22**][CF_3SO_3]): Yield: 0.154 g, > 86.6 %. ^{1}H NMR (400 MHz, *CD_2Cl_2*) δ ppm 9.30 (d, *J* = 6 Hz, 4H, NC_5H_4), 8.08 (d, *J* = 6 Hz, 4H, NC_5H_4), 7.07 (d, ^3J = 9 Hz, 4H, C_6H_4), 6.91 (d, ^3J = 9 Hz, 4H, C_6H_4), 6.12 (s, 6H, C_6H_6), 3.95 (t, ^3J = 6 Hz, 4H, OCH_2), 1.80 (m, 4H, CH_2), 1.46-1.26 (m, 28H, $(CH_2)_7$), 0.89 (t, ^3J = 6 Hz, 6H, CH_3) ppm. ^{13}C(^{1}H) NMR (100 MHz, $CDCl_3$): δ = 162.5 (2C, C=O), 157.5 (2C, C–O), 156.0 (4C, NCH), 143.6 (2C, C–O), 139.8 (4C, C_{py}), 125.7 (4C, CH_{py}), 122.0 (4C, CH), 115.1 (4C, CH), 87.2(6C, C_6H_6), 68.6 (2C, OCH_2), 32.0-22.8 (16C, $(CH_2)_8$), 14.3 (2C, CH_3) ppm.

[(*p*-$MeC_6H_4Pr^i$)Ru(L^1)$_2$Cl]CF_3SO_3 ([**23**][CF_3SO_3]): Yield: 0.0.147 g, > 86.1 %. ^{1}H NMR (400 MHz, *$CDCl_3$*) δ ppm 9.48 (d, *J* = 6.4 Hz, 4H, NC_5H_4), 8.14 (d, *J* = 6.8 Hz, 4H, NC_5H_4), 7.09 (d, *J* = 9.2 Hz, 4H, C_6H_4), 6.91 (d, *J* = 9.2 Hz, 4H, C_6H_4), 6.06 (d, *J* = 6.0 Hz, 2H, RuC_6H_4), 5.90 (d, *J* = 6.0 Hz, 2H, RuC_6H_4), 3.95 (t, *J* = 6.4 Hz, 4H, OCH_2), 2.58 (m, 1H, CH), 1.80-1.73 (m, 7H, CH_3 and CH_2), 1.46-1.27 (m, 28H, $(CH_2)_7$), 1.17 (d, *J* = 6.8 Hz, 6H, $(CH_3)_2$), 0.87 (t, *J* = 6.8 Hz, 3H, CH_3) ppm. ^{13}C(^{1}H) NMR (100 MHz, $CDCl_3$): δ = 162.5 (2C, C=O), 157.6 (2C, C–O), 156.0 (4C, NCH), 143.6 (2C, C–O), 139.8 (2C, C_{py}), 125.8 (4C, CH_{py}), 122.0 (4C, CH), 115.3 (4C, CH), 103.6(1C, RuC), 102.3(1C, RuC), 89.0(2C, RuCH), 83.0(2C, RuCH), 68.6 (2C, OCH_2), 32.0-18.0 (36C), 14.3 (2C, CH_3) ppm.

[(C_6Me_6)Ru(L^1)$_2$Cl]CF_3SO_3 ([**24**][CF_3SO_3]): Yield: 0.146 g, > 87.2 %. ^{1}H NMR (400 MHz, *$CDCl_3$*) δ ppm 9.44 (d, ^3J = 6 Hz, 4H, NC_5H_4), 8.25 (d, ^3J = 6 Hz, 4H, NC_5H_4), 7.12 (d, ^3J = 9 Hz, 4H, C_6H_4), 6.93 (d, ^3J = 9 Hz, 4H, C_6H_4), 3.97 (t, ^3J = 6 Hz, 4H, OCH_2), 2.02 (s, 18H, $C_6(CH_3)_6$), 1.81 (m, 4H, CH_2), 1.47-1.28 (m, 14H, $(CH_2)_7$), 0.90 (t, ^3J = 7 Hz, 3H, CH_3). ^{13}C(^{1}H) NMR (100 MHz, $CDCl_3$): δ = 157.0 (2C, C=O), 155.5 (2C, C–O), 143.0 (4C, NCH), 138.0 (2C, C–O), 125.7 (4C, C_{py}), 121.8 (4C, CH_{py}), 115.1 (4C, CH), 94.6 (12C, $CH_3(C_6)$), 68.4 (2C, OCH_2), 31.8-15.43 (16C, $(CH_2)_8$), 14.1 (2C, CH_3) ppm.

[(C_6H_6)Ru(L^4)Cl]Cl ([**45**][Cl]): A mixture of [(C_6H_6)Ru_2Cl_4] dimer (0.0168 g, 0.03 mmol) and 2 equivalents of the ligand $\mathbf{L^4}$ in CH_3OH (20 mL) was refluxed. After 2 h, the yellow solution was cooled and filtered. The solvent was evaporated to dryness, and the final product was collected and dried *in vacuo*. Yield: 0.0625 g, > 99%. IR (KBr, cm^{-1}): 3435(s), 2925(m), 2098(w), 1638(s), 1508(s), 1232(m), 837(w), 619(m). ^{1}H NMR (400 MHz, CD_2Cl_2) δ ppm 9.79 (s, 2H, NCH), 8.17 (d, ^3J = 8 Hz, 2H, NCCH), 8.12 (d, ^3J = 8 Hz, 2H, CCH), 6.99 (d, ^3J = 9 Hz, 4H, C_6H_4), 6.88 (d, ^3J = 9 Hz, 4H, C_6H_4), 6.30 (s, 6H, C_6H_6), 5.50-5.26 (dd, ^2J = 14, 4H, CCH_2O), 3.92 (t, ^3J = 7 Hz, 4H, OCH_2), 1.78 (p, ^3J = 7 Hz, 4H, CH_2), 1.46-1.26 (m, 28H, $(CH_2)_7$), 0.90 (t, ^3J = 6 Hz, 6H, CH_3).

[(C_6H_6)Ru(L^4)(H_2O)]SO_4 ([**48**][SO_4]): A mixture of [(C_6H_6)Ru(L^4)Cl]Cl (0.0625 g, 0.067 mmol) and 1 equivalent of Ag_2SO_4 in CH_3OH (10 mL) was stirred and treated with ultrasonic bath. After 1 h, the yellow solution was filtered off, the solvent was evaporated to dryness, and the final product was collected and dried *in vacuo*. Yield: 0.0616 g, > 94 %. ^{1}H NMR (400 MHz, CD_2Cl_2) δ ppm 9.66 (s, 2H, NCH), 8.44 (m, 2H, NCCH), 7.97 (m, 2H, CCH), 6.95 (d, ^3J = 9 Hz, 4H, C_6H_4), 6.80 (d, ^3J = 9 Hz, 4H, C_6H_4), 6.17-6.11 (m, 4 H, RuC_6H_4), 5.51-5.19 (dd, ^2J = 14, 4H, CCH_2O), 3.84 (t, ^3J = 7 Hz, 4H, OCH_2), 2.55 (sept, ^3J = 7 Hz, 1H, $CH(CH_3)_2$), 2.16 (s, 3H, CH_3), 1.75 (p, ^3J = 7 Hz, 4H, CH_2), 1.41-1.27 (m, 28H, $(CH_2)_7$), 0.99 (d, ^3J = 7 Hz, 6H, $(CH_3)_2$), 0.90 (t, ^3J = 6 Hz, 6H, CH_3).

[(*p*-$MeC_6H_4Pr^i$)Ru(L^4)Cl]Cl ([**46**][Cl]): A mixture of [(*p*-$MeC_6H_4Pr^i$)Ru_2Cl_4] dimer (0.0238 g, 0.04 mmol) and 2 equivalents of the ligand $\mathbf{L^4}$ in CH_2Cl_2/CH_3OH (1:1, 20 mL) was refluxed. After 2 h, the yellow solution was cooled, the solvent was evaporated to dryness, and the final product was collected and dried *in vacuo*. Yield: 0.0766 g, > 99 %. (Found: C, 64.55; H, 7.83; N, 2.67. Calc. for $C_{54}H_{74}Cl_2N_2O_4Ru$ (*M* = 987.2): C, 64.70; H, 7.88; N, 2.67%). IR (KBr, cm^{-1}): 3434(s), 2924(m), 2039(w), 1638(s), 1508(m), 1233(m), 1050(m), 620(m). ^{1}H NMR (400 MHz, CD_2Cl_2) δ ppm 9.71 (s, 2H, NCH), 8.22 (d, ^3J = 8 Hz, 2H, NCCH), 8.14 (d, ^3J = 8 Hz, 2H, CCH), 6.99 (d, ^3J = 9 Hz, 4H, C_6H_4), 6.87 (d, ^3J = 9 Hz, 4H, C_6H_4), 6.14 (d, ^3J = 6 Hz, 2H, RuC_6H_4), 6.04 (d, ^3J = 6 Hz, 2H, RuC_6H_4), 5.58-5.30 (dd, ^2J = 14, 4H, CCH_2O), 3.91 (t, ^3J = 7 Hz, 4H, OCH_2), 2.57 (sept, ^3J = 7 Hz, 1H, $CH(CH_3)_2$), 2.27 (s, 3H, CH_3), 1.78 (p, ^3J = 7 Hz, 4H, CH_2), 1.46-1.26 (m, 28H, $(CH_2)_7$), 0.99 (d, ^3J = 7 Hz, 6H, $(CH_3)_2$), 0.90 (t, ^3J = 7 Hz, 6H, CH_3). MS(ESI) *m/z*: 951.5 [M-Cl].

[(*p*-$MeC_6H_4Pr^i$)Ru(L^4)(H_2O)]SO_4 ([**49**][SO_4]): A mixture of [(*p*-$MeC_6H_4Pr^i$)Ru($\mathbf{L^4}$)Cl]Cl (0.0766 g, 0.08 mmol) and 1 equivalent of Ag_2SO_4 in CH_3OH (10 mL) was stirred and

treated with ultrasonic bath. After 1 h, the yellow solution was filtered off, the solvent was evaporated to dryness, and the final product was collected and dried *in vacuo*. Yield: 0.0741 g, > 92.7 %. ^{1}H NMR (400 MHz, CD_2Cl_2) δ ppm 9.66 (s, 2H, NCH), 8.45 (m, 2H, NCCH), 7.97 (m, 2H, CCH), 6.95 (d, ^{3}J = 9 Hz, 4H, C_6H_4), 6.80 (d, ^{3}J = 9 Hz, 4H, C_6H_4), 6.17-6.11 (m, 4 H, RuC_6H_4), 5.51-5.19 (dd, ^{2}J = 14, 4H, CCH_2O), 3.84 (t, ^{3}J = 7 Hz, 4H, OCH_2), 2.55 (sept, ^{3}J = 7 Hz, 1H, $CH(CH_3)_2$), 2.16 (s, 3H, CH_3), 1.75 (p, ^{3}J = 7 Hz, 4H, CH_2), 1.41-1.27 (m, 28H, $(CH_2)_7$), 0.99 (d, ^{3}J = 7 Hz, 6H, $(CH_3)_2$), 0.90 (t, ^{3}J = 6 Hz, 6H, CH_3). MS(ESI) *m/z*: 951.6 $[(M-\{SO_4\})+H_2O]^+$.

$[(C_6Me_6)Ru(L^4)Cl]Cl$ ([**47**][Cl]): A mixture of $[(C_6Me_6)Ru_2Cl_4]$ dimer (0.0244 g, 0.04 mmol) and 2 equivalents of the ligand $\mathbf{L^4}$ in CH_2Cl_2/CH_3OH (2:1, 15 mL) was refluxed. After 2 h, the yellow solution was cooled, the solvent was evaporated to dryness, and the final product was collected and dried *in vacuo*. Yield: 0.0741 g, > 99 %. IR (KBr, cm^{-1}): 3436(s), 2925(w), 2026(w), 1638(m), 1506(w), 1188(w), 617(w). ^{1}H NMR (400 MHz, $CDCl_3$) δ ppm 9.08 (d, ^{3}J = 6 Hz, 4H, NC_5H_4), 7.96 (d, ^{3}J = 6 Hz, 4H, NC_5H_4), 7.11 (d, ^{3}J = 9 Hz, 4H, C_6H_4), 6.93 (d, ^{3}J = 9 Hz, 4H, C_6H_4), 3.96 (t, ^{3}J = 6 Hz, 4H, OCH_2), 2.02 (s, 18H, $C_6(CH_3)_6$), 1.79 (m, 4H, CH_2), 1.47-1.27 (m, 28H, $(CH_2)_7$), 0.88 (t, ^{3}J = 7 Hz, 6H, CH_3).

$[(C_6Me_6)Ru(L^4)(H_2O)]SO_4$ ([**48**][SO_4]): A mixture of $[(C_6Me_6)Ru(\mathbf{L^4})Cl]Cl$ (0.0741 g, 0.08 mmol) and 1 equivalent of Ag_2SO_4 in CH_3OH (10 mL) was stirred and treated with ultrasonic bath. After 1 h, the yellow solution was filtered off, the solvent was evaporated to dryness, and the final product was collected and dried *in vacuo*. Yield: 0.0741 g, > 92.7 %. ^{1}H NMR (400 MHz, CD_2Cl_2) δ ppm 9.85 (m, 2H, NCH), 8.16 (m, 2H, NCCH), 8.05 (m, 2H, CCH), 6.82 (m, 4H, C_6H_4), 6.20 (m, 4H, CCH_2), 3.86 (t, 4 H, OCH_2), 1.75 (p, ^{3}J = 7 Hz, 4H, CH_2), 1.75-1.27 (m, 44H, $(CH_2)_7$ and $C_6(CH_3)_6$), 0.88 (t, 6H, CH_3) ppm.

$[(C_6H_6)Ru(L^5)Cl]Cl$ ([**53**][Cl]): A mixture of $[(C_6H_6)Ru_2Cl_4]$ dimer (0.0056 g, 0.01 mmol) and 2 equivalents of the ligand $\mathbf{L^5}$ in CH_3OH/CH_2Cl_2 (1:1, 20 mL) was refluxed. After 2 h, the yellow solution was cooled and filtered. The solvent was evaporated to dryness, and the final product was collected and dried *in vacuo*. Yield: 0.02 g, > 99%. ^{1}H NMR (400 MHz, CD_2Cl_2) δ ppm 9.64 (d, ^{3}J = 4 Hz, 2H, NCH), 8.37 (s, 2H, NCCH), 7.74 (d, ^{3}J = 4 Hz, 2H, CCH), 6.91 (d, ^{3}J = 8 Hz, 4H, C_6H_4), 6.86 (d, ^{3}J = 8 Hz, 4H, C_6H_4), 6.26 (s, 6H, C_6H_6), 5.23 (s, 4H, CCH_2O), 3.91 (t, ^{3}J = 8 Hz, 4H, OCH_2), 1.79 (p, ^{3}J = 8 Hz, 4H, CH_2), 1.46-1.27 (m, 28H, $(CH_2)_7$), 0.89 (t, ^{3}J = 6 Hz, 6H, CH_3). MS (ESI) *m/z*: 895.6 $[(M-Cl)+H]^+$

*Preparation of the Ruthenium Nanoparticles **26 - 29***

The **5**-stabilized Ru nanoparticles **26** were prepared by reducing **13** (5 mg, 8.26 x 10^{-3} mmol) under solvent-free conditions in a magnetically stirred stainless-steel autoclave (volume 100 mL) with H_2 (50 bar) at 100 ˚C for 64 h. Alternatively, the **5**-stabilized Ru nanoparticles **27 - 29** were obtained by reacting 5 mg of [(arene)Ru$(H_2O)_3$]SO_4 (for **27** arene = C_6H_6; for **28** arene = *p*-$MeC_6H_4Pr^i$; for **29** arene = C_6Me_6) with one equivalent of ligand **5** in absolute ethanol (1 mL) in a magnetically stirred stainless-steel autoclave (volume 100 mL) under 50 bar pressure of H_2 at 100 ˚C for 14 h. After pressure release, the solvent was removed and the nanoparticles were dried *in vacuo*.

*Preparation of the Ruthenium Nanoparticles **30 - 31***

The pyridine stabilized Ru nanoparticles **30** – **31** were prepared by reducing 5 mg of [(arene)Ru$(H_2O)_3$]SO_4 (for **30** arene = *p*-$MeC_6H_4Pr^i$; for **31** arene = C_6H_6) with one equivalent of pyridine in absolute ethanol (5 mL) in a magnetically stirred stainless-steel autoclave (volume 100 mL) under 50 bar pressure of H_2 at 100 ˚C for 14 h. After pressure release, the solvent was removed and the nanoparticles were dried *in vacuo*.

*Preparation of the Ruthenium Nanoparticles **36***

The **32**-stabilized Ru nanoparticles **36** were prepared by reducing 5 mg of [(*p*-$MeC_6H_4Pr^i$)Ru$(H_2O)_3$]SO_4 with one equivalent of **32** in absolute ethanol (5 mL) in a magnetically stirred stainless-steel autoclave (volume 100 mL) under 50 bar pressure of H_2 at 100 ˚C for 14 h. After pressure release, the brownish black solution was isolated and treated with CH_2Cl_2 followed by centrifugation in order to remove excess of **32**.

*Preparation of the Ruthenium Nanoparticles **43***

The **39**-stabilized Ru nanoparticles **43** were prepared by reducing 5 mg of **20** with one equivalent of **39** in absolute ethanol (5 mL) in a magnetically stirred stainless-steel autoclave (volume 100 mL) under 40 bar pressure of H_2 at 100 ˚C for 14 h. After pressure release, the brownish black solution was isolated and treated with CH_2Cl_2 followed by centrifugation in order to remove excess of **39**.

*Preparation of the Ruthenium Nanoparticles **54***

The **52**-stabilized Ru nanoparticles **54** were prepared by reducing 5 mg of **20** with one equivalent of **52** in absolute ethanol (5 mL) in a magnetically stirred stainless-steel autoclave (volume 100 mL) under 40 bar pressure of H_2 at 100 ˚C for 14 h. After pressure release, the brownish black solution was isolated and treated with CH_2Cl_2 followed by centrifugation in order to remove excess of **52**.

Experimental Details – Chapter 3

Instrumentation

NMR spectra were measured using Bruker DRX-400 MHz spectrometer. For the particle size determination, a transmission electron microscope Philips CM 200 operating at 200 kV was used, the hectorite sample being deposited on a 300 mesh copper grid covered by a carbon thin film. The hydrogenation of arenes, furfuryl alcohol and α,β-unsaturated ketones was carried out in a magnetically stirred stainless-steel autoclave. The air in the autoclave was displaced by purging three times with hydrogen prior to use. The experiments were carried out at different operating conditions. Quantitative chemical analysis of hydrogenation products was done by ^1H NMR spectroscopy in $CDCl_3$ using Bruker® DRX-400 MHz spectrometer and by GC-MS analysis. The GC separation was carried out on a ZB-5MS column (30m x 0.25mm, 0.25µm) using a temperature program of 25-200°C at 5°C/min. The instrument used was a ThermoFinnigan® Trace GC-Polaris Q. The data were collected by using extracted ion chromatograms of marker m/z values for each molecule from the total ion chromatograms (TIC).

Syntheses

White sodium hectorite (**1**) was prepared according to the method of Bergk and Woldt.[116] The sodium cation exchange capacity, determined according to the method of Lagaly,[117] was found to be 104 mEq per 100 g. The dimeric complex $[(C_6H_6)_2RuCl_2]_2$ was synthesized following the procedure reported by Arthur and Stephenson.[118]

*Preparation of Ruthenium(II)-Containing Hectorite **56***

The neutral complex $[(C_6H_6)_2RuCl_2]_2$ (83.8 mg, 0.17 mmol) was dissolved in distilled and Ar-saturated water (50 mL), giving a clear yellow solution after intensive stirring for 1 h.

The pH of this solution was adjusted to 8 (using a glass electrode) by adding the appropriate amount of 0.1 M NaOH. After filtration, this solution was added to 1 g of finely powdered and degassed (1 h high vacuum, then Ar-saturated) sodium hectorite **55**. The resulting suspension was stirred for 4 h at 20˚C. Then the yellow ruthenium(II)-containing hectorite **56** was filtered off and dried *in vacuo*.

*Preparation of Ruthenium(0)-Containing Hectorite **57** for Arene Hydrogenation by Reduction with Molecular Hydrogen*

The ruthenium(0)-containing hectorite **57** was obtained by reacting a suspension of the yellow ruthenium(II)-containing hectorite **56** (50 mg, 0.01592 mmol Ru) in a magnetically stirred stainless-steel autoclave (volume 100 mL) under a pressure of H_2 (50 bar) at 100˚C for 14 h using water or different alcohols (2.5 mL) as solvent. After pressure release and cooling, **57** was isolated as a black material.

*Preparation of Ruthenium(0)-Containing Hectorite **57** for Arene Hydrogenation by Reduction with Refluxing Alcohols*

Alternatively, the ruthenium(0)-containing hectorite **57** was prepared by reducing yellow hectorite **56** (50 mg, 0.01592 mmol Ru) without hydrogen in refluxing alcohols (10 mL), the reaction time varying from 12 to 96 h for completion, depending on the alcohol.

*Preparation of Ruthenium(0)-Containing Hectorite **3** for Furfuryl Alcohol Hydrogenation*

The ruthenium(0)-containing hectorite **57** was obtained by reacting a suspension of the yellow ruthenium(II)-containing hectorite **56** (50 mg, 0.01592 mmol Ru) in a magnetically stirred stainless-steel autoclave (volume 100 mL) under a pressure of H_2 (50 bar) at 100˚C for 14 h using different solvents and different volumes. After pressure release and cooling, **57** was isolated as a black material.

*Regeneration of Ruthenium(0)-Containing Hectorite **57** for Furfuryl Alcohol Hydrogenation*

Regenerated ruthenium(0)-containing hectorite **57** was obtained by reacting a suspension of recycled ruthenium(0)-containing hectorite in a magnetically stirred stainless-steel autoclave (volume 100 mL) under a pressure of H_2 (50 bar) at 100˚C for 14 h using methanol (18 mL).

*Preparation of Ruthenium(0)-containing Hectorite **57** for Selective Hydrogenation of C=C Bond in α,β-Unsaturated Ketones*

The ruthenium(0)-containing hectorite **57** was obtained by reacting a suspension of the yellow ruthenium(II)-containing hectorite **56** (50 mg, 0.01592 mmol Ru) in a magnetically stirred stainless-steel autoclave (volume 100 mL) under a pressure of H_2 (50 bar) at 100 °C for 14 h using ethanol (5 mL) as solvent. After pressure release and cooling for 48 h, **57** was isolated as a black material.

*Preparation of Ruthenium(0)-containing Hectorite **3** for Selective Hydrogenation of C=O Bond in α,β-Unsaturated Ketones*

The ruthenium(0)-containing hectorite **57** was obtained by reacting a suspension of the yellow ruthenium(II)-containing hectorite **56** (50 mg, 0.01592 mmol Ru) in a magnetically stirred stainless-steel autoclave (volume 100 mL) under a pressure of H_2 (50 bar) at 100 °C for 14 h using ethanol (10 mL) as solvent. After pressure release and cooling, **57** was isolated as a black material.

*Preparation of Ruthenium(II)-Containing Hectorites **64 – 66***

The neutral complex $[(arene)_2Ru_2Cl_4]$ (0.17 mmol), arene being $[(C_6H_6)_2Ru_2Cl_4]$, $[(p\text{-}MeC_6H_4Pr^i)_2Ru_2Cl_4]$ and $[(C_6Me_6)_2Ru_2Cl_4]$, was dissolved in distilled and Ar-saturated water (50 mL), giving a clear yellow solution after intensive stirring for 1 h. The yellow solution was passed through a strongly basic anion exchange resin to give **61 – 63**. After filtration, this solution **61 – 63** was added to 1 g of finely powdered and degassed (1 h high vacuum, then Ar-saturated) sodium hectorite **55**. The resulting suspension was stirred for 4 h at 20˚C. Then the yellow ruthenium(II)-containing hectorite **64 – 66** was filtered off and dried *in vacuo*.

*Preparation of Ruthenium(0)-Containing Hectorites **67 – 69***

The ruthenium(0)-containing hectorites **67 – 69** were obtained by reacting a suspension of the yellow ruthenium(II)-containing hectorite **64 – 66** (50 mg) in a magnetically stirred stainless-steel autoclave (volume 100 mL) under a pressure of H_2

(50 bar) at 100˚C for 14 h using ethanol (2.5 mL) as solvent. After pressure release and cooling, **67 – 69** were isolated as black materials.

*Preparation of Ruthenium(II)-Containing Montmorillonite **73***

The neutral complex $[(C_6H_6)_2RuCl_2]_2$ (83.8 mg, 0.17 mmol) was dissolved in distilled and N_2-saturated water (50 mL), giving a clear yellow solution after intensive stirring for 1 h. The pH of this solution was adjusted to 8 (using a glass electrode) by adding the appropriate amount of 0.1 M NaOH. After filtration, this solution was added to 1 g of finely powdered and degassed (1 h high vacuum, then Ar-saturated) sodium montmorillonite **72**. The resulting suspension was stirred for 4 h at 20˚C. Then the yellow ruthenium(II)-containing montmorillonite was filtered off and dried *in vacuo*.

*Preparation of Ruthenium(0)-Containing Montmorillonite **74***

The ruthenium(0)-containing montmorillonite was obtained by reacting a suspension of the yellow ruthenium(II)-containing Montmorillonite **73** (50 mg, 0.01592 mmol Ru) in a magnetically stirred stainless-steel autoclave (volume 100 mL) under a pressure of H_2 (50 bar) at 100˚C for 14 h using either water or ethanol (2.5 mL) as solvent or no solvent. After pressure release and cooling, ruthenium(0)-containing montmorillonite was isolated as a black material.

*Preparation of Ruthenium(II)-Containing Y-Zeolite **76***

The neutral complex $[(C_6H_6)_2RuCl_2]_2$ (334 mg, 0.67 mmol) was dissolved in distilled and N_2-saturated water (50 mL), giving a clear yellow solution after intensive stirring for 1 h. The pH of this solution was adjusted to 8 (using a glass electrode) by adding the appropriate amount of 0.1 M NaOH. After filtration, this solution was added to 0.5 g of finely powdered and degassed (1 h high vacuum, then Ar-saturated) Y-NH_4 zeolite **75**. The resulting suspension was stirred for 4 h at 20˚C. Then the yellow ruthenium(II)-containing Y-zeolite was filtered off, washed with water (25 mL) and dried *in vacuo*.

*Preparation of Ruthenium(0)-Containing Y-Zeolites **77***

The ruthenium(0)-containing Y-zeolite was obtained by reacting a suspension of the yellow ruthenium(II)-containing Y-zeolite **76** (50 mg, 0.04029 mmol Ru) in a magnetically stirred stainless-steel autoclave (volume 100 mL) under a pressure of H_2 (50 bar) at 100˚C for 14 h using either water or ethanol (2.5 mL) as solvent or no

solvent. After pressure release and cooling, ruthenium(0)-containing Y-zeolite was isolated as a black material.

*Preparation of Ruthenium(II)-Containing USY-Zeolite **79***

The neutral complex $[(C_6H_6)_2RuCl_2]_2$ (243 mg, 0.49 mmol) was dissolved in distilled and N_2-saturated water (50 mL), giving a clear yellow solution after intensive stirring for 1 h. The pH of this solution was adjusted to 8 (using a glass electrode) by adding the appropriate amount of 0.1 M NaOH. After filtration, this solution was added to 0.5 g of finely powdered and degassed (1 h high vacuum, then Ar-saturated) USY-NH_4 zeolite **78**. The resulting suspension was stirred for 4 h at 20˚C. Then the yellow ruthenium(II)-containing USY-zeolite was filtered off, washed with water (25 mL) and dried *in vacuo*.

*Preparation of Ruthenium(0)-Containing USY-Zeolite **80***

The ruthenium(0)-containing USY-zeolite was obtained by reacting a suspension of the yellow ruthenium(II)-containing USY-zeolite **79** (50 mg, 0.03510 mmol Ru) in a magnetically stirred stainless-steel autoclave (volume 100 mL) under a pressure of H_2 (50 bar) at 100˚C for 14 h using either water or ethanol (2.5 mL) as solvent or no solvent. After pressure release and cooling, ruthenium(0)-containing USY-Zeolites was isolated as a black material.

*Preparation of Ruthenium(II)-Containing GRACE SP-1522 Silica **82***

The neutral complex $[(C_6H_6)_2RuCl_2]_2$ (211 mg, 0.42 mmol) was dissolved in distilled and N_2-saturated water (50 mL), giving a clear yellow solution after intensive stirring for 1 h. The pH of this solution was adjusted to 8 (using a glass electrode) by adding the appropriate amount of 0.1 M NaOH. After filtration, this solution was added to 0.5 g of finely powdered and degassed (1 h high vacuum, then Ar-saturated) GRACE SP-1522 silica **81**. The resulting suspension was stirred for 4 h at 20˚C. Then the yellow ruthenium(II)-containing GRACE SP-1522 silica was filtered off, washed with water (25 mL) and dried *in vacuo*.

*Preparation of Ruthenium(0)-Containing GRACE SP-1522 Silica **83***

The ruthenium(0)-containing GRACE SP-1522 silica was obtained by reacting a suspension of the yellow ruthenium(II)-containing GRACE SP-1522 Silica **82** (50 mg, 0.01936 mmol Ru) in a magnetically stirred stainless-steel autoclave (volume 100 mL) under a pressure of H_2 (50 bar) at 100˚C for 14 h using either water or ethanol (2.5 mL)

as solvent or no solvent. After pressure release and cooling, ruthenium(0)-containing GRACE SP-1522 Silica was isolated as a black material.

*Preparation of Ruthenium(II)-Containing SBA-15 Silica **85***

The neutral complex $[(C_6H_6)_2RuCl_2]_2$ (169 mg, 0.34 mmol) was dissolved in distilled and N_2-saturated water (50 mL), giving a clear yellow solution after intensive stirring for 1 h. The pH of this solution was adjusted to 8 (using a glass electrode) by adding the appropriate amount of 0.1 M NaOH. After filtration, this solution was added to 0.5 g of finely powdered and degassed (1 h high vacuum, then Ar-saturated) SBA-15 silica **84**. The resulting suspension was stirred for 4 h at 20˚C. Then the yellow ruthenium(II)-containing SBA-15 silica was filtered off, washed with water (25 mL) and dried *in vacuo*.

*Preparation of Ruthenium(0)-Containing SBA-15 Silica **86***

The ruthenium(0)-containing SBA-15 silica was obtained by reacting a suspension of the yellow ruthenium(II)-containing SBA-15 silica **85** (50 mg, 0.02331 mmol Ru) in a magnetically stirred stainless-steel autoclave (volume 100 mL) under a pressure of H_2 (50 bar) at 100˚C for 14 h using either water or ethanol (2.5 mL) as solvent or no solvent. After pressure release and cooling, ruthenium(0)-containing SBA-15 silica was isolated as a black material.

Catalysis

The catalytic hydrogenation of arenes was carried out in a magnetically stirred stainless-steel autoclave. The air in the autoclave was removed by purging three times with hydrogen.

*Benzene Hydrogenation with Freshly Prepared Ruthenium(0)-Hectorite **57** in the Original Solvent*

A freshly prepared suspension (2.5 mL) of ruthenium(0)-containing hectorite **57** was used, 2.5 mL of the same solvent as well as 5.0 mL of benzene were added. Then the autoclave was heated under rigorous stirring to 50˚C for 2 h (preheating period) and then pressurized with hydrogen (50 bar). When the pressure had dropped to 35 bar (15

min to 4 h), the autoclave was cooled in an ice-bath. After pressure release, the solution was decanted from the solid and analyzed.

*Benzene Hydrogenation with Ruthenium(0)-Hectorite **57** in Ethanol*

A freshly prepared suspension (2.5 mL) of ruthenium(0)-containing hectorite **57** was allowed to settle down, the black precipitates were isolated by decanting and washing with ethanol (3 times, 10 mL) without drying. Then **57** was suspended in 5 mL of ethanol. After addition of 5 mL of benzene, the autoclave was heated under rigorous stirring to 50 °C for 2 h (preheating period) and then pressurized with hydrogen (50 bar). When the pressure had dropped to 35 bar (20 min to 57 h), the autoclave was cooled in an ice-bath. After pressure release, the solution was decanted from the solid and analyzed.

Arene Hydrogenation with Other Supported Ruthenium(0) Catalysts (Silicas, Zeolites)

A freshly prepared suspension (2.5 mL) of ruthenium(0)-containing catalyst was used, 2.5 mL of the same solvent as well as 5.0 mL of corresponding arene were added. Then the autoclave was heated under rigorous stirring at 50 °C for 2 h (preheating period) and then pressurized with hydrogen (50 bar). When the pressure had dropped to 35 bar, the autoclave was cooled in an ice-bath. After pressure release, the solution was decanted from the solid and analyzed.

*Catalytic Hydrogenation of Furfuryl Alcohol with Freshly Prepared **57***

A freshly prepared suspension (10 mL) of the ruthenium(0)-containing hectorite **57** in the appropriate solvent was introduced into 100 mL stainless-steel autoclave and 1.0 mL of FA was added. After pressurizing with hydrogen (15-30 bar), the autoclave was subjected to rigorous stirring at 40-60 °C. After 2 h, the pressure was released, and the autoclave was cooled in an ice-bath. Then the solution was decanted from the solid and analyzed.

In order to determine the catalytic activity (TON, TOF) and selectivity, a freshly prepared suspension of ruthenium(0)-containing hectorite **57** in methanol (18 mL) was used, 0.2 mL of FA was added, pressurized with hydrogen (20 bar) and subjected to rigorous stirring at 40 °C. After 1 h, pressure was released, and the autoclave was cooled in an ice-bath. Then a sample was taken, filtered and analyzed.

The turnover number was determined by adding 0.2 mL of FA after regular intervals (1 h) until the catalyst became inactive, the total volume of substrate added being 2 mL. The selectivity was checked by GC-MS. The same catalytic procedure was followed for the recycled and regenerated ruthenium(0)-containing hectorite **57**.

*Selective C=C bond Hydrogenation in α,β-Unsaturated Ketones with Freshly Prepared **57***

A freshly prepared suspension (5 mL) of ruthenium(0)-containing hectorite **57** was used, ethanol (15 mL) as well as the corresponding α,β-unsaturated ketone (12.2 mmol) were added. Then the autoclave was heated at 35 °C under constant hydrogen pressure (1-10 bar). After 1h, the pressure was released, the solution was filtered (0.22 µm, PTFE) and analyzed by GC-MS in order to determine the substrate conversion and selectivity (in %). The turnover number for 3-buten-2-one and 3-penten-2-one was determined by adding 12.2 mmol of substrate in regular intervals, until the catalyst lost its selectivity. However, in the case of 4-methyl-3-penten-2-one, 122 mmol of substrate was added in regular intervals, until the catalyst lost its activity.

*Selective C=O bond Hydrogenation in α,β-Unsaturated Ketones with Freshly Prepared **57***

A freshly prepared suspension (10 mL) of ruthenium(0)-containing hectorite **57** was used, ethanol (40 mL) as well as the corresponding α,β-unsaturated ketone (12.2 mmol) were added. Then, the reaction mixture was stirred vigorously at 0 °C under constant hydrogen pressure (15 bar). After 5h, the pressure was released, the solution was filtered (0.22 µm, PTFE) and analyzed by GC-MS in order to determine the substrate conversion and selectivity (in %).

Experimental Details – Chapter 4

Preparation of Fe_3O_4 Nanoparticles:

Fe_3O_4 nanoparticles were prepared by the co-precipitation method:[96,213a] Freshly prepared aqueous solution of 1M $FeCl_3$ (10 mL) was mixed with 2M $FeCl_2$ (2.5 mL) dissolved in 2M HCl. Both solutions were prepared in deoxygenated water. Immediately

after being mixed under nitrogen, the solution containing the iron chlorides was added to 0.7M NH_3 (125 mL) under N_2. After 30 min of vigorous stirring, the pH was adjusted to 10 by using 2M NaOH. After 1h, the black Fe_3O_4 nanoparticles formed were separated magnetically.

*Preparation of Fe_3O_4/$[(C_6H_6)Ru(H_2O)_3]^{2+}$ Nanoparticles **87***

Fe_3O_4 nanoparticles were redispersed in 50 mL water containing 0.1 g of $[(C_6H_6)_2Ru_2Cl_4]$. This mixture was heated at 80 °C overnight. The resulting precipitate was separated magnetically, washed with H_2O (3 x 25 mL), and dried *in vacuo*.

*Preparation of Fe_3O_4/Ru Nanoparticles **88***

88 was obtained by reacting a suspension of **87** (0.5 g) in n-BuOH (20 mL) in a magnetically stirred stainless-steel autoclave (volume 100 mL) under a pressure of H_2 (50 bar) at 100 °C for 14 h. After pressure release and cooling, **88** was isolated by magnetic decantation and dried *in vacuo*.

Hydrogenation of trans-4-Phenyl-3-buten-2-one :

Freshly prepared **88** (0.5 g) was added to a solution of *trans*-4-phenyl-3-buten-2-one (1.78 g) in n-BuOH (20 mL). This solution was placed in an autoclave (100 mL), while rigorously stirring at 30 °C under H_2 (15 bar) was applied. After 8 h, the pressure was released, the solution was magnetically decanted from the solid and analyzed. The turnover number was determined by adding 1.78 g of substrate dissolved in n-BuOH (20 mL) after regular intervals, until the catalyst became inactive, the total volume of substrate added being 5.34 g. The selectivity was checked by GC-MS. For recycling, a permanent magnet was externally applied to isolate **88** on the side wall of the reactor. The reaction solution was decanted off, and the catalyst was re-used directly for the next run.

X-ray crystallographic details

The intensity data were collected at 173K (-100°C) on a Stoe Mark II-Image Plate Diffraction System equiped with a two-circle goniometer and using MoKα graphite monochromated radiation (λ = 0.71073 Å). The structure was solved by Direct methods using the programme SHELXS-97. The refinement and all further calculations were carried out using SHELXL-97.[219] The hydrogen atoms could be located in difference Fourier maps. The H_2O, OH^- and H-atoms were refined with distance restraints, O-H = 0.84(2) Å, with $U_{iso}(H) = 1.5U_{eq}(O)$. The C-bound H-atoms were included in calculated positions and treated as riding atoms: C-H = 0.95 with $U_{iso}(H) = 1.2U_{eq}$ (parent C-atom). The non-H atoms were refined anisotropically, using weighted full-matrix least-squares on F^2. A semi-empirical absorption correction was applied using the MULscanABS routine in PLATON.[220] Crystallographic details are summarised in Tables 24 and 25. Figure 4 and Figure 23 were drawn with ORTEP.[221]

Table 25. Crystallographic and structure refinement parameters for complex [(*p*-$MeC_6H_4Pr^i$)Ru(L^1)Cl_2]

Chemical formula	$C_{24}H_{27}Cl_2NO_3Ru$
Formula weight	549.44
Crystal system	Monoclinic
Space group	*P* $2_1/c$
Crystal colour and shape	orange block
Crystal size (mm)	0.19 x 0.16 x 0.15
a (Å)	14.3079(9)
b (Å)	8.4712(4)
c (Å)	19.3588(9)
α (°)	90
β (°)	99.463(4)
γ (°)	90
V (Å^3)	2314.5(2)
Z	4
T (K)	173(2)
D_c (g·cm^{-3})	1.577
μ (mm^{-1})	0.934
Scan range (°)	$1.44 < \theta < 25.11$
Unique reflections	4107
Observed refls [I > 2σ(I)]	2909
R_{int}	0.1062
Final *R* indices [I > 2σ(I)]*	R_1 0.0489, wR_2 0.0563
R indices (all data)	R_1 0.0877, wR_2 0.0620
Goodness-of-fit	0.978
Max., min. Δρ (e Å^{-3})	0.566, -0.699

* Structures were refined on F_0^2: $R_1 = \Sigma \big| \, |F_o| - |F_c| \, \big| / \Sigma |F_o|$, $wR_2 = [\Sigma [w (F_0^2 - F_c^2)^2] / \Sigma w (F_0^2)^2]^{1/2}$, where $w^{-1} = [\Sigma(F_0^2) + (aP)^2 + bP]$ and $P = [\max(F_0^2, 0) + 2F_c^2]/3$

Table 26. Crystallographic and structure refinement parameters for $[(C_6H_6)_2Ru_2(OH)_2(O)] \cdot 8H_2O$

Chemical formula	$C_{12}H_{30}O_{11}Ru_2$
Formula weight	551.49
Crystal system	Monoclinic
Space group	$P\ 2_1/m$
Crystal colour and shape	Yellow plate
Crystal size (mm)	0.23 × 0.22 × 0.10
a (Å)	8.5615 (1)
b (Å)	12.2582 (1)
c (Å)	9.6970 (2)
α (°)	90
β (°)	105.600 (1)°
γ (°)	90
V (Å^3)	980.2 (2)
Z	2
T (K)	173(2)
D_c (g·cm^{-3})	1.869
μ (mm^{-1})	1.59
Scan range (°)	2.2< θ < 29.60
Unique reflections	1807
Observed refls [I > 2σ(I)]	1534
R_{int}	0.028
Final R indices [I > 2σ(I)]*	R_1 0.0239, wR_2 0.0542
R indices (all data)	R_1 0.0315, wR_2 0.0562
Goodness-of-fit	1.01
Max., min. Δρ (e Å^{-3})	0.54, -0.66

* Structures were refined on F_0^2: $R_1 = \Sigma \left| \left| F_o \right| - \left| F_c \right| \right| / \Sigma \left| F_o \right|$, $wR_2 = [\Sigma\ [w\ (F_0^2 - F_c^2)^2] / \Sigma w\ (F_0^2)^2]^{1/2}$, where $w^{-1} = [\Sigma(F_0^2) + (aP)^2 + bP]$ and $P = [\max(F_0^2, 0) + 2F_c^2]/3$

7

References

1. J. S. Bradley, in *Cluster and Colloids* (ed. G. Schmid), Wiley VCH Weinheim, **1994**, p.459.
2. I. Freestone, N. Meeks, M. Sax, C. Higgitt, *Gold Bulletin*, **2007**, *40*, 270–277.
3. M. Faraday, *Phil. Trans. R. Soc.* **1857**, *147*, 145–181.
4. J. M. Thomas, *Pure Appl. Chem.* **1988**, *60*, 1517–1528.
5. C. P. Poole Jr., F. J. Owens, in *Introduction to Nanotechnology*, Wiley VCH Weinheim, **2003**, p. 02.
6. W. Ostwald, *Colloid-Zeitschrift.* **1907**, *1*, 291–331.
7. D. L. Rapino, F. F. Nord, *J. Am. Chem. Soc.* **1941**, *63*, 2745–2749.
8. http://www.zyvex.com/nanotech/feyman.html
9. M. Brust, M. Walker, D. Bethell, D. J. Schiffrin, R. Whyman, *J. Chem. Soc., Chem. Commun.* **1994**, 801–802.
10. D. Astruc, in *Nanoparticles and Catalysis* (ed. D. Astruc), Wiley VCH Weinheim, **2008**, p.01.
11. C. L. Donley, J. Zaumseil, J. W. Andreasen, M. M. Nielsen, H. Sirringhaus, R. H. Friend, J. S. Kim, *J. Am. Chem. Soc.* **2005**, *127*, 12890–12899.
12. A. S. W. Wong, G. W. Ho, S. L. Liew, K. C. Chua, D. Z. Chi, *Prog. Photovolt: Res. Appl.* **2011**, *19*, 464–472.
13. J. R. Chen, Y. Q. Miao, N. Y. He, X. H. Wu, S. J. Li, *Nanotech. Biosens. Biotech. Advances*, **2004**, *22*, 505–518.
14. D. Astruc, in *Nanoparticles and Catalysis* (ed. D. Astruc), Wiley VCH Weinheim, **2007**.

15. D. J. Irvine, *Nature Mater.* **2011**, *10*, 342–343.
16. X. L. Wu, L. Y. Jiang, F. F. Cao, Y. G. Guo, L. J. Wan, *Adv. Mater.* **2009**, *21*, 2710–2714.
17. Y. Suganuma, P. -E. Trudeau, A. Dhirani, *Nanotech.* **2005**, *16*, 1196–1203.
18. A. E. Kestell, G. T. Delorey, in *Nanoparticles : Properties, Classification, Characterization and Fabrication*, Nova Sci. Pub. Inc. NY, **2010**.
19. (a) K. Pelzer, M. Hävecker, M. Boualleg, J. -P. Candy, J. -M. Basset, *Angew. Chem. Int. Ed.* **2011**, *50*, 5170–5073; (b) G. Cao, Y. Wang, *Nanostructures and Nanomaterials* (vol. 2), in Chapter 2, World Sci. Publishing Singapore, **2004**.
20. J. P. Liu, in *Nanoscale Magnetic Materials and Applications*, (ed. J. P. Liu) Springer Science **2009**, p. 35.
21. C. Gautier, *Ph.D thesis*, University of Neuchâtel, **2008**.
22. C. Sanchez, *C. R. Chimie* 2010, *13*, 1–2.
23. http://www.strem.com/catalog/d/nanomaterials
24. S. -I. Marahashi, in *Ruthenium in Organic Synthesis* (ed. S. –I. Marahashi), Wiley VCH Weinheim, **2004**, p.01.
25. G. C. Trivino, K. J. Klabunde, E. B. Dale, *Langmuir* **1987**, *3*, 986–992.
26. (a) D. Astuc, *Nanoparticles and catalysis*, Wiley VCH Weinheim, **2008**, p.07; (b) B. Chaudret, *C. R. Physique* **2005**, *6*, 117–131.
27. R. J. White, R. Luque, V. L. Budarin, J. H. Clark, D. J. Macquarrie, *Chem. Soc. Rev.* **2009**, *38*, 481–494.
28. K. J. Klabunde, Y. -X. Li, B. -J. Tan, *Chem. Mater*. **1991**, *3*, 30–39.
29. S. Tsubota, M. Haruta, T. Kobayashi, A. Ueda, Y. Nakahara, G. Poncelet, P. Grange, P. A. Jacobs, *Preparation of Catalysts V*, Elsevier Science Publishers B.V. Amsterdam, **1991**, p. 695.
30. I. Dékàny, L. Turi, G. Galbacs, J. H. Fendler, *J. Colloid Interface Sci.* **1999**, *213*, 584–591.
31. A. Sandoval, A. Gómez-Cortés, R. Zanella, G. Diaz, J. M. Saniger, *J. Mol. Catal. A: Chem.* **2007**, *278*, 200–208.
32. (a) M. T. Reetz, W. Helbig, *J. Am. Chem. Soc.* **1994**, *116*, 7401-7402; (b) S. Dominguez-Dominguez, J. Arias-Pardilla, A. Berenguer-Murcia, E. Morallon, D. Cazorla-Amoros, *J. Appl. Electrochem.* **2008**, *38*, 259–268.
33. K. Pelzer, K. Philippot, B. Chaudret, *Z. Anorg. Allg. Chem.* **2003**, *629*, 1217–1222.
34. (a) G. Süss-Fink, B. Mollwitz, B. Therrien, M. Dadras, G. Laurenczy, A. Meister, G. Meister, *J. Clust. Sci.* **2007**, *18*, 87–95; (b) S. Shimazu, T. Hirano, T. Uematsu, *Appl. Catal.* **1987**, *34*, 255–261; (c) A. Meister, G. Meister, G. Süss-Fink, J. Mol. Catal. **1994**, *92*, L123–L126.
35. G. Winkhaus, H. Singer, *J. Organomet. Chem.* **1967**, *7*, 487–491.
36. R. A. Zelonka, M. C. Baird, *Can. J. Chem.* **1972**, *50*, 3063–3072.

37. M. A. Bennett, A. K. Smith, *J. Chem. Soc., Dalton Trans.* **1974**, 233–241.
38. J. W. Kang, K. Moseley, P. M. Maitlis, *J. Am. Chem. Soc.* **1969**, *91*, 5970–5977.
39. M. A. Bennett, T. N. Huang, T. W. Matheson, A. K. Smith, *Inorg. Synth.* **1982**, *21*, 74–78.
40. M. A. Bennett, J. P. Ennett, *Organometallics* **1984**, *3*, 1365–1374.
41. M. A. Bennett, L. Y. Goh, I. J. McMahon, T. R. B. Mitchell, G. B. Robertson, T. W. Turney, W. A. Wickramasinghe, *Organometallics* **1992**, *11*, 3069–3085.
42. (a) K. Pelzer, O. Vidoni, K. Philippot, B. Chaudret, V. Collière, *Adv. Funct. Mater.* **2003**, *13*, 118–126; (b) S. Gao, J. Zhang, Y. -F. Zhu, C. -M. Che, *New J. Chem.* **2000**, *24*, 739–740.
43. O. Vidoni, C. Amiens, K. Philippot, B. Chaudret, O. Balmes, J. -O. Malm, J. -O. Bovin, F. Senocq, M. -J. Casanove, *Angew. Chem. Int. Ed.* **1999**, *38*, 3736–3738.
44. M. Králik, A. Biffis, *J. Mol. Catal. A: Chem.* **2001**, *177*, 113–138.
45. R. A. Sánchez-Delgado, N. Machalaba, N. Ng-a-qui, *Catal. Commun.* **2007**, *8*, 2115–2118.
46. (a) A. N. Grace, K. Pandian, *Mater. Chem. Phys.* **2007**, *104*, 191-198; (b) X. Yan, H. Liu, K. Y. Liew, *J. Mater. Chem.* **2001**, *11*, 3387–3391.
47. (a) A. Duteil, R. Queau, B. Chaudret, *Chem. Mater.* **1993**, *5*, 341–347; (b) C. Pan, K. Pelzer, K. Philippot, B. Chaudret, F. Dassenoy, P. Lecante, M. -J. Casanove, *J. Am. Chem. Soc.* **2001,** *123*, 7584–7593.
48. I. Favier, D. Picurelli, C. Pradel, J. Durand, B. Milani, M. Gómez, *Inorg. Chem. Commun.* **2010**, *13*, 766–768.
49. (a) X. Kang, N. B. Zuckerman, J. P. Konopelski, S. Chen. *Angew. Chem. Int. Ed.* **2010**, *49*, 9496–9499; (b) W. Chen, N. B. Zuckerman, X. Kang, D. Ghosh, J. P. Konopelski, S. Chen. *J. Phys. Chem. C* **2010,** *114*, 18146–18152.
50. (a) G. Viau, R. Brayner, L. Poul, N. Chakroune, E. Lacaze, F. Fiévet-Vincent, F. Fiévet, *Chem. Mater.* **2003,** *15*, 486–494; (b) T. Tsukatani, H. Fujihara, *Langmuir* **2005,** *21*, 12093–12095.
51. C. Pan, K. Pelzer, K. Philippot, B. Chaudret, F. Dassenoy, P. Lecante, M. –J. Casanove, *J. Am. Chem. Soc.* **2001,** *123*, 7584–7593.
52. W. Chen, D. Ghosh, J. Sun, M. C. Tong, F. Deng, S. Chen, *Electrochim. Acta*, **2007**, *53*, 1150–1156.
53. W. Chen, N. B. Zuckerman, J. P. Konopelski, S. Chen, *Anal. Chem.* **2010,** *82*, 461–465.
54. (a) K. Pelzer, O. Vidoni, K. Phillipot, B. Chaudret, V. Collière, *Adv. Funct. Matter.* **2003**, *13*, 118–126. (b) Y. Wang, J. Ren, K. Deng, L. Gui, Y. Tang, *Chem. Mater.* **2000,** *12*, 1622–1627.
55. J. Yang, J. Y. Lee, T.C. Deivaraj, H. -P. Too, *J. Colloid Interface Sci.* **2004**, *271*, 308–312.
56. O. Vidoni, K. Philippot, C. Amiens, B. Chaudret, O. Balmes, J. -O. Alm, J. -O. Bovin, F. Senocq, M. -J. Casanove, *Angew. Chem. Int. Ed.* **1999**, *38*, 3736–3738.
57. K. Pelzer, K. Philippot, B. Chaudret, *Z. Phys. Chem.* **2003**, *217***,** 1539–1547.

58. M. Takasaki, Y. Motoyama, K. Higashi, S. -H. Yoon, I. Mochida, H. Nagashima, *Chem. Asian J.* **2007**, *2*, 1524–1533.
59. C. -M. Ho, W. -Y. Yu, C.-M. Che, *Angew. Chem., Int. Ed.* **2004**, *43*, 3303–3307.
60. J. Yang, T. C. Deivaraj, H. -P. Too, J. Y. Lee, *Langmuir* **2004**, *20*, 4241–4245.
61. N. Chakroune, G. Viau, S. Ammar, L. Poul, D. Veautier, M. M. Chehimi, C. Mangeney, F. Villain, F.Fiévet, *Langmuir* **2005,** *21*, 6788–6796.
62. L. M. Rossi, G. Machado, P. F. P. Fichtner, S. R. Teixeira, J. Dupont, *Catal. Lett.* **2004**, *92*, 149–155.
63. M. H. G. Prechtl, M. Scariot, J. D. Scholten, G. Machado, S. R. Teixeira, J. Dupont, *Inorg. Chem.* **2008**, *47*, 8995–9001.
64. (a) T. Gutel, J. Garcia-Anton, K. Pelzer, K. Philippot, C. C. Santini, Y. Chauvin, B. Chaudret, J. -M. Basset, *J. Mater. Chem.* **2007**, *17*, 3290–3292; (b) M. H.G. Prechtl, J. D. Scholten, J. Dupont, *J. Mol. Catal. A: Chem.* **2009**, *313*, 74–78; (c) L. M. Rossi, G. Machado, *J. Mol. Catal. A: Chem.***2009**, *298*, 69–73.
65. J. Pan, J. Li, C. Wang, Z. Yang, *React. Kinet. Catal. Lett.* **2007**, *90*, 233–242.
66. (a) G. Zehl, G. Schmithals, A. Hoell, S. Haas, C. Hartnig, I. Dorbandt, P. Bogdanoff, S. Fiechter, *Angew. Chem. Int. Ed.* **2007**, *46*, 7311–7314; (b) M. Besson, P. Gallezot, A. Perrard, C. Pinel, *Catal. Today*, **2005**, *160*, 102–103; (c) S. Mori, M. Takubo, K. Makida, T. Yanase, S. Aoyagi, T. Maegawa, Y. Monguchi,H. Sajiki, *Chem. Commun.* **2009**, 5159–5161; (d) A. Denicourt-Nowicki, A. Roucoux, F. Wyrwalski, N. Kania, E. Monflier, A. Ponchel, *Chem. Eur. J.* **2008**, *14*, 8090–8093.
67. J. Liu, P. Bai, X. S. Zhao, *Phys. Chem. Chem. Phys.* **2011**, *13*, 3758–3763.
68. J. M. Planeix, N. Coustel, B. Coq, V. Brotons, P. S. Kumbhar, R. Dutartre, P. Geneste, P. Bernier, P. M. Ajayan, *J. Am. Chem. Soc*. **1994**, *116*, 7935–7936.
69. Q. -C. Xu, J. -D. Lin, J. Li, X. -Z. Fu, Y. Liang, D. -W. Liao, *Catal. Commun.* **2007**, *8*, 1881–1885.
70. (a) Z. Y. Sun, Z. M. Liu, B. X. Han, Y. Wang, J. M. Du, Z. L. Xie, G. J. Han, *Adv. Mater.* **2005**, *17*, 928–932; (b) S. Guo, K. Y. Liew, J. Li, *J. Am. Oil Chem. Soc*. **2009**, *86*, 1141–1147.
71. (a) B. J. Arena, Des Plaines, US Pat. 4503274 (**1985**); (b) B.J. Arena, Des Plaines, US Pat. 4380680 (**1983**); (c) B.J. Arena, Des Plaines, US Pat. 4471144 (**1984**); (e) P. Veerakumar, Z. Z. Lu, M. Velayudham, K. -L. Lub, S. Rajagopala, *J. Mol. Catal. A: Chem.* **2010**, *332*, 128–137.
72. B.J. Arena, Des Plaines, US Pat. 4413152 (**1983**).
73. B.J. Arena, Des Plaines, US Pat. 4487980 (**1984**).
74. (a) P. G. Hoogewys, Fr 2526782(**1982**); (b) J. Ning, J. Lui, F. Lu, *Catal. Lett.* **2006**, *109*, 175–180.

75. H. Nishimoto, K. Nakagawa, N. Ikenaga, T. Suzuki, *Catal. Lett*. **2002**, *82*, 161–172.
76. F. Vocanson, Y. P. Guo, J. L. Namy, H. B. Kagan, *Synth. Commun.* **1998**, *28*, 2577–2582.
77. (a) P. Seetharamulu, V. S. Kumar, A. H. Padmasri, B. D. Raju, K. S. R. Rao, *J. Mol. Catal. A*: *Chem* **2007**, *263*, 253–258; (b) J. Zhang, H. Xu, Q. Ge, W. Li, *Catal. Comm.* **2006**, *7*, 148–152.
78. (a) V. Hulea, D. Brunel, A. Galarneau, K. Philippot, B. Chaudret, P. J. Kooyman, F. Fajula, *Microporous Mesoporous Mater.* **2005**, *79*, 185–194; (b) K. Pelzer, K. Philippot, B. Chaudret, W. Meyer-Zaika, G. Z. Schmid, *Z. Anorg. Allg. Chem.* **2003**, *629*, 1217–1222; (c) F. Schröder, D. Esken, M. Cokoja, M. W. E. van den Berg, O. I. Lebedev, G. Van Tendeloo, B. Walaszek, G. Buntkowsky, H. -H. Limbach, B. Chaudret, R. A. Fischer, *J. Am. Chem. Soc.* **2008**, *130*, 6119–6130; (d) F. Su, L. Lv, F. Yin, T. Tao-Liu, A. I. Cooper, A. Song-Zhao, *J. Am. Chem. Soc.* **2007**, *129*, 14213–14223.
79. F. Bergaya, B. K. G. Theng, G. Lagaly, in *Handbook of Clay Sci*. Elsevier Science Publishers B.V. Amsterdam, **2006**.
80. J. D. F. Ramsay, S. W. Swanton, J. Bunce, *J. Chem. Soc., Faraday Trans.* **1990**, *86*, 3919–3926.
81. (a) H. -B. Dai, X. -D. Kang, P. Wang, *Int. J. Hydrogen Energ.* **2010**, *35*, 10317–10323. (b) S. Miao, Z. Liu, B. Han, J. Huang, Z. Sun, J. Zhang, T. Jiang, Angew. *Chem. Int. Ed.* **2006**, *45*, 266–269.
82. V. Polshettiwar, R. Luque, A. Fihri, H. Zhu, M. Bouhrara, J. -M. Basset, *Chem. Rev*. **2011**, *111*, 3036–3075.
83. A. H. Lu, E. L. Salabas, F. Schuth, *Angew. Chem. Int. Ed.* **2007**, *46*, 1222–1244.
84. M. J. Jacinto, P. K. Kiyohara, S. H. Masunaga, R. F. Jardim, L. M. Rossi, *Appl. Catal. A-Gen*. **2008**, *338*, 52–57.
85. S. P. Gubin (ed.), *Magnetic Nanoparticles*, Wiley VCH Weinheim, **2009**.
86. A. -H. Lu, W. Schmidt, N. Matoussevitch, H. Bönnemenn, B. Spliethoff, B. Tesche, E. Bill, W. Kiefer, F. Schüth, *Angew. Chem. Int. Ed.* **2004**, *43*, 4303–4306.
87. L. M. Rossi, F. P. Silva, L. L. R. Vono, P. K. Kiyohara, E. L. Duarte, R. Itri, R. Landers, G. Machado, *Green Chem.* **2007**, *9*, 379–385.
88. A. Hu, G. T. Yee, W. Lin, *J. Am. Chem. Soc.* **2005**, *127*, 12486–12487.
89. V. Polshettiwar, R. S. Varma, *Chem. Eur. J.* **2009**, *15*, 1582–1586.
90. B. Baruvati, V. Polshettiwar, R. S. Varma, *Tetrahedr. Lett.* **2009**, *50*, 1215–1218.
91. (a) M. Auzias, G. Süss-Fink, P. Stěpnicka, J. Ludvik, *Inorg. Chimic. Acta* **2007**, *360*, 2023–2028; (b) M. Marcos, M. B. Ros, J. L. Serrano, M. A. Esteruelas, E. Sola, L. A. Oro, J. Barbera, *Chem. Mater*. **1990**, *2*, 748–758.
92. G. V. Tsarichenko, V. I. Bobrov and M. V. Smarkov, *Pharm. Chem. J*. **1977**, *11*, 481–483.

93. J. Suarez, K. Ranguelova, A. A. Jarzecki, *J. Biol. Chem.* **2009**, *284*, 7017–7029.
94. A. Gil, S. A. Korili, R. Trujillano, M. A. Vicente, in *Pillard Clays and Related Catalysts*, **2010**.
95. L. M. Rossi, L. L. R. Vono, F. P. Silva, P. K. Kiyohara, E. L. Duarte, J. R. Matos, *Appl. Catal. A* **2007**, *330*, 139–144.
96. R. Massart, *IEEE Trans. Magn.* **1981**, *17*, 1247–1248.
97. G. Süss-Fink, *Dalton Trans.* **2010**, *39*, 1673–1688.
98. P. J. Dyson, *Chimia* **2007**, *61*, 698–703.
99. S. J. Dougan, P. J. Sadler, *Chimia* **2007**, *61*, 704–715.
100. L. D. Dale, J. H. Tocher, T. M. Dyson, D. I. Edwards, D. A. Tocher, *Anti-Cancer Drug Design*, **1992**, *7*, 3–14.
101. C. S. Allardyce, P. J. Dyson, D. J. Ellis, S. L. Heath, *Chem. Commun.* **2001**, 1396–1397.
102. R. E. Morris, R. E. Aird, P. d. S. Murdoch, H. Chen, J. Cummings, N. D. Hughes, S. Pearsons, A. Parkin, G. Boyd, D. I. Jodrell, P. J. Sadler, *J. Med. Chem.* **2001**, *44*, 3616–3621.
103. J. G. Małecki, R. Kruszynski, M. Jaworska, P. Lodowski, Z. Mazurak, *J. Organomet. Chem.* **2008**, *693*, 1096–1108.
104. (a) Y. Malam, M. Loizidou, A. M. Seifalian, *Trends Pharm. Sci.* **2009,** *30*, 592–599. (b) P. P. Jumade, A. M. Gupta, P. W. Dhore, P. S. Wake, V. V. Pande, A. Deshmukh, *J. Chem. Pharm. Sci.* **2009**, *2*, 158–164. (c) M. E. Gindy, R. K. Prud'homme, *Opinion Drug Deliv.* **2009**, *6*, 865–878. (d) W. Lin, T. Hyeon, G. M. Lanza, M. Zhang, T. J. Meade, *MRS Bulletin* **2009**, *34*, 441–448.
105. D. F. Baban. L. W. Seymour, *Adv. Drug Delivery Rev.* **1998**, *34*, 109–119.
106. M. Vaccaro, R. Del Litto, G. Mangiapia, A. M. Carnerup, G. D'Errico, F. Ruffoa, L. Paduano, *Chem. Commun.* **2009**, 1404–1406.
107. W. H. Ang, P. J. Dyson, *Eur. J. Inorg. Chem.* **2006**, 4003–4018.
108. (a) F. Schmitt, P. Govindaswamy, G. Süss-Fink, W. H. Ang, P. J. Dyson, L. Juillerat-Jeanneret, B. Therrien, *J. Med. Chem.* **2008**, *51*, 1811–1816. (b) P. Govender, N. C. Antonels, J. Mattsson, A. K. Renfrew, P. J. Dyson, J. R. Moss, B. Therrien, G. S. Smith, *J. Organomet. Chem.* **2009**, *694*, 3470–3476. (c) J. Mattsson, P. Govindaswamy, A. K. Renfrew, P. J. Dyson, P. Štěpnička, G. Süss-Fink, B. Therrien, *Organometallics* **2009**, *28*, 4350–4357. (d) M. G Mendoza-Ferri, C. G. Hartinger, A. A. Nazarov, R. E. Eichinger, M. A. Jakupec, K. Severin, B. K. Keppler, *Organometallics* **2009**, *28*, 6260–6265.
109. B. Therrien, W. H. Ang, F. Chérioux, L. Vieille-Petit, L. Juillerat-Jeanneret, G. Süss-Fink, P. J. Dyson, *J. Cluster Sci.* **2007**, *18*, 741–752.
110. (a) Coll. in *Organic Syntheses*, **1973**, *5*, p.251; (b) A. Williamson, *Philosophical Magazine*, **1850**, *37*, 350–356.

111. T. W. Green, P. G. M. Wuts, *Protective Groups in Organic Synthesis*, Wiley-Interscience, New York, **1999**, 76–86, 708–711.
112. R. Salmon, "Oxalyl Chloride" in Encyclopedia of Reagents for Organic Synthesis, **2001**, John Wiley & Sons, New York.
113. K. I. Nättinen, K. Rissanen, *Cryst. Growth Design* **2003**, *3*, 339–353.
114. J. A. Creighton, D. G. Eadon, *J. Chem. Soc. Faraday Trans.* **1991**, *87*, 3881–3891.
115. M. D. Abramoff, P. J. Magelhaes, S.J. Ram, *Biophotonics Int.* **2004**, *11*, 36–42.
116. M. Auzias, B. Therrien, G. Süss-Fink, P. Štěpnička, W. H. Ang, P. J. Dyson, *Inorg. Chem.* **2008**, *47*, 578–583.
117. C. A. Vock, C. Scolaro, A. D. Phillips, R. Scopelliti, G. Sava, P. J. Dyson *J. Med. Chem.* **2006**, *49*, 5552–5561.
118. (a) D. J. Goldschmith, E. Kennedy, R. G. Campbello, *J. Org. Chem.* **1995**, *40*, 3571–3574; (b) S. K. Kang, W. S. Kim, B. H. Moon, *Synth.***1985**, *12*, 1161–1162; (c) A. Ravikrishnan, P. Sudhakara, P. Kannan, *J. Mater. Sci.* **2010**, *45*, 435–442; (d) J. M. Chong, M. A. Heuft, P. Rabbat, *J. Org. Chem.* **2000**, *65*, 5837–5838.
119. Y. Fu, Y. Li, J. Li, S. Yan, Z. Bo, *Macromolecules* **2004**, *37*, 6395–6400.
120. C. Milone, R. Ingoglia, A. Pistone, G. Neri, F. Frusteri, S. Galvagno, *J. Catal.* **2004**, *222*, 348–356.
121. U. S. Schubert, C. Eschbaumer, G. Hochwimmer, *Synth.* **1999**, *5*, 779–782.
122. I. Gillaizeau-Gauthier, F. Odobel, M. Alebbi, R. Argazzi, E. Costa, G. J. Meyer, *Inorg. Chem.* **2001**, *40*, 6073–6079.
123. D. Astruc, F. Lu, J. R. Aranzaes, *Angew. Chem. Int. Ed.* **2005**, *44*, 7852–7872.
124. J. Ma, H. Ma, D. Pan, R. Li, K. Xie, *React. Kinet. Catal. Lett.* **2005**, *86*, 225–231.
125. M. Zahmakiran, Y. Tonbul, S. Özkar, *J. Am. Chem. Soc.* **2010**, *132*, 6541–6549.
126. N. Yan, C. Zhao, C. Luo, P. J. Dyson, H. Liu, Y. Kou, *J. Am Chem. Soc.* **2006**, *128*, 8714–8715.
127. M. Poliakoff, J. M. Fitzpatrik, T. R. Farren, P. T. Anastas, *Science* **2002**, *297*, 807–810.
128. R. Berthoud, A. Baudouin, B. Fenet, W. Lukens, K. Pelzer, J. –M. Basset, J. –P. Candy, C. Copéret, *Chem. Eur. J.* **2008**, *14*, 3523–3526.
129. (a) M. Womes, T. Cholley, F. Le Peltier, S. Morin, B. Didillon, N. Szydlowski-Schildknecht, *Appl. Catal. A* **2005**, *283*, 9–22; (b) B. Chaudret, *Top. Organomet. Chem.* **2005**, *16*, 233–259; (c) R. M. Rioux, H. Song, M. Grass, S. Habas, K. Niesz, J. D. Hoefelmeyer, P. Yang, G. A. Somorjai, *Top. Catal.* **2006**, *39*, 167–174.
130. S. H. Joo, J. Y. Park, J. R. Renzas, D. R. Butcher, W. Huang, G. A. Somorjai, *Nano Lett.* **2010**, *10*, 2709–2713.
131. X. Yan, H. Liu, K.Y. Liew, *J. Mater. Chem.* **2001**, *11*, 3387–3391.

132. F. Bonet, V. Delmas, S. Grugeon, R. H. Urbina, P. Y. Silvert, K. Tekaia-Elhsissen, *Nanostruct. Mater.* **1999**, *11*, 1277–1284.
133. Y. Chen, K. Y. Liew, J. Li, *Mater. Lett.* **2008**, *62*, 1018–1021.
134. G. Meister, G. Süss-Fink, unpublished, see G. Meister (**1994**), Ph. D. Thesis, University of Neuchâtel, Switzerland.
135. A. Meister, G. Süss-Fink, unpublished, see A. Meister (**1994**). Ph. D. Thesis, University of Neuchâtel, Switzerland.
136. M. Stebler-Röthlisberger, W. Hummel, P. -A. Pittet, H. -B. Bürgi, A. Ludi, A. E. Merbach, *Inorg. Chem.* **1988**, *27*, 1358–1363.
137. G. Lagaly, H. Tributh, *Ber. Dt. Tonmineralgruppe* **1991**, 86–130.
138. T. D. Kim, T. J. Mc Neese, *Inorg. Chem.* **1988**, *27*, 2554–2555.
139. J. Weitkamp, L. Puppe, in *Catalysis and Zeolites*, by Springer Sci. **1999**.
140. J. Cejka, S. Zones, A. Corma, in *Zeolites and Catalysis*, by John Wiley & Sons, **2010**.
141. S. M. Zhu, S. H. Zhou, M. Hibino, I. Honma, *J. Mater. Chem.* **2003**, *13*, 1115–1118.
142. G. Laugel, J. Arichi, H. Guerba, M. Molière, A. Kiennemann, F. Garin, B. Louis, *Catal. Lett.* **2008**, *125*, 14–21.
143. P. J. Dyson, *Dalton Trans.* **2003**, 2964–2974.
144. S. Lu, C. A. Menning, Y. Zhu, J. G. Chen, *ChemPhysChem.* **2009**, *10*, 1763–1765.
145. E. Bayram, M. Zahmakıran, S. Ozkar, R. G. Finke, *Langmuir* **2010**, *26*, 12455–12464.
146. S. K. Sharma, K. B. Sidhpuria, R. V. Jasra, *J. Mol. Catal. A: Chem.* **2011**, *335*, 65–70.
147. M. Zahmakıran, Y. Tonbulz, S. Özkar, *Chem. Commun.* **2010**, *46*, 4788–4790.
148. (a) K. Weissermel, H.-J. Arpe, in *Industrial Organic Chemistry*, **2003**, Wiley-VCH, Weinheim; (b) L. Llyod, in Handbook of Industrial Catalysts, 1st ed. 2011, p.100, Springer.
149. C. Vangelis, A. Bouriazos, S. Sotiriou, M. Samorski, B. Gutsche,G. Papadogianakis, *J. Catal.* **2010**, *274*, 21–28.
150. (a) G. W. Parshall, S. D. Ittel, in *Homogeneous Catalysis*, **2010**, John Wiley,New York; (b) H. Brunner, in: B. Cornils, W.A. Herrmann (Eds.), *Applied Homogeneous Catalysis with Organometallic Compounds*, vol. 1, Wiley-VCH, Weinheim, **1996**, p.201–219.
151. J. A. Widegren, R. G. Finke, *J. Mol. Catal. A: Chem.* **2003**, *191*, 187–207.
152. Y. Motoyama, M. Takasaki, S. -H. Yoon, I. Mochida, H. Nagashima, *Org. Lett.* **2009**, *11*, 5042–5045.
153. B. Yoon, H. -B. Pan, C. M. Wa, *J. Phys. Chem. C* **2009,** *113*, 1520–1525.
154. N. Yan, Y. Yuan, Paul J. Dyson, *Chem. Commun.* **2011**, *47*, 2529–2531.
155. M. E. Halttunen, M. K. Niemela, A. O. I. Krause, A. I. Vuori, *J. Mol. Catal. A: Chem.* **1996**, *109*, 209–217.

156. A. B. Boricha, H. M. Mody, H. C. Bajaj, R. V. Jasra, *Appl. Clay Sci.* **2006**, *31*, 120–125.
157. D. Marquardt, C. Vollmer, R. Thomann, P. Steurer, R. Mülhaupt, E. Redel, C. Janiak, *Carbon* **2011**, *49*, 1326–1332.
158. L. V. Allen Jr., Compounding Topical Dosage Forms: Ointments, Creams, Pastes and Lotions, Paddock Laboratories, Inc. (1993). http://www.paddocklabs.com/html/resource/pdf/Sec%20Artem%203.2.pdf
159. G. W. Huber, S. Iborra, A. Corma, *Chem. Rev*. **2006**, *106*, 4044–4098.
160. A. Hull, I. Golubkov, US Pat. 7323020 (**2008**).
161. J.-P. Lange, W. D. van de Graaf, R. J. Haan, *ChemSusChem*. **2009**, *2*, 437–441.
162. National Organic Standards Board Technical Advisory Panel Review for FA, Compiled by University of California Sustainable Agriculture Research and Education Program (UCSAREP) for the USDA National Organic Program (2003).
163. N. Merat, C. Godawa, A. Gaset, *J. Chem. Tech. Biotechnol*. **1990**, *48*, 145–159.
164. M. A. Tike, V. V. Mahajani, *Ind. Eng. Chem. Res*. **2007**, *46*, 3275–3282.
165. S. Winterle, A. Kraynov, J. Klankermayer, W. Leitner, M. A. Liauw, personal communication (**2010**).
166. X. Chen, W. Sun, N. Xiao, Y. Yan, S. Liu, *Chem. Eng. J*. **2007**, *126*, 5–11.
167. Y. Song, W. Li, M. Zhang, K. Tao, Front. *Chem. Eng. China*. **2007**, *2*, 151–154.
168. W. -L. Wei, H. -Y. Zhu, C. -L. Zhao, M. -Y. Huang, Y. -Y. Jiang, *React. Funct. Polym*. **2004**, *59*, 33–39.
169. R. A. Rajadhyaksha, S.L. Karwa, *Chem. Engg. Sci*. **1986**, *41*, 1765–1770.
170. W. H. Carothers, R. J. Adams, *J. Am. Chem. Soc*.**1924**, *46*, 1675–1683.
171. A. S. Hussey, G. W. Keulks, G. P. Nowack, R. H. Baker, *J. Org. Chem.***1968**, *33*, 610–616.
172. H. Adkins, Reactions of Hydrogen, University of Wisconsin Press, Madison, **1937**, p. 135.
173. G. J. Leuck, J. Pokorny, F. N. Peters, U. S. Pat. 2097493, (**1937**).
174. S. Sawadesh, A. P. Dunlop, *J. Org. Chem*. **1949**, *14*, 692–695.
175. (a) Y. -C. Son, S. L. Suib, R. E. Malz, *Catalysis of Organic Reactions* D. G. Morrel, Ed. Marcel Dekker Inc., New York, **2003**, p. 559–564. (b) W. K. O'Keefe, F. T. T. Ng, G. L. Rempel, *Ind. Eng. Chem. Res.* **2007**, *46*, 716–725. (c) P. G. N. Mertens, P. Vandezande, X. Ye, H. Poelman, I. F. J. Vankelecoma, D. E. De Vos, *Appl. Catal. A: Gen.* **2009**, *355*, 176–183.
176. P. Kluson, L. Cerveny, *Appl. Catal. A: Gen.* **1995**, *128*, 13–31.
177. T. J. Pinnavaia, *Science*. **1983**, *220*, 365–371.
178. J. L. Valverde, A. de Lucas, P. Sànchez, F. Dorado, A. Romero, *Appl. Catal. B.* **2003**, *43*, 43–56.

179. B. M. Choudary, M. L. Kantam, K. V. S. Ranganath, K. K. Rao, Angew. *Chem. Int. Ed.* **2005**, *44*, 322–325.

180. S. Shimazu, T. Hirano, T. Uematsu, *Appl. Catal.* **1987**, *34*, 255–261.

181. F. -A. Khan, A. Vallat, G. Süss-Fink, *Catal. Commun.* **2011**, *12*, 1428–1431.

182. (a) V. Ponec, *Appl. Catal. A: Gen.* **1997**, *149*, 27–48. (b) J. G. de Vries, L. Lefort, P. H. Phua, PCT Int. Appl. WO 2009/150173 A1, (**2009**).

183. (a) E. Breitner, E. Roginski, P. N. Rylander, *J. Org. Chem.* **1959**, *24*, 1855–1857; (b) C. Milone, R. Ingoglia, A. Pistone, G. Neri, F. Frusteri, S. Galvagno, *J. Catal.* **2004**, *222*, 348–356; (c) C. Milone, R. Ingoglia, M. L. Tropeano, G. Neri and S. Galvagno, *Chem. Commun.* **2003**, 868–869; (d) K. Yu. Koltunov, I. B. Repinskaya, G. I. Borodkin, Russ. *J. Org. Chem.* **2001**, *37*, 1534–1541.

184. (a) B. P. S. Chauhan, J. S. Rathore, T. Bandoo, *J. Am. Chem. Soc.* **2004**, *126*, 8493–8500 ; (b) U. R. Pillai, E. Sahle-Demessie, *J. Mol. Catal. A: Chem.* **2004**, *222*, 153–158; (c) W. K. O'Keefe, M. Jiang, F. T. T. Ng, G. L. Rempel, *Chem. Eng. Sci.* **2005**, *60*, 4131–4140; (d) Q. Liu, J. Li, X. –X. Shen, R. -G. Xing, J. Yang, Z. Liu, B. Zhou, *Tetrahedron Lett.* **2009**, *50*, 1026–1028.

185. (a) G. Szöllósi, Á. Mastalir, Á. Molnár, M. Bartók, *React. Kinet. Catal. Lett.* **1996**, *57*, 29–33; (b) M. L. A. von Holleben, M. Zucolotto, C. A. Zini, E. R. Oliveira, *Tetrahedron.* **1994**, *50*, 973–978; (c) K. Kindler, K. Liihrs, *Justus Liebigs Ann. Chem.* **1965**, *685*, 36; (d) T. Yasuhiko, N. Toschio, Jpn. Pat. 61085343A, (**1986**); (e) O. Norio, T. Masayuki, N. Yoshitaka, H. Shigeo, Jpn. Pat. 229904A, (**2000**); (f) O. Norio, T. Masayuki, K. Takako, H. Shigetada, Jpn. Pat. 219649 A, (**2000**); (g) Y. Hu, H. Yang, Y. Zhang, Z. Hou, X. Wang, Y. Qiao, H. Li, B. Feng, Q. Huang, *Catal. Commun.* **2009**, *10*, 1903–1907; (h) A. M. R. Galletti, C. Antonetti, A. M. Venezia, G. Giambastiani, *Appl. Catal. A: Gen.* **2010**, *386*, 124–131.

186. (a) L. Mordenti, J. J. Brunet, P. Caubere, *J. Org. Chem.* **1979**, *44*, 2203–2205; (b) J. J. Brunet, L. Mordenti, B. Loubinoux, P. Caubere, *Tetrahedron Lett*. **1977**, *18*, 1069–1072; (c) S. Masamune, G. S. Bates, P. E. Georghiou, *J. Am. Chem. Soc*. **1974**, *96*, 3686–3688; (d). J. Lipowitz, S. A. Bowman, *J. Org. Chem.* **1973**, *38*, 162–165; (e) P. Gallois, J. J. Brunet, P. Caubere, *J. Org. Chem.* **1980**, *45*, 1946–1950; (f) D. H. Gibson, Y. S. El-Omrani, *Organometallics* **1985**, *4*, 1473–1475; (g) E. Keinan, D. Perez, *J. Org. Chem.* **1987**, *52*, 2576–2580; (h) Y. Fort, R. Vanderesse, P. Caubere, *Tetrahedron Lett.* **1986**, *27*, 5487–5490; (i) K. E. Kim, S. B. Park, N. M. Yoon, *Synth. Commun.* **1988,** *18*, 89–90; (j) K. R. Russell, *e-EROS Encyclopedia of Reagents for Organic Synthesis, John Wiley & Sons, Inc*. **2001.**

187. (a) M. Sommovigo, H. Alper, *Tetrahedron Lett.* **1993**, *34*, 59–62; (b) I. S. Cho, H. Alper, *J. Org. Chem.* **1994**, *59*, 4027–4028; (c) H. Jiang, D. Song, *Organometallics* **2008**, *27*, 3587–3592; (d) A. M. Caporusso, G. Giacomelli, L. Lardicci, *J. Org. Chem.* **1982**, *47*, 4640–4640;

(e) Z. Yang, M. Ebihara, T. Kawamura, *J. Mol. Catal. A: Chem.* **2000**, *158*, 509–514; (f) C. A. Mebi, B. J. Frost, *Organometallics.* **2005**, *24*, 2339–2346; (g) H. M. Ali, A. A. Naiini, C. H. Brubaker Jr., *J. Mol. Catal.* **1992**, *77*, 125–134; (h) H. M. Ali, A. A. Naiini, C. H. Brubaker Jr., *Tetrahedron Lett.* **1991**, *32*, 5489–5492; (i) R. van Asselt, C. J. Elsevier, *J. Mol. Catal.* **1991**, *65*, L13–L19; (j) Y. Himeda, N. Onozawa-Komatsuzaki, S. Miyazawa, H. Sugihara, T. Hirose, K. Kasuga, *Chem. Eur. J.* **2008**, *14*, 11076–11081; (k) H. Jiang, E. Stepowska, D. Song, *Eur. J. Inorg. Chem.* **2009**, 2083–2089; (l) J. H. van Tonder, C. Marais, D. J. Cole-Hamilton, B. C. B. Bezuidenhoudt, *Synthesis.* **2010**, *3*, 421–424; (m) M. Mirza-Aghayan, R. Boukherroub, M. Bolourtchian, M. Rahimifard, *J. Organomet. Chem.* **2007**, *692*, 5113–5116.

188. (a) T. Kimura, T. Takahashi, M. Nishiura, K. Yamamura, Org. lett. 8 (2006) 3137–3139; (b) P. Goswami, S. Ali, Md. M. Khan, B. Das, *Lett. Org. Chem.* **2008**, *5*, 659–664.

189. (a) J. A. Trejo, J. Tate, D. Martenak, F. Huby, S. M. Baxter, A. K. Schultz, R. J. Olsen, *Top. Catal.* **2010**, *53*, 1156–1162; (b) E. O. C. Greiner, C. Funada, *The Chemical Economics Handbook (CEH)*, SRI Consulting Report Number 675.6000, (**2008**).

190. (a) J. I. Di Cosimo, G. Torres, C. R. Apesteguía, *J. Catal.* **2002**, *208*, 114–123; (b) K. H. Lin, A. N. Ko, *Appl. Catal. A: Gen.*, **1996**, *147*, L259–L265; (c) P. Y. Chen, S. J. Chu, K. C. Wu, W. C. Lin, *U.S. Pat.* **1997**, 5684207; (d) L. V. Mattos, F. B. Noronha, J. L. F. Monteiro, *J. Catal.* **2002**, *209*, 166–176; (e) R. H. Crabtree, P. T. Anastas, *Green catalysis: Heterogeneous catalysis, Wiley-VCH Verlag*, **2009**.

191. (a) L. P. Bevey, *Progress in Catalysis Research* (ed. L. P. Bevey), Nova Science Publisher, Inc. New York, **2005**, pp. 178; (b) N. Cheikhi, M. Kacimi, M. Rouimi, M. Ziyad, L. F. Liotta, G. Pantaleo, G. Deganello, *J. Catal.* **2005**, *232*, 257–267; (c) M. Mediavilla, L. Melo, Y. Díaz, A. Albornoz, A. Llanos, J. L. Brito, *Micropor. Mesopor. Mat.* **2008**, *116*, 627–632.

192. (a) F. Maclean, C. C. Hobbs, US Pat. 2825743, (**1955**); (b) J. Kasumi, M. Kuniyoshi, Jpn. Pat. 7215809, 1972; (c) Y. Qi, Z. Wang, R. Wang, *Appl. Catal.* **1989**, *53*, 63–70; (d) S. Nishimura, *Handbook of Heterogeneous Catalytic Hydrogenation for Organic Synthesis*, John Wiley & Sons, Inc. **2001**, p. 226.

193. (a) F. Delbecq, P. Sautet, J. Catal. 152 (1995) 217–236 ; (b) P. Sautet, J. F. Paul, *Catal. Lett.* **1991**, *9*, 245–260.

194. a) P. Mäki-Arvela, J. Hájek, T. Salmi, D. Yu. Murzin, *Appl. Catal. A-Gen.* **2005**, *292*, 1–49. b) S. N. Coman, V. I. Parvulescu, M. De Bruyn, D. E. De Vos, P. Jacobs, *J. Catal*. **2002**, *206*–218.

195. E. Breitner, E. Roginski, P. N. Rylander, *J. Org. Chem.* **1959**, *24*, 1855–1857.

196. a) C. Milone, R. Ingoglia, A. Pistone, G. Neri, F. Frusteri, S. Galvagno, *J. Catal.* **2004**, *222*, 348–356. b) V. Ponec, *App. Catal. A: Gen.* **1997**, *149*, 27–48.

197. Gy. Szöllósi, Á. Mastalir, Á. Molnár, M. Bartók, *React. Kinet. Catal. Lett.* **1996**, *57*, 29–36.

198. M. von Arx, T. Mallat, A. Baiker, *J. Mol. Catal. A: Chem.* **1999**, *148*, 275–283.

199. (a) C. Milone, R. Ingoglia, M. L. Tropeano, G. Neri, S. Galvagno, *Chem. Commun.* **2003**, 868–869 ; (b) C. Milone, R. Ingoglia, L. Schipilliti, C. Crisafulli, G. Neri, S. Galvagno, *J. Catal.* **2005**, *236*, 80–90; (c) P. G. N. Mertens, J. Wahlen, X. Ye, H. Poelman, D. E. De Vos, *Catal. Lett*. **2007**, *117*, 15–21; (d) C. Milone, R. Ingoglia, S. Galvagno, *Gold Bulletin*, **2006**, *39*, 54–64.

200. M. -M. Wang, L. He, Y.-M. Liu, Y. Cao, H. -Y. He, K. -N. Fan, *Green Chem.* **2011**, *13*, 602–607.

201. (a) N. M. Yoon, T. B. Sim, *Bull. Korean Chem. Soc.* **1993**, **14**, 749–752; (b) A. L. Gemal, J. L. Luche, *J. Am. Chem. Soc.* **1981**, *103*, 5454–5459; (c) K. E. Wilson, R. T. Seider, S. Masamune, *J. Chem. Soc. D,* **1970**, 213b–214; (d) L. Mordenti, J. J. Brunet, P. Caubere, *J. Org. Chem.* **1979**, *44*, 2203–2205.

202. (a) H. Ozasa, K. Kondo, T. Aoyama, *Chem. Pharm. Bull.* **2010**, *58*, 989–990; (b) T. Inagaki, Y. Yamada, L. T. Phong, A. Furuta, J. Ito, H. Nishiyama, *Synlett.* **2009**, 253–256; (c) D. Addis, S. Zhou, S. Das, K. Junge, H. Kosslick, J. Harloff, H. Lund, A. Schulz, M. Beller, *Chem. Asian J.* **2010**, *5*, 2341–2345; (d) D. Addis, N. Shaikh, S. Zhou, S. Das, K. Junge, M. Beller, *Chem. Asian J.* **2010**, *5*, 1687–1691.

203. (a) N. Erathodiyil, S. Ooi, A. M. Seayad, Y. Han, S. S. Lee, J. Y. Ying, *Chem. Eur. J.* **2008**, *14*, 3118–3125; (b) A. J. Blacker, S. M. Brown, C. Bubert, J. M. J. Williams, *WO 0244111*, **2002**; (c) A. J. Blacker, B. V. Mellor, US Pat. 2002/0156282, (**2002**); (d) J. I. Di Cosimo, A. Acosta, C. R. Apesteguia, *J. Mol. Catal. A: Chem.* **2004**, *222*, 87–96.

204. (a) Y. Ishii, T. Nakano, A. Inada, Y. Kishigami, K. Sakurai, M. Ogawa, *J. Org. Chem.* **1986**, *51*, 240–242; (b) M. Gargano, V. D'Orazio, N. Ravasio, M. Rossi, *J. Mol. Catal.* **1990**, *58*, L5–L8.

205. (a) K. Junge, B. Wendt, D. Addis, S. Zhou, S. Das, S. Fleischer, M. Beller, *Chem. Eur. J.* **2011**, *17*, 101–105; (b) X. Chen,W. Jia, R. Guo, T. W. Graham, M. A. Gullons, K. Abdur-Rashid, *Dalton Trans.* **2009**, 1407–1410; (c) I. Warad, Z. Al-Othman, S. Al-Resayes, S. S. Al-Deyab, E. -R. Kenawy, *Molecules*, **2010**, *15*, 1028–1040; (d) R. Noyori, T. Ohkuma, *Pure Appl. Chem.* **1999**, *71*, 1493–1501; (e) C. A. Mebi, R. P. Nair, B. J. Frost, *Organometallics*, **2007**, *26*, 429–438.

206. R. A. Sheldon, *Pure Appl. Chem.* **2000**, *72*, 1233–1246.

207. V. Polshettiwar, R. Luque, A. Fihri, H. Zhu, M. Bouhrara, J. -M. Basset, *Chem. Rev.* **2011**, *111*, 3036–3075.

208. (a) J. Špringerova, P. Kacher, L. Červeny, *Res. Chem. Intermed.* **2005**, *31*, 785–795; (b) B. S. Furniss, A. J. Hannaford, P. W. G. Smith, A. R. Tatchell in *Vogel's Textbook of Practical Organic Chemistry* (ed: 5th A. Longman), Wiley-VCH, New York, **1989**, p. 519.

209. B. Panella, A. Vargas, A. Baiker, *J. Catal.* **2009**, *261*, 88–93.

210. M. J. Jacinto, P. K. Kiyohara, S. H. Masunaga, R. F. Jardim, L. M. Rossi, *Appl. Catal. A-Gen*. **2008**, *338*, 52–57.

211. A. H. Lu, E. L. Salabas, F. Schuth, *Angew. Chem. Int. Ed.* **2007**, *46*, 1222–1244.

212. A. Hu, G. T. Yee, W. Lin, *J. Am. Chem. Soc.* **2005**, *127*, 12486–12487.

213. (a) L. M. Rossi, L. L. R. Vono, F. P. Silva, P. K. Kiyohara, E. L. Duarte, J. R. Matos, *Appl. Catal. A-Gen*. **2007**, *330*, 139–144; (b) R. Massart, *IEEE Trans. Magn.* **1981**, *17*, 1247–1248.

214. W. Wu, Q. He, C. Jiang, *Nanoscale Res Lett.* **2008**, *3*, 397–415.

215. R. M. Cornell, U. Schwertmann in *The Iron Oxides: Structure, Properties, Reactions, Occurences and Uses*, Wiley-VCH, Weinheim, **1996**.

216. (a) M. Kotani, T. Koike, K. Yamaguchi, N. Mizuno, *Green Chem.* **2006**, *8*, 735–741; (b) M. A. Vergés, R. Costo, A. G. Roca, J. F. Marco, G. F. Goya, C. J. Serna, M. P. Morales, *J. Phys. D: Appl. Phys.* **2008**, *41*, 134003–134013.

217. (a) H.P. Klug, L.E. Alexander, *X-Ray Diffraction Procedures*, 2nd Ed. John Wiley & Sons Inc., **1974**, p 687-703; (b) A. Patterson, *Phys. Rev.* **1939**, *56*, 978–982.

218. A. Hu, G. T. Yee, W. Lin, *J. Am. Chem. Soc.* **2005**, *127*, 12486–12487.

219. G. M. Sheldrick, *Acta Cryst.* **2008**, *A64*, 112–122.

220. A. L. Spek, *Acta Cryst.* **2009**, *D65*, 148–155.

221. L. J. Farrugia, *J. Appl. Cryst.* **1997**, *30*, 565–566.

8

List of Publications

1. Arene Ruthenium Complexes Contianing Long-Chain Isonicotinic Ester Ligands: Synthesis, Molecular Sturucture and Anticancer Activity, **F. -A. Khan**, B. Therrien, G. Süss-Fink, O.Zava, P. J. Dyson, *J. Organomet. Chem.* in process.

2. Superparamagnetic Core-Shell Type Fe_3O_4/Ru Nanoparticles as Catalysts for the Selective Hydrogenation of an Unconstrained α,β-Unsaturated Ketone, **F. -A. Khan**, G. Süss-Fink, *Eur. J. Inorg. Chem.* **2012**, 727–732.

3. Highly selective C=C bond hydrogenation in α,β-unsaturated ketones catalyzed by hectorite-supported ruthenium nanoparticles, **F. -A. Khan**, A. Vallat, G. Süss-Fink, *J. Mol. Catal. A: Chem.***2012**, *355*, 168–173.

4. Highly Selective Low Temperature Hydrogenation of Furfuryl Alcohol to Tetrahydrofurfuryl Alcohol Catalyzed by Hectorite-Supported Ruthenium Nanoparticles, **F. -A. Khan**, A. Vallat, G. Süss-Fink, *Catal. Commun.* **2011**, *12*, 1428–1431.

5. Synthesis and Anticancer Activity of Long-Chain Isonicotinic Ester Ligand-Containing Arene Ruthenium Complexes and Nanoparticles, G. Süss-Fink, **F. -A. Khan**, L. J. Jeanneret, P. J. Dyson, A. K. Renfrew, *J. Clust. Sci.* **2010**, *21*, 313–324.

6. Shape- and Size-Selective Preparation of Hectorite-Supported Ruthenium Nanoparticles for the Catalytic Hydrogenation of Benzene, G. Süss-Fink, **F. -A. Khan**, J. Boudon, V. Spassov, *J. Clust. Sci.* **2009**, *20*, 341–353.

Other Publications

7. Coordination of Septran drug with Trace Metal ions in the Biological System, F. S. Rehmani, **F. -A. Khan**, F. Hassan, *Int. J. Bio.& Biotech.* **2006**, *3*, 439 – 442.

In recent years, nano-sized molecular materials recieved much attention due to their potential applications. Isonicotinic acid is widely used for the synthesis of antibiotics and antituberculosis preparations, and it has strong bactericide effects. We have been interested in the use of long-chain isonicotinic esters as lipohilic components in order to increase the anticancer activity of arene ruthenium complexes, while using them as stabilizers for ruthenium nanoparticles with the aim of exploring self-organization and biological (anticancer) properties of these new hybrid materials.

Developing green chemical transformations to reduce waste in liquid phase organic reactions is a major challenge today. Heterogeneous catalysts are considered clean technologies, because they help minimize the consumption of energy and raw materials used in the synthesis. In this study, arene ruthenium complexes intercalated in hectorite were used as precursor for the size- and shape-selective preparation of ruthenium nanoparticles and in exploiting their possible catalytic potential in hydrogenation reactions.

Based on the experience gained from hectorite-supported nano-ruthenium and on well established procedures to make magnetite nanoparticles by co-precipitation from aqueous solutions of Fe^{2+} and Fe^{3+} salts using the Massart method, we have been interested in developing ruthenium-coated magnetite nanoparticles by the aqueous organometallic route. The easy separability of these superparamagnetic nanoparticles from reaction mixture by means of an external magnet makes nano Ru@Fe_3O_4 an interesting material for catalytic transformations.

It was, therefore, the aim of this study to develop metallic ruthenium nanoparticles stabilized by mesogenic isonicotinic ester ligands, intercalated in hectorite and supported on magnetite for catalytic and biological applications.